eLife

Reviewed Preprint
v1 • August 4, 2026
Not revised

Engulfment by brain macrophages in a short-lived vertebrate

For correspondence:
bedbrook@stanford.edu
ravinath@stanford.edu
abrunet1@stanford.edu

* equal contribution

Rahul Nagvekar[1,2], Angela N Pogson[1,3,4], Prateek R Kalakuntla[3,4], Helena J Barr[5,6,7], Azalia M Martínez Jaimes[4,8], SV Perry[1], Emma K Costa[9,10,11], Jingxun Chen[1], Felix Boos[1], Paloma Navarro Negredo[1,12], Luise A Seeker[13], James B Jaggard[14], Rogelio Barajas[1,15], Philippe Mourrain[14], Param Priya Singh[15,16], Stephen R Quake[13,17], Tony Wyss-Coray[9,11,18], Kristy Red-Horse[8,19,20], Beth Stevens[5,6,19], Bo Wang[3,13], Claire N Bedbrook[1,21,*], Ravi D Nath[1,21,22,*], Anne Brunet[1,11,18,23,*]

[1]Department of Genetics, Stanford University, Stanford, United States • [2]Genetics Graduate Program, Stanford University School of Medicine, Stanford, United States • [3]Department of Developmental Biology, Stanford University, Stanford, United States • [4]Developmental Biology Graduate Program, Stanford University School of Medicine, Stanford, United States • [5]Boston Children's Hospital, Kirby Neurobiology Center, Boston, United States • [6]Broad Institute of MIT and Harvard, Cambridge, United States • [7]Harvard Division of Medical Sciences, Graduate Program in Neuroscience, Boston, United States • [8]Department of Biology, Stanford University, Stanford, United States • [9]Department of Neurology and Neurological Sciences, Stanford University, Stanford, United States • [10]Neurosciences Interdepartmental Program, Stanford University School of Medicine, Stanford, United States • [11]Wu Tsai Neurosciences Institute, Stanford University, Stanford, United States • [12]Global Health Institute, École Polytechnique Fédérale de Lausanne (EPFL), Lausanne, Switzerland • [13]Department of Bioengineering, Stanford University, Stanford, United States • [14]Department of Psychiatry and Behavioral Sciences, Stanford University, Stanford, United States • [15]Department of Anatomy, University of California San Francisco, San Francisco, United States • [16]Bakar Aging Research Institute, University of California San Francisco, San Francisco, United States • [17]Department of Applied Physics, Stanford University, Stanford, United States • [18]Phil and Penny Knight Initiative for Brain Resilience, Stanford, United States • [19]Howard Hughes Medical Institute, Chevy Chase, United States • [20]Institute for Stem Cell Biology and Regenerative Medicine, Stanford, United States • [21]Lewis-Sigler Institute for Integrative Genomics, Princeton University, Princeton, United States • [22]Department of Molecular Biology, Princeton University, Princeton, United States • [23]Glenn Center for the Biology of Aging, Stanford University, Stanford, United States

Competing interests: A.B. is a scientific advisory board member of Calico. B.S. is a member of the scientific advisory board and minority shareholder of Annexon Bioscience and a member of the scientific advisory board and minority shareholder of TenVie. The other authors declare no competing interests.

Funding: See page 38

Reviewing editor: Florent Ginhoux, Singapore Immunology Network, Singapore

eLife Assessment

This **valuable** study establishes a novel genetic model for chronic, in vivo visualization of protein engulfment in brain macrophages from the naturally short-lived African turquoise killifish. The **solid** data presented here show that brain phagocytes exhibit transcriptional features resembling mammalian border associated macrophages and monocyte derived macrophages rather than classical microglia and that their engulfment capacity declines with age, providing a resource for future studies on brain immune cells in teleosts. This research will interest a broad audience across developmental biology, genetics, neuroimmunology, aging research, and evolutionary biology.

[Editors' note: this paper was reviewed by *Review Commons*.]

https://doi.org/10.7554/eLife.112503.1.sa4

Abstract

Engulfment by macrophages is critical for waste clearance in the vertebrate brain. Understanding clearance mechanisms may open new therapeutic possibilities to counter brain aging and neurodegenerative diseases. However, few *in vivo* models exist to study engulfment in the brain and characterize this process during aging and across species. Here we present a genetic model for

secretion of a fluorescent protein by neurons in the brain of the African turquoise killifish, the shortest-lived vertebrate that can be bred in captivity. We use this model to identify a population of brain macrophages in the killifish responsible for engulfment of material from the brain extracellular space. Intriguingly, many of these cells bear similarities to mammalian border-associated and monocyte-derived macrophages, rare subsets of macrophages in mouse and human brains noted for their engulfment capabilities. We also find that in our model, killifish brain macrophages decline in engulfment capacity with age. This work highlights how vertebrate brain macrophages, particularly those at brain border regions, can play a critical role in clearance and provides an opportunity to test interventions that can boost engulfment by these macrophages to promote brain resilience in old age and disease.

Introduction

The vertebrate brain uses varied strategies to clear extracellular material such as extracellular matrix and aggregation-prone proteins[1–3]. Engulfment by specialized cells[4–7] – including macrophages such as microglia[8–16] – permits degradation and clearance of extracellular proteins and other macromolecules in the brain. Disruptions in clearance can lead to dysregulated accumulation of extracellular material in the brain interstitial space and cerebrospinal fluid (CSF), with detrimental consequences during aging and in neurodegenerative diseases[17–30]. Thus, clearance mechanisms could represent key strategies for maintaining brain homeostasis, with promising therapeutic potential to counter brain aging and neurodegenerative diseases[31–37]. Studying clearance strategies in varied species could reveal mechanisms not present in mammals and help determine how they could be used to counter brain aging.

An interesting model system in which to study clearance strategies is the African turquoise killifish *Nothobranchius furzeri* – the shortest-lived vertebrate that can be bred in captivity[38]. The killifish has a median lifespan of only six months, 5 times shorter than the mouse[38], enabling scalable studies of processes that are disrupted with age[39–59]. The killifish also recapitulates many conserved hallmarks of brain aging, including neurodegeneration[60–62], cognitive decline[63–65], and behavioral deficits[66]. However, waste clearance in the brain has not been examined in this species. A short-lived vertebrate model in which to study clearance would enable longitudinal studies as well as the identification of interventions that boost clearance in the aged brain.

Here, we present a genetic model for studying clearance of a secreted fluorescent protein in the brain of the killifish. Using this genetic model, we show that a population of macrophages in the killifish brain is responsible for engulfment of diverse extracellular molecules. Intriguingly, we find that many killifish brain macrophages exhibit similarities to mammalian border-associated macrophages (BAMs) and monocyte-derived macrophages (MDMs), which are rare cell types in the adult mammalian brain. We also find that in our model, the engulfment capacity of killifish brain macrophages declines with age, which could contribute to clearance dysregulation and abnormal accumulation of extracellular material in brain aging.

A model for engulfment by vertebrate brain myeloid cells

To model clearance of extracellular proteins in the brain, we engineered a killifish strain using a CRISPR knockin method developed for killifish[67]. In this strain, a secreted form of the red fluorescent protein oScarlet is expressed from one allele of the *ELAVL3* locus, a vertebrate-conserved gene predominantly expressed in neurons[68] (Fig. 1a). We chose oScarlet for visualizing clearance processes due the relatively high stability of mScarlet-derived red fluorescent proteins[69,70]. Importantly, to allow the secretion of oScarlet into the interstitial space, we added a signal peptide (SP, derived from the killifish HSPA5 protein[71]) to the N-terminal region of oScarlet. We also added a P2A self-cleaving peptide to prevent fusion of oScarlet to the ELAVL3 protein[72] (Fig. 1a). We maintained the killifish line at the heterozygous state and refer to it as SP-oScarlet.

We confirmed insertion of the SP-oScarlet knockin construct at the *ELAVL3* locus by PCR and long-read sequencing of the entire locus, which confirmed appropriate junctions with the *ELAVL3* gene and the presence of the SP-oScarlet insertion (Fig. 1 – Fig. Supplement 1a). We noted the

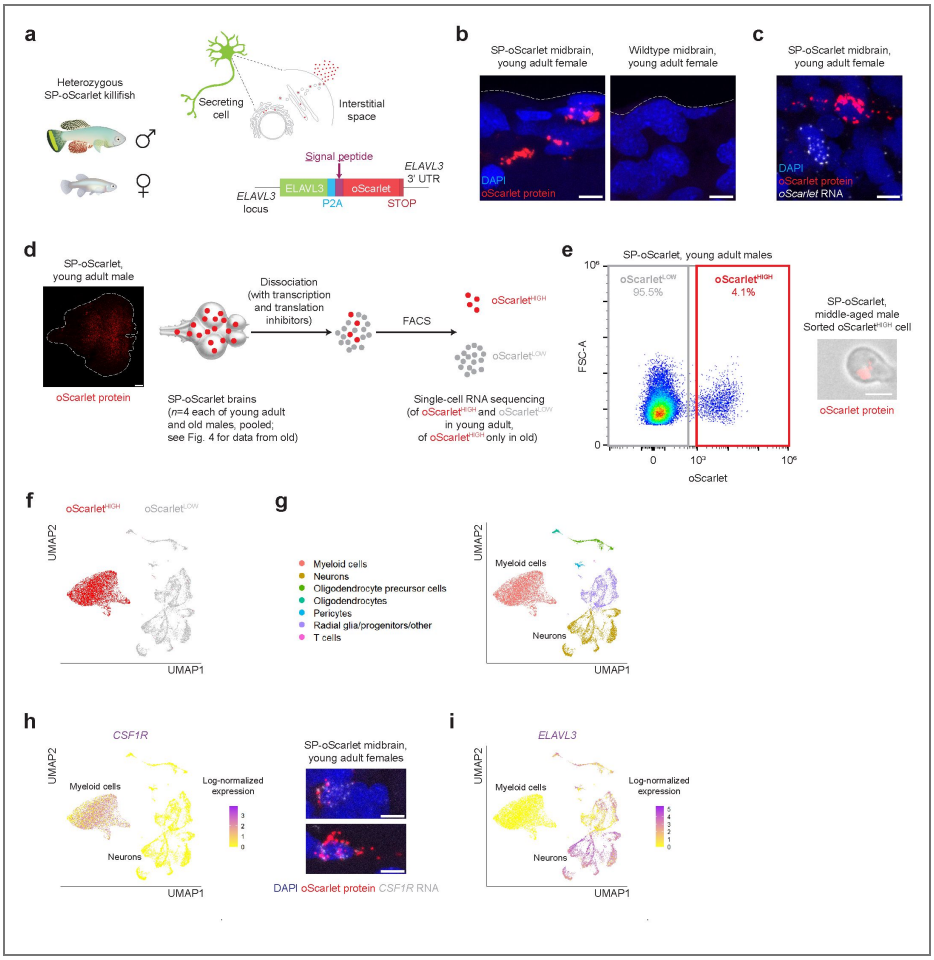

Figure 1. A model for engulfment by vertebrate brain myeloid cells.

a, Schematic for the SP-oScarlet killifish line, which features expression and secretion of a red fluorescent protein, oScarlet, from non-immune cells of the killifish brain using CRISPR knockin at the *ELAVL3* locus. P2A, self-cleaving peptide; UTR, untranslated region. The SP-oScarlet line is maintained in the heterozygous state. Art by Rogelio Barajas (killifish). **b,** Representative images of brain sections from young adult (59 days) female heterozygous SP-oScarlet and young adult (59 days) female wildtype killifish, highlighting oScarlet protein signal (native fluorescence plus anti-mCherry immunofluorescence staining) in the SP-oScarlet brain (representative of n = 13 SP-oScarlet fish over three experiments and n = 3 wildtype fish in one experiment). Scale bars = 5 µm. **c,** Representative image of a young adult (59 days) female heterozygous SP-oScarlet killifish brain section, highlighting oScarlet protein signal (native fluorescence plus anti-mCherry immunofluorescence staining) in a cell that does not express *oScarlet* RNA (representative of n = 10 fish, 59-63 days females, over two experiments). Scale bar = 5 µm. **d,** (Left) 3D image of a cleared (modified Adipo-Clear method) young adult (50 days) male heterozygous SP-oScarlet killifish midbrain/hindbrain, highlighting punctate oScarlet protein signal (native fluorescence plus anti-RFP immunofluorescence staining) (n = 1 fish). (Right) Schematic for single-cell RNA sequencing of cells with and without oScarlet protein signal in young adult (49 days) and old (134 days) male heterozygous SP-oScarlet killifish brains (n = 4 fish, pooled, per age group, in one experiment). For data from old fish and for an independent experiment in old fish, see Fig. 4. **e,** (Left) Fluorescence-activated cell sorting (FACS) plot for young adult pooled brains from experiment in **d**, highlighting oScarlet^{LOW} and oScarlet^{HIGH} cells. Each dot represents one cell. (Right) Image of an oScarlet^{HIGH} cell isolated from a middle-aged (76 days) male heterozygous SP-oScarlet killifish brain by FACS, highlighting oScarlet protein signal (native fluorescence only) (n = 1 fish). Scale bar = 2 µm. **f,** Uniform Manifold Approximation and Projection (UMAP) of 11,503 oScarlet^{LOW} and 9,680 oScarlet^{HIGH} high-quality young adult cells from experiment in **d**. Each dot represents one cell. **g**, UMAP as in **f** colored according to manually annotated cell types, labeled in legend. Each dot represents one cell. **h,** (Left) UMAP as in **f** colored according to log-normalized *CSF1R* (*LOC107387189*) expression. Each dot represents one cell. (Right) Representative images of young adult (59-63 days) female heterozygous SP-oScarlet killifish brain sections, highlighting oScarlet protein signal (native fluorescence plus anti-mCherry immunofluorescence staining) in cells expressing *CSF1R* RNA (representative of n = 10 fish, 59-63 days females, over two experiments). Scale bars = 5 µm. **i,** UMAP as in **f** colored according to log-normalized *ELAVL3* (*LOC107378364*) expression. Each dot represents one cell.

presence of two tandem copies of the SP-oScarlet insertion, although the presence of a stop codon at the C-terminus of oScarlet likely leads to the production of a single oScarlet protein (Fig. 1 – Fig. Supplement 1a).

We verified that *ELAVL3* and *oScarlet* transcripts were expressed in the same cells of SP-oScarlet fish, as expected, using *in situ* hybridization chain reaction (HCR)[73] on adult brain sections (Fig. 1 – Fig. Supplement 1b-c). By immunofluorescence staining for oScarlet, we also observed bright, punctate oScarlet signal in adult SP-oScarlet brains (Fig. 1b, Fig. 1 – Fig. Supplement 1d). Using HCR on brain sections, we verified the presence of cells with bright oScarlet protein signal (oScarlet^{HIGH}) that did not express *oScarlet* transcripts in the brains of SP-oScarlet fish (Fig. 1c, Fig. 1 – Fig. Supplement 1d). This suggests that the oScarlet protein is efficiently secreted from the neurons that express the *oScarlet* transcript, resulting in oScarlet protein that is likely engulfed by other cell types in the brain. Thus, the bright oScarlet puncta in the brains of SP-oScarlet fish can be found within cells that likely engulf, and do not produce, this protein.

To identify the cells that engulf oScarlet, we developed a flow cytometry strategy to distinguish cells with bright oScarlet protein signal (oScarlet^{HIGH}) from other cells in the adult brain (oScarlet^{LOW}) (Fig. 1d-e, Fig. 1 – Fig. Supplement 1e). We isolated oScarlet^{HIGH} cells from adult SP-oScarlet brains (Fig. 1e), and we verified that these cells were not present in the brains of wildtype killifish, even at older ages where more autofluorescent cells might be expected (Fig. 1 – Fig. Supplement 1f).

To unbiasedly characterize oScarlet^{HIGH} cells, we performed single-cell RNA sequencing on enriched oScarlet^{HIGH} cells FACS-isolated from the brains of young adult (49 days) and old (134 days) male SP-oScarlet killifish (n = 4 fish per age group, pooled), as well as oScarlet^{LOW} cells isolated from the young adult fish. We used transcription and translation inhibitors to minimize gene expression changes due to dissociation, as done in studies of mammalian brain macrophages[74–76]. We performed Uniform Manifold Approximation and Projection (UMAP)[77] analysis of the single-cell RNA sequencing data from young adult animals (for analysis of the old dataset, see Fig. 4). This analysis revealed that most oScarlet^{HIGH} cells were transcriptionally distinct from their oScarlet^{LOW} counterparts (Fig. 1f).

By manually annotating cell types based on matching top UMAP cluster marker genes (Fig. 1 – Fig. Supplement 2a-b) to cell type markers known from literature in mammals, zebrafish, and killifish[68,78–80], we identified the vast majority (99.6%) of oScarlet^{HIGH} cells as myeloid immune cells (Fig. 1g).

oScarlet^{LOW} cells included neurons, oligodendroglia, radial glia and progenitors, pericytes, and T cells (Fig. 1g). We noted that endothelial cells were not well represented in our dataset, possibly due to our use of dissociation and FACS in our workflow. Only a very small percentage (0.5%) of oScarlet^{LOW} cells were myeloid cells, indicating that most myeloid cells likely engulfed oScarlet (Fig. 1g).

We could confirm by HCR on brain sections *in situ* that oScarlet^{HIGH} cells expressed a homolog of the conserved myeloid marker *CSF1R*[81,82] (Fig. 1h). We also verified that oScarlet^{HIGH} cells largely did not express *ELAVL3*, the driver for *oScarlet* expression (Fig. 1i).

Collectively, these data show that most oScarlet^{HIGH} cells are myeloid cells that have likely engulfed secreted oScarlet protein in the brains of SP-oScarlet fish. Thus, we have generated a genetic model for chronic engulfment by brain myeloid cells in a short-lived vertebrate.

The killifish brain includes a population of macrophages with transcriptional similarities to mammalian monocyte-derived macrophages

What type of myeloid cells engulf oScarlet in the killifish brain? Analysis of our single-cell RNA sequencing data indicated that oScarlet^{HIGH} cells are likely macrophages. Indeed, in addition to *CSF1R*, oScarlet^{HIGH} cells were enriched for *APOEB* (a homolog of human *APOE*) as well as antigen presentation-associated (e.g., *HLA-DPB1*, *CD74*), complement-associated (e.g., *C1QC*, *C1QA*), and

scavenger receptor-encoding (e.g., *MRC1*, *MARCO*) genes (Fig. 2a). Moreover, by analyzing gene signatures from our single cell RNA sequencing dataset, we found that oScarlet^{HIGH} cells were enriched for signatures characteristic of macrophage functions, such as endocytosis-related and lysosomal genes (Fig. 2b). We also observed punctate oScarlet protein signal in proximity to late endosomes and lysosomes (marked by the protein marker LAMP1) by immunofluorescence staining (Fig. 2 – Fig. Supplement 1a), consistent with endocytosis and attempted degradation of extracellular material by macrophages. mScarlet, from which oScarlet is derived[70], is known to be relatively stable at the acidic lysosomal pH[69], which could explain the persistence of oScarlet signal in cells that engulf the protein.

In the mammalian brain, most macrophages fall into one of three main classes[75,83]: parenchymal microglia (derived from the embryonic yolk sac), and two classes of macrophages found at interfaces between the brain and periphery (blood vessels, meninges, and choroid plexus) – border-associated macrophages (BAMs) (also derived from the embryonic yolk sac), and monocyte-derived macrophages (MDMs) (of peripheral, hematopoietic origin)[84–93]. BAMs and MDMs can strongly engulf substrates from the CSF[10], with BAMs noted for their exceptional endocytic capacity[75].

Using principal component analysis (PCA) with marker genes, mouse brain macrophages from a dataset from Barr et al.[75] could be clearly transcriptionally separated into microglia, BAMs, and MDMs (Fig. 2c, Fig. 2 – Fig. Supplement 1b). In contrast, using principal component analysis with killifish homologs of the same marker genes, oScarlet^{HIGH} cells from SP-oScarlet killifish could not be transcriptionally separated into these classes (Fig. 2c, Fig. 2 – Fig. Supplement 1b). Consistent with this finding, wildtype killifish forebrain macrophages (i.e., cells from an *APOEB+ IBA1+ LCP1+* cluster, originally annotated as “Microglia”) from an independent dataset from Ayana et al.[68] could not be transcriptionally separated into microglia, BAMs, and MDMs in the same analysis (Fig. 2c, Fig. 2 – Fig. Supplement 1b). Thus, we did not find evidence for the existence of transcriptionally distinct microglia, BAMs, and MDMs in killifish brains, possibly suggesting a more plastic population of brain macrophages in the killifish.

Killifish homologs of many of the strongest markers of mouse microglia, BAMs, and MDMs were not detected in killifish brain macrophages, while some killifish brain macrophage markers (e.g., *CLDN5*) were not detected in mouse brain macrophages (Fig. 2a, Fig. 2d, Fig. 2 – Fig. Supplement 2a, Fig. 2 – Fig. Supplement 3a, Fig. 2 – Fig. Supplement 4a).

Nonetheless, the expression profile of oScarlet^{HIGH} cells overlapped most with that of mouse MDMs (Fig. 2d, Fig. 2 – Fig. Supplement 2a, Fig. 2 – Fig. Supplement 3a). Similar expression of key MDM markers was observed in many wildtype macrophages in the Ayana et al. dataset (Fig. 2d, Fig. 2 – Fig. Supplement 2a, Fig. 2 – Fig. Supplement 4a). Hence, the adult killifish brain includes a population of macrophages with some transcriptional similarities to mammalian monocyte-derived macrophages (consistent with studies in zebrafish[80,94,95]).

Macrophages in the killifish brain are endocytic and present at brain borders

To functionally test whether oScarlet^{HIGH} cells have *in vivo* engulfment capabilities like mammalian BAMs and MDMs, we injected the macromolecule dextran (a 70 kDa polysaccharide, conjugated to a fluorophore) into the brains of young adult to middle-aged (63-91 days) female SP-oScarlet animals (Fig. 3a). We aimed our injection for the brain ventricle to maximize dextran distribution via the CSF[96]. In mice, similar approaches have been shown to result in engulfment of fluorescently-tagged substrates by BAMs and MDMs, and less so by microglia[10,97,98].

We performed HCR and immunofluorescence staining on brain sections of fish one day post-injection. Cells with bright oScarlet protein signal were enriched for dextran engulfment, as well as for expression of *APOEB*, as predicted by our single-cell RNA sequencing data ($p = 0.031$ for each, paired Wilcoxon test) (Fig. 3a, Fig. 3 – Fig. Supplement 1a). We verified that the colocalization seen between dextran and oScarlet signal (Fig. 3a) was not a result of bleed-through or autofluorescence (Fig. 3 – Fig. Supplement 1b-c) and likely resulted from these

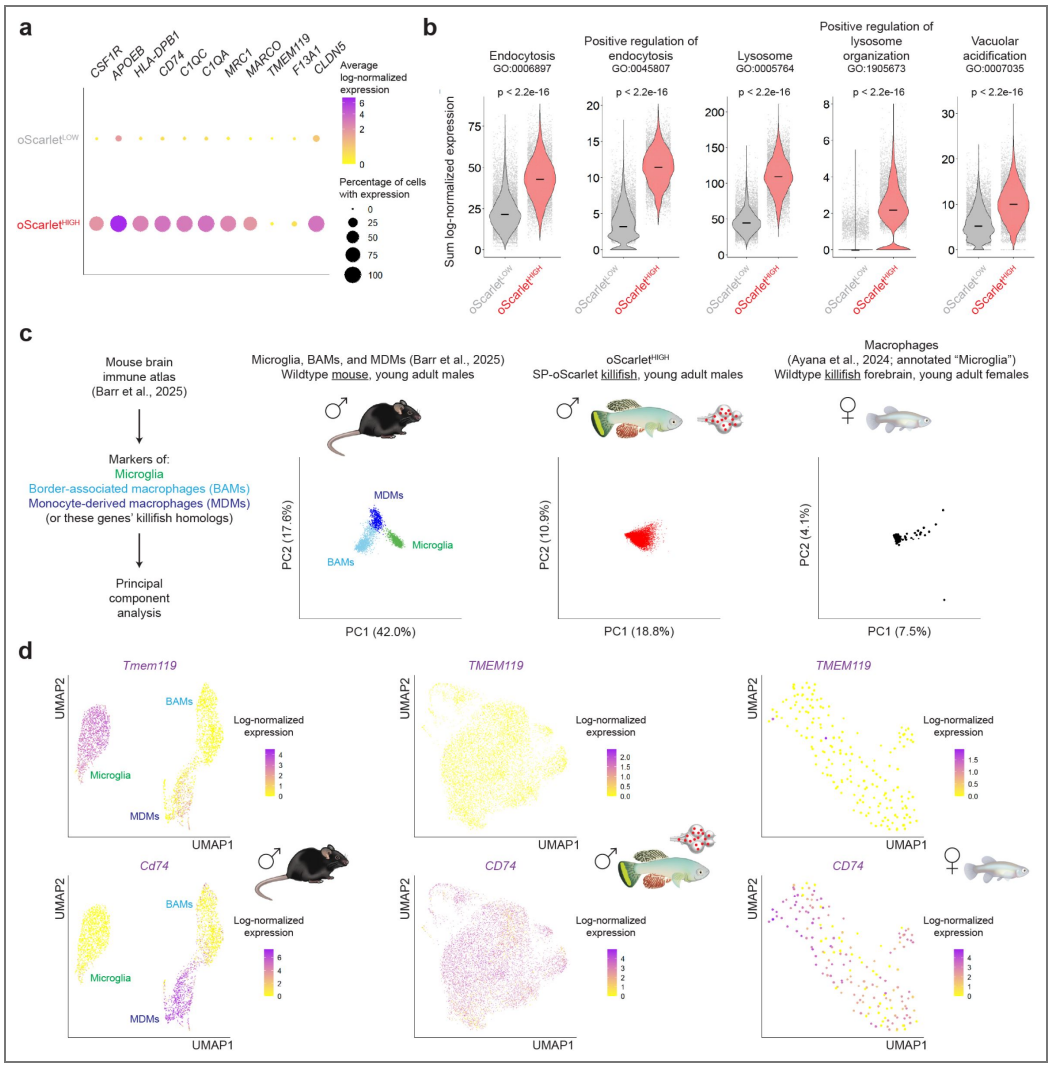

Figure 2. The killifish brain includes a population of macrophages with transcriptional similarities to mammalian monocyte-derived macrophages.

a, Dotplot highlighting expression of selected genes (*CSF1R* (*LOC107387189*), *APOEB* (*LOC10737395*), *HLA-DPB1* (*LOC107372638*), *CD74* (*LOC107375728*), *C1QC* (*LOC107385068*), *C1QA* (*LOC107385067*), *MRC1* (*LOC107383768*), *MARCO* (*LOC107390282*), *TMEM119* (*LOC107393987*), *F13A1* (*LOC107377057*), and *CLDN5* (*LOC107394244*)) in young adult oScarlet^{LOW} and oScarlet^{HIGH} cells from experiment in **1d**. The color of each circle corresponds to average log-normalized expression among cells with detectable expression of the respective gene. The size of each circle corresponds to percentage of cells in each population with detectable expression of the gene. **b,** Violin plots for sum log-normalized expression of genes in Gene Ontology: Biological Process terms "endocytosis" (GO:0006897), "positive regulation of endocytosis" (GO:0045807), "lysosome" (GO:0005764), "positive regulation of lysosome organization" (GO:1905673), and "vacuolar acidification" (GO:0007035) in young adult oScarlet^{LOW} and oScarlet^{HIGH} cells from experiment in **1d**. Each dot represents one cell. Lines: medians; p-values, unpaired Wilcoxon rank-sum test at per-cell level (fish were pooled for single cell RNA-sequencing experiments to obtain sufficient numbers of oScarlet^{HIGH} cells). **c,** Principal component analysis (PCA) plots (principal components 1 vs. 2) of wildtype young adult mouse microglia, border-associated macrophages (BAMs), and monocyte-derived macrophages (MDMs) (Barr et al., 2025[75]; 3,230 high-quality cells from clusters manually annotated by Barr et al.), young adult oScarlet^{HIGH} cells from experiment in **1d**, and wildtype young adult killifish forebrain macrophages (Ayana et al., 2024[68]; 176 high-quality cells from *APOEB+ IBA1+ LCP1+* cluster) using marker genes of microglia, BAMs, and MDMs from the Barr et al. dataset, or all killifish homologs of these genes. Each dot represents one cell. Percentages on axes represent the percentage of variance explained by each respective principal component. Art by Rogelio Barajas. **d,** UMAPs of wildtype young adult mouse brain macrophages (Barr et al., 2025[75]; 3,488 high-quality cells from clusters manually annotated by Barr et al.), young adult oScarlet^{HIGH} cells from experiment in **1d**, and wildtype young adult killifish forebrain macrophages (Ayana et al., 2024[68]) colored according to log-normalized *Tmem119* (or killifish homolog *TMEM119* (*LOC107393987*)) or *CD74* (or killifish homolog *CD74* (*LOC107375728*)). Each dot represents one cell.

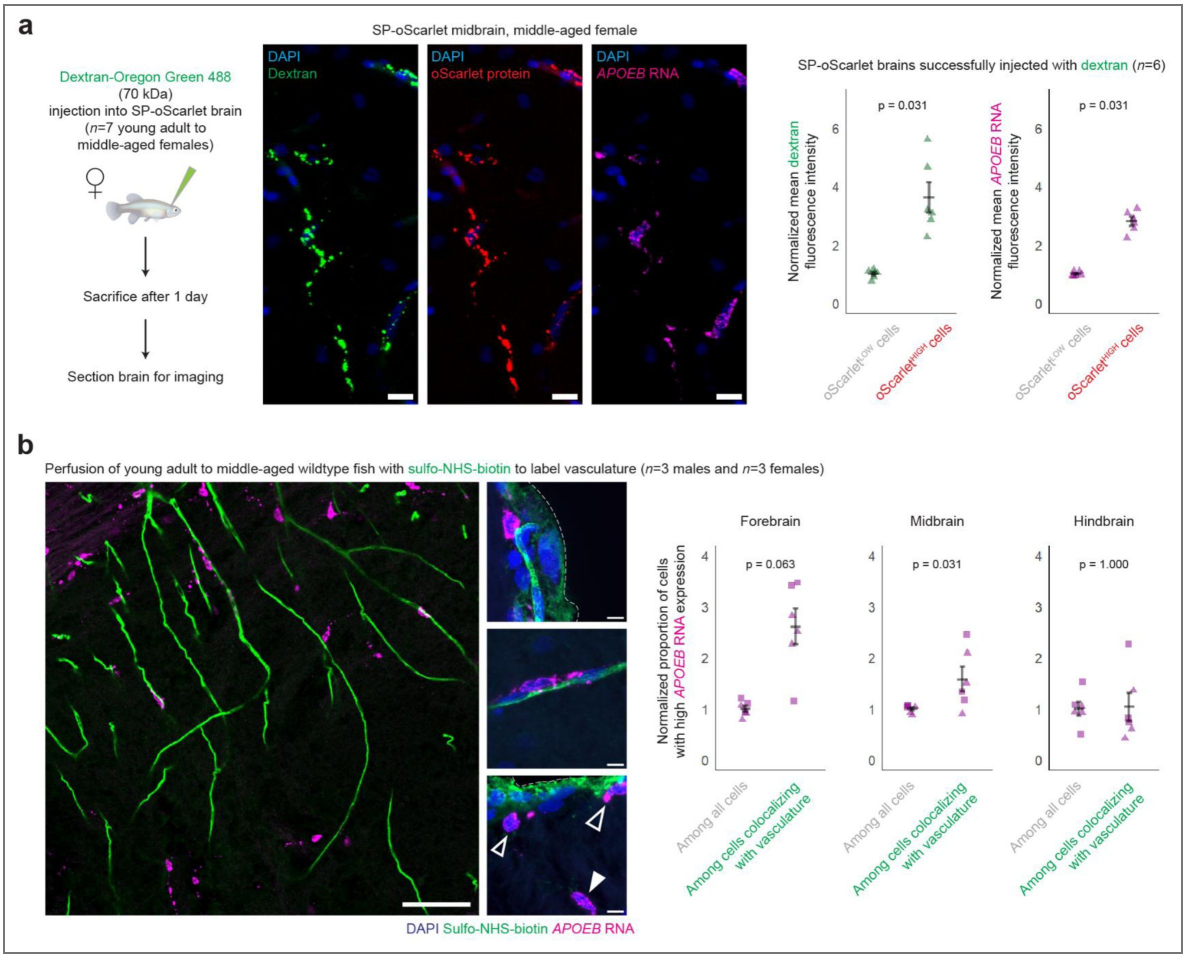

Figure 3. Macrophages in the killifish brain are endocytic and present at brain borders.

a, (Left) Schematic for injection of dextran-Oregon Green 488 (70 kDa) into the brains of young adult to middle-aged (63-91 days) female heterozygous SP-oScarlet killifish (n = 7 fish over two experiments). (Center) Representative images of middle-aged (91 days) female heterozygous SP-oScarlet killifish brain sections highlighting co-occurrence of injected dextran signal, oScarlet protein signal (native fluorescence plus anti-mCherry immunofluorescence staining), and *APOEB* RNA in the same cells. Scale bars = 10 μm. (Right) Quantification of mean dextran fluorescence intensity and mean *APOEB* RNA fluorescence intensity in oScarlet^{LOW} and oScarlet^{HIGH} cells (n = 6 successfully injected fish, 63-91 days females, with 5-6 regions of interest over 1-2 sagittal brain sections per fish, over two experiments). Four images (one image per fish for each of four fish) of regions of interest with a visually apparent very high density of cells with high *APOEB* RNA expression, which could plausibly reflect an injection-related injury, were excluded from quantifications. The excluded images are listed in Supplementary Table 4. Each triangle represents one fish. Mean +/-standard error of mean; p-values, paired Wilcoxon rank-sum test at per-animal level. **b,** (Left) Representative images of young adult to middle-aged (74-101 days) male and female wildtype killifish brain sections, highlighting cells with high *APOEB* RNA expression that do and do not colocalize with vasculature as labeled by perfused sulfo-NHS-biotin (representative of n = 6 fish, 3 males, 74-101 days, and 3 females, 74-101 days, over two experiments). Scale bars = 50 μm (leftmost image), 5 μm (all others). Dashed lines: brain outside border. (In bottom right image) Filled arrows: example of cell with high *APOEB* RNA expression that does not colocalize with vasculature or other brain borders. Unfilled arrows: examples of cells with high *APOEB* RNA expression that are found near brain borders. (Right) Quantification of proportion of cells with high *APOEB* RNA expression among all cells and among cells colocalizing with vasculature, as defined by centroid-centroid distance to nearest sulfo-NHS-biotin-positive cell, in forebrain, midbrain, and hindbrain regions imaged (n = 6 fish, 74-101 days, with 1-2 regions of interest per brain region over 1-2 sagittal brain sections per fish, over two experiments). Regions of interest imaged generally avoided brain outside borders due to very high brightness of sulfo-NHS-biotin signal at some parts of brain outside borders, which could bias quantification. Each square (male) or triangle (female) represents one fish.

substrates being localized to the same endosomes and lysosomes. Collectively, these data show that killifish brain macrophages can engulf diverse extracellular substrates (protein, polysaccharide) (see Fig. 5 for additional, *ex vivo* engulfment assays).

As noted above, in mammals, engulfment of substrates injected into the brain ventricles is a distinguishing functional characteristic of BAMs and MDMs, consistent with their localization at brain borders exposed to CSF flow[10,11]. To determine the spatial localization of killifish brain macrophages, we perfused young adult to middle-aged (74-101 days) male and female wildtype killifish with sulfo-NHS-biotin to label vasculature[99] and performed HCR on brain sections for *APOEB*. We observed cells with high *APOEB* expression adjacent to (and on the parenchymal-facing side of, not within) vasculature in wildtype killifish brains, both near the brain's external borders and within the brain interior (Fig. 3b). While we also observed some cells with high *APOEB* expression within the parenchyma, away from any detectable vasculature or other brain border, the distribution of cells with high *APOEB* expression was enriched toward sulfo-NHS-biotin-labeled vasculature in some brain regions (Fig. 3b, see Source Data Table 5 for additional metrics of colocalization with vasculature).

Thus, we have identified a population of macrophages in the killifish brain with several characteristics of mammalian BAMs and MDMs – expressing several markers associated with brain macrophages including complement components and scavenger receptors, exhibiting endocytic functions, and being at least in part localized near brain borders.

Killifish brain macrophages change transcriptionally with age in our model

We leveraged the killifish's short lifespan to characterize brain macrophages with aging. We first used single-cell RNA sequencing to characterize oScarlet^{HIGH} cells from old SP-oScarlet killifish (same experiment as described in Fig. 1d). By performing UMAP analysis of oScarlet^{HIGH} cells from young adult and old SP-oScarlet brains, we found evidence of transcriptional differences between young adult and old oScarlet^{HIGH} cells (Fig. 4a). We found that oScarlet^{HIGH} cells from old brains were also predominantly macrophages, expressing markers (*CSF1R*, *APOEB*, *HLA-DPB1*, *C1QC*, *MRC1*) at similar levels to young adult oScarlet^{HIGH} cells (Fig. 4b).

What transcriptional pathways in these killifish brain macrophages are impacted during aging? Gene ontology (GO) analysis showed an upregulation of translation-related pathways with age in oScarlet^{HIGH} cells (Fig. 4c-d). GO analysis also identified a modest downregulation in vacuolar acidification with age (Fig. 4c-d). Analysis of specific pathways relevant to engulfment and endolysosomal functions showed that these were also modestly decreased during aging (Fig. 4 – Fig. Supplement 1a). Inflammation-related genes were not strongly upregulated with age in oScarlet^{HIGH} cells (Fig. 4 – Fig. Supplement 1b), unlike in brain macrophage populations described in mammals[75,79,100,101].

Could some of the transcriptional responses observed with age be due to the lifelong, chronic engulfment of oScarlet, particularly given the relative resistance of oScarlet to rapid degradation? To address this possibility, we performed an independent single-cell RNA sequencing experiment of oScarlet^{HIGH} cells FACS-sorted from the brains of old (130 days) SP-oScarlet male animals (n = 3 fish, pooled), as well all Live cells FACS-sorted from the brains of old (122 days) wildtype male brains (n = 3 fish, pooled) (Fig. 4e). We subset each population to macrophages (i.e., cells from *APOEB+ IBA1+ LCP1+* clusters).

We found that neither old oScarlet^{HIGH} nor old wildtype macrophages could be transcriptionally separated into microglia, BAMs, and MDMs (Fig. 4f, Fig. 4 – Fig. Supplement 1c). When comparing old oScarlet^{HIGH} macrophages to old wildtype macrophages, we found that these populations expressed marker genes (*CSF1R*, *APOEB*, *HLA-DPB1*, *C1QC*, *MRC1*) at similar levels (Fig. 4g-h).

GO analysis showed that translation-related pathways were enriched in old oScarlet^{HIGH} macrophages compared to wildtype macrophages (Fig. 4i, Fig. 4 – Fig. Supplement 1d).

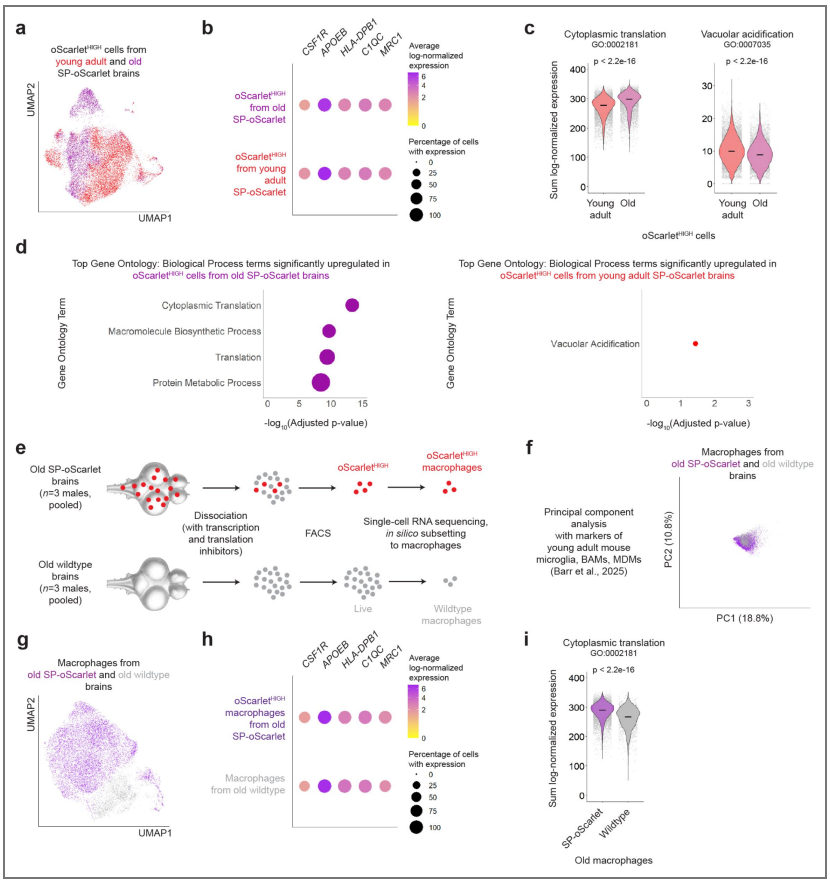

Figure 4. Killifish brain macrophages change transcriptionally with age in our model.

a, UMAP of 6,489 oScarlet^{HIGH} high-quality cells from old (134 days) male heterozygous SP-oScarlet brains (n = 4 fish, pooled, in one experiment), as well as 9,680 young adult oScarlet^{HIGH} high-quality cells from experiment in **1d** (same experiment). **b,** Dotplot highlighting expression of selected homologs of mammalian brain macrophage marker genes (*CSF1R* (*LOC107387189*), *APOEB* (*LOC10737395*), *HLA-DPB1* (*LOC107372638*), *C1QC* (*LOC107385068*), and *MRC1* (*LOC107383768*)) in old and young adult oScarlet^{HIGH} cells from experiment in **1d**. The color of each circle corresponds to average log-normalized expression among cells with detectable expression of the respective gene. The size of each circle corresponds to percentage of cells in each population with detectable expression of the gene. **c,** Violin plots for sum log-normalized expression of genes in Gene Ontology: Biological Process terms "cytoplasmic translation" (GO:0002181) and "vacuolar acidification" (GO: 0007035) in young adult and old oScarlet^{HIGH} cells from experiment in **1d**. Each dot represents one cell. Lines: medians; p-values, unpaired Wilcoxon rank-sum test at per-cell level. **d**, Top Gene Ontology: Biological Process terms upregulated in old (left) and young adult (right) oScarlet^{HIGH} cells from experiment in **1d**, as ranked by adjusted p-value (Fisher's exact test, Benjamini-Hochberg false discovery rate (FDR)-corrected). Size of each circle corresponds to number of distinct human homologs among differentially expressed genes from each term. Full lists of differentially expressed genes and upregulated terms in Supplementary Tables 9-11. **e,** Schematic for single-cell RNA sequencing of oScarlet^{HIGH} cells from old (130 days) male heterozygous SP-oScarlet killifish brains and all Live cells from old (122 days) male wildtype killifish brains (n = 3 fish per genotype, pooled in one experiment; for an independent experiment involving old SP-oScarlet fish, see **1d**). **f**, PCA plot (principal components 1 vs. 2) of oScarlet^{HIGH} and wildtype old killifish brain macrophages from experiment in **e** using all killifish homologs of marker genes of microglia, BAMs, and MDMs (Barr et al., 2025[75]). Each dot represents one cell. Percentages on axes represent the percentage of variance explained by each respective principal component. **g,** UMAP of 12,575 old oScarlet^{HIGH} and old wildtype macrophages, as defined by *APOEB+ IBA1+ LCP1+* clusters among all cells from experiment in **e** (resolution = 0.2). Each dot represents one cell. **h,** Dotplot highlighting expression of selected homologs of mammalian brain macrophage marker genes (*CSF1R* (*LOC107387189*), *APOEB* (*LOC10737395*), *HLA-DPB1* (*LOC107372638*), *C1QC* (*LOC107385068*), and *MRC1* (*LOC107383768*)) in old oScarlet^{HIGH} and old wildtype macrophages from experiment in **e**. The color of each circle corresponds to average log-normalized expression among cells with detectable expression of the respective gene. The size of each circle corresponds to percentage of cells in each population with detectable expression of the gene. **i,** Violin plot for sum log-normalized expression of genes in Gene Ontology: Biological Process term "cytoplasmic translation" (GO:0002181) in old oScarlet^{HIGH} and old wildtype macrophages from experiment in **e**. Each dot represents one cell. Lines: medians; p-values, unpaired Wilcoxon rank-sum test at per-cell level.

Some inflammation- and pathogen-response-related pathways were mildly depleted in old oScarlet^{HIGH} macrophages compared to old wildtype macrophages (Fig. 4 – Fig. Supplement 1d). The engulfment-related pathways examined showed no consistent directional pattern when comparing old oScarlet^{HIGH} to old wildtype macrophages (Fig. 4 – Fig. Supplement 1e). These results suggest that the translation-related changes observed with age in oScarlet^{HIGH} cells may reflect a response to lifelong oScarlet exposure, rather than to aging *per se*. In contrast, changes in engulfment-related pathways are unlikely to be solely driven by lifelong, chronic oScarlet exposure.

Overall, our single-cell RNA sequencing results indicate that killifish brain macrophages in SP-oScarlet animals experience notable transcriptional changes with age, with translation-related genes increasing in expression with age (possibly as part of a response to chronic oScarlet engulfment) and some engulfment-relevant (vacuolar acidification) genes decreasing in expression with age.

Engulfment capacity of killifish brain macrophages declines with age in our model

We next functionally characterized killifish brain macrophages with age, using oScarlet^{HIGH} status as a proxy for macrophage identity – as supported by our single-cell RNA sequencing data – given the lack of antibodies and reporter lines in killifish to otherwise identify these cells. By performing flow cytometry on the brains of young adult (41-63 days) and old (148-167 days) male and female SP-oScarlet killifish (n = 6 fish per age group and per sex), we noted a decline with age in the oScarlet fluorescence intensity of oScarlet^{HIGH} cells in both males and females (p = 0.002 for each sex, unpaired Wilcoxon test) (Fig. 5a, Fig. 5 – Fig. Supplement 1a). These observations are consistent with the possibility that aging is accompanied by a potential decline in engulfment by brain macrophages, though the decline in oScarlet brightness in old oScarlet^{HIGH} cells could also be due to changes in oScarlet expression, secretion, or degradation, especially given that *ELAVL3* gene expression has been shown to decrease with age in the killifish brain (Fig. 5 – Fig. Supplement 1b)[55].

To assess more directly if the engulfment capacity of brain macrophages changes with age, we developed an acute *ex vivo* assay in the context of SP-oScarlet animals. In this assay, macromolecule substrates such as ovalbumin (a 45 kDa protein) and dextran (a 70 kDa polysaccharide) (conjugated to far-red and green fluorophores, respectively) were mixed *ex vivo* with brain cells during the 30 minutes of tissue dissociation[75], followed by flow cytometry to quantify fluorescent substrate engulfment by cells (Fig. 5b). Using this assay, we verified that oScarlet^{HIGH} cells from young adult SP-oScarlet brains were enriched for their ability to rapidly engulf ovalbumin compared to oScarlet^{LOW} cells (p = 0.031 for each sex, paired Wilcoxon test) (Fig. 5c, see Fig. 5 – Fig. Supplement 1c for additional metrics of engulfment).

We used this *ex vivo* engulfment assay to examine ovalbumin engulfment differences with age among oScarlet^{HIGH} cells in both males and females (n = 6 fish per age and per sex). Crucially, we showed that oScarlet^{HIGH} cells in old brains showed a decreased capacity to engulf ovalbumin compared their counterpart cells in young adult brains, in both males (p = 0.002, unpaired Wilcoxon test) and females (p = 0.009, unpaired Wilcoxon test) (Fig. 5d). Fewer old oScarlet^{HIGH} cells engulfed ovalbumin, and those that did showed reduced ovalbumin brightness compared to young adult oScarlet^{HIGH} cells that engulfed ovalbumin (Fig. 5 – Fig. Supplement 1d, see Fig. 5 – Fig. Supplement 2a-c for alternative gating schemes).

In a separate experiment, we also performed this *ex vivo* engulfment assay using dextran as a substrate (n = 4 male fish per age) and verified that oScarlet^{HIGH} cells from young adult (56 days) male SP-oScarlet brains also showed a trending, non-significant increased capacity to rapidly engulf dextran compared to oScarlet^{LOW} cells (p = 0.125, unpaired Wilcoxon test) (Fig. 5e, see Fig. 5 – Fig. Supplement 1e for additional metrics of engulfment). oScarlet^{HIGH} cells in old (156 days) male brains also showed a trending, non-significant decreased capacity to engulf dextran compared their counterpart cells in young adult brains (p = 0.057, unpaired Wilcoxon test) (Fig.

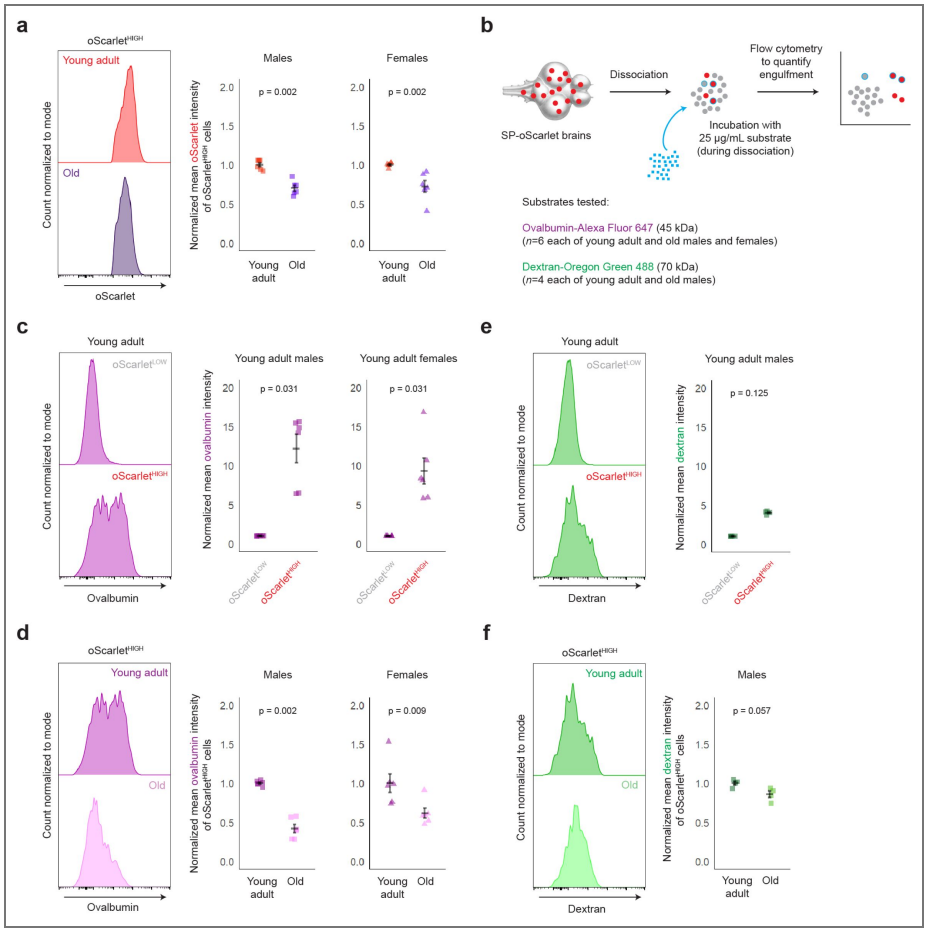

Figure 5. Engulfment capacity of killifish brain macrophages declines with age in our model.

a, (Left) Representative flow cytometry histograms from young adult (41 days, above) and old (160 days, below) male heterozygous SP-oScarlet killifish brains, highlighting mean oScarlet fluorescence intensity in oScarlet^{HIGH} cells. (Right) Quantification of mean oScarlet fluorescence intensity among young adult and old oScarlet^{HIGH} cells (n = 6 fish per age per sex, over two experiments per sex; young adult males: 41-63 days; old males: 148-160 days; young adult females: 57-63 days; old females: 161-167 days). Each square (male) or triangle (female) represents one fish. Mean +/- standard error of mean; p-values, unpaired Wilcoxon rank-sum test at per-animal level. **b,** Schematic for *ex vivo* engulfment assays performed on young adult and old heterozygous SP-oScarlet killifish brains (for ovalbumin-Alexa Fluor® 647: n = 6 fish per age and sex, over two experiments per sex; young adult males: 41-63 days; old males: 148-160 days; young adult females: 57-63 days; old females: 161-167 days; for dextran-Oregon Green 488 (70 kDa): n = 4 male fish per age in one experiment; young adult: 56 days; old: 156 days). **c,** (Left) Representative flow cytometry histograms from young adult (41 days) male heterozygous SP-oScarlet killifish brains, highlighting mean ovalbumin fluorescence intensity in oScarlet^{LOW} and oScarlet^{HIGH} cells. (Right) Quantification of mean ovalbumin fluorescence intensity among young adult oScarlet^{LOW} and oScarlet^{HIGH} cells (same experiments as in **a**). Each square (male) or triangle (female) represents one fish. Mean +/- standard error of mean; p-values, paired Wilcoxon rank-sum test at per-animal level. **d,** (Left) Representative flow cytometry histograms from young adult (41 days) (above) and old (160 days) (below) male heterozygous SP-oScarlet killifish brains, highlighting mean ovalbumin fluorescence intensity in oScarlet^{HIGH} cells. (Right) Quantification of mean ovalbumin fluorescence intensity among young adult and old oScarlet^{HIGH} cells (same experiments as in **a**). Each square (male) or triangle (female) represents one fish. Mean +/- standard error of mean; p-values, unpaired Wilcoxon rank-sum test at per-animal level. **e,** (Left) Representative flow cytometry histograms from young adult (56 days) male heterozygous SP-oScarlet killifish brains, highlighting mean dextran fluorescence intensity in oScarlet^{LOW} and oScarlet^{HIGH} cells. (Right) Quantification of mean dextran fluorescence intensity among young adult oScarlet^{LOW} and oScarlet^{HIGH} cells. Each square represents one fish. Mean +/- standard error of mean; p-values, paired Wilcoxon rank-sum test at per-animal level. **f,** (Left) Representative flow cytometry histograms from young adult (56 days) (above) and old (156 days) (below) male heterozygous SP-oScarlet killifish brains, highlighting mean dextran fluorescence intensity in oScarlet^{HIGH} cells. Each dot represents one cell. (Right) Quantification of mean dextran fluorescence intensity among young adult and old oScarlet^{HIGH} cells (same experiment as in **e**). Each square represents one fish. Mean +/- standard error of mean; p-values, unpaired Wilcoxon rank-sum test at per-animal level.

5f). Fewer old oScarlet^{HIGH} cells engulfed dextran, and those that did showed reduced dextran brightness compared to young adult oScarlet^{HIGH} cells that engulfed dextran (Fig. 5 – Fig. Supplement 1f, see Fig. 5 – Fig. Supplement 2d-e for alternative gating schemes).

Collectively, these data suggest that brain macrophages in killifish exhibit a functional decline in engulfment capacity with age.

Discussion

In this study, we generated a genetically modified killifish line to investigate engulfment of a secreted protein in the vertebrate brain, providing a model to study clearance. Using the secreted red fluorescent protein oScarlet as a model extracellular protein (here secreted principally from neurons), we found that a macrophage population in the adult killifish brain exhibits a high engulfment capacity. Our *in vivo* genetic model could be used to study secretion and engulfment in the vertebrate brain, help elucidate functional roles of brain macrophages, and identify interventions that boost engulfment in the aged or diseased brain. We note that some limitations of this genetic model include that oScarlet is expressed constitutively and is relatively resistant to degradation, precluding acute examination of oScarlet engulfment and potentially even affecting the state of cells that engulf oScarlet. We therefore developed additional methods in this study to assess acute engulfment with other substrates both *in vivo* and *ex vivo* in the killifish brain. Together, these tools in killifish complement recent approaches to study engulfment in mouse brains[10,75], and they provide a resource to understand the functions of brain macrophages in a short-lived vertebrate.

We found that many killifish brain macrophages display similarities to border-associated macrophages (BAMs) and monocyte-derived macrophages (MDMs), known engulfment-capable macrophage populations in mammalian central nervous systems[10,75,76,89,102–115]. These similarities include: expression of marker genes such as scavenger receptors, localization to brain border regions, and functional enrichment for engulfment capacity for several substrates (the protein oScarlet *in vivo*, the polysaccharide dextran *in vivo* and the protein ovalbumin and polysaccharide dextran *ex vivo*). Our findings suggest that the adult killifish brain – in contrast to the mouse brain[102] – represents a system where the need for waste clearance may be addressed by relatively abundant cells with characteristics of BAMs and MDMs, parallel to findings from adult zebrafish brains[80,94,95]. This potential evolutionary difference is intriguing and could be due to differences in myelination[116–118], neurogenesis[119–121], or demands for pathogen response[122,123] or immune regulation[124] between fish and mammals or between aquatic and terrestrial environments. These observations also suggest there may be more plasticity among fish brain macrophages than previously anticipated. Understanding how macrophages other than microglia perform brain clearance in species where they are abundant could provide new avenues to promote clearance in mammals.

We showed that in our model, killifish brain macrophages decline in engulfment capacity with age. This is in line with recent mammalian studies highlighting that BAMs and MDMs, despite being rare populations in the mammalian brain, play key functional roles but experience alterations with age and under pathological conditions[10,11,75,97,98,100,125–167]. Thus, BAMs and MDMs could represent promising avenues for therapeutic intervention in age-associated and other brain diseases. In mammalian BAMs, decline in engulfment with age has been linked to decreased expression of clathrin-mediated endocytosis receptors[75]. While similar transcriptional changes with age were not observed in our single-cell RNA sequencing datasets, key endocytic machinery in the killifish brain may be regulated at the level of translation (which has been shown to decrease globally with age in the killifish brain[54]), or at a post-translational level (e.g., decreased efficiency of proton pumping to acidify lysosomes[168]), resulting in an evolutionarily conserved decline in scavenging capacity with age.

Overall, our findings highlight the underappreciated role that engulfment by macrophages, particularly those at brain borders, could play in critical waste clearance processes in the brain. This study also underscores the potential of the killifish as a powerful vertebrate model to

investigate questions relevant to aging, disease, and evolution of the complex and specialized cell types of the vertebrate brain.

Methods

Killifish husbandry

The short-lived *Nothobranchius furzeri* GRZ strain[38] was used as the background killifish strain in this study. Fish were maintained using an Aquaneering recirculating aquatic system at a temperature of ~27°C, pH of 7-7.5, conductivity of 1200 µS with a 12 hour/12 hour light/dark cycle with the light on between ~7 a.m. and ~7 p.m. For the first 1 month of life, fish were fed live brine shrimp (Brine Shrimp Direct, BSEP6LB). Brine shrimp feeding solution was generated by mixing 50 mL of brine eggs hatched over 48 hours at ~27°C in a cone with 10 L reverse osmosis (RO) water and 1.5 cups salt (approximately 350 mL; Instant Ocean; Amazon, B000256EUS)). Fish were fed brine shrimp twice daily at ~9 a.m. and ~3 p.m. on weekdays (0.5-2 mL per feeding, with volume per feeding approximately scaling with each week of development). Fish were fed once daily on weekends and holidays. After 1 month, fish were fed food pellets (Reed Mariculture, Otohime C1) twice daily at ~9 a.m. and ~3 p.m. (and once daily on weekends and holidays) with ~18 mg per feeding. Tests for pathogens were conducted every three months (Charles River Labs). Fish were housed in Stanford ChEM-H/Neuro Vivarium and Research Animal Facility (RAF), according to IACUC protocol 13645.

For breeding and collecting killifish embryos, plastic weigh boats (e.g., Heathrow Scientific, HS1420BB) filled up to halfway with sand were dropped in breeding tanks containing 1 male and 1-10 females (all 1-4 months old, 1.5-2.5 month old breeding females used when available; 2.8 L breeding tank for up to 3 females, 6.8 L breeding tank for up to 6 females; 9.8 L breeding tank for up to 10 females) to initiate mating, and approximately 3-6 hours later the embryos were collected by pouring the contents of the sand tray through a sieve.

Collected embryos were placed in 5-15 mL embryo solution liquid (embryo solution was made by adding 2 Ringer tablets (EMD Millipore, 1.15525.0001) and 100 µL methylene blue (Kordon, 37344) to 1 L Milli-Q water, for a final concentration of 0.01% methylene blue) in 35 or 60 mm diameter Petri dishes (Greiner, 627102 and 628161 respectively; dish size used dependent on number of embryos, with a maximum of ~40 embryos in a 35 mm and ~150 embryos in a 60 mm Petri dish) for 2 weeks at 28°C in a dark incubator (e.g., Thermo 50125590H). Dead embryos were removed each day, with the embryo solution exchanged on the first day and on an as-needed basis thereafter. Embryos were generally treated with Povidone Iodine Prep Solution U.S.P. (Dynarex; Amazon, B00859URLK) (added to the Petri dish with embryo solution at ~1:1000 dilution, followed by 2-3 washes with embryo solution) immediately after collection.

At 14-16 days post fertilization (dpf), embryos were placed on autoclaved coconut fiber (Fluker's; Amazon, B01HO27S4M) in 35 or 60 mm diameter Petri dishes (with a maximum of ~40 embryos in a 35 mm and ~150 embryos in a 60 mm Petri dish) and maintained at 27-30°C for an additional 2 weeks before hatching by placing in ~5 mL cold (4°C) humic acid solution (Sigma-Aldrich, 53680, 1 g/L in RO water) in a 35 mm Petri dish left overnight at room temperature, followed by transfer to the aquatic system. In certain cases (noted in Supplementary Table 1), some embryos entered diapause, even at 28°C (this did not appear to be linked to maternal age or any other obviously noticeable parameter), and had to be induced out of diapause using a thermocycler program of 6 hours at 28°C and 6 hours at 37°C repeated 6 times before being allowed to continue to develop at 28°C and transferred to coconut fiber followed by hatching in cold humic acid.

Newly hatched killifish (fry) were housed on the system at a density of up to 20 fry per 0.8 L tank, with successive reductions in density as the fish grew older until reaching a density of 1 male fish per 1.8-2.8 L tank, or 1-10 female fish per 1.8-9.8 L tank (2.8 L tank for up to 4 females, 6.8 L breeding tank for up to 6 females; 9.8 L breeding tank for up to 10 females), beyond 1 month of age (sexual maturity).

Unless otherwise noted, original data in this study from all figures were collected from animals raised in Stanford ChEM-H/Neuro Vivarium after a general system bleaching (January 2025) and treated as described above. Data from Fig. 1b, Fig. 1c, Fig. 1h (images), Fig. 1 – Fig. Supplement 1c, Fig. 1 – Fig. Supplement 1d (4 of 10 fish), and Fig. 3b were obtained in another facility at Stanford (RAF), with specific husbandry variations noted in Supplementary Table 1 (see "Notes"). Data from Fig. 1 – Fig. Supplement 1a, Fig. 1 – Fig. Supplement 1f, Fig. 4f-i, and Fig. 4 – Fig. Supplement 1c-e were collected in ChEM-H/Neuro Vivarium before system bleaching (with bryozoans and mycobacteria prevalent), with specific husbandry variations noted in Supplementary Table 1 (see "Notes"). A list of animals used in each experiment/figure panel, with information on age (with hatch and sacrifice dates), notes on husbandry conditions, sex, and genotype, can be found in Supplementary Table 1. Importantly, the key phenotypes observed in this study were robust to variations in husbandry conditions.

Generation of SP-oScarlet killifish

To generate a killifish knockin strain expressing a secreted form of the red fluorescent protein oScarlet in the nervous system, we used our CRISPR-based knockin method[67]. Overall, a construct encoding a signal peptide (SP) from killifish HSPA5 (signal peptide predicted using SignalP 5.0[71]) fused to the N-terminus of the red fluorescent protein oScarlet[70] was inserted by homology-directed repair just 5' of the endogenous stop codon of the *ELAVL3* (*LOC107378364*) locus in the killifish GRZ wildtype strain. Across multiple vertebrate species, *ELAVL3* encodes an RNA-binding protein expressed strongly in neurons, as well as some glia such as oligodendrocytes[68,78], and has successfully be used in killifish as a driver for pan-neuronal expression[67].

The signal peptide allows the secretion of oScarlet from ELAVL3-expressing cells. To prevent unwanted fusion of oScarlet to ELAVL3, the construct also encodes a P2A self-cleaving peptide[72] at the C-terminal end of ELAVL3 (full sequence of construct, including 200 bp homology arms at either end, in Supplementary Table 2; annotated SnapGene map file in Supplement 1).

To generate the killifish strain expressing this secreted form of oScarlet, which we refer to as SP-oScarlet, we followed the step-by-step CRISPR knockin protocol described by Bedbrook et al., 2023[67]. For each round of injection attempted, a sand tray was dropped in a harem breeding tank (6.8-9.8L tank) containing 1 GRZ wildtype male and 5-10 GRZ wildtype females (all 1-4 months old, with 1.5-2.5 months old breeders used when available) to initiate mating, and approximately 3-4 hours later the embryos were collected by pouring the contents of the sand tray through a sieve.

Injection needles were generated from borosilicate glass capillaries (Sutter, BF100-58-10) pulled on P-97 pipette pullers (Sutter Instruments). A ramp test was performed and a Heat value of [RAMP value + 30] was used. Other settings used were Pull = 20-30, Velocity = 19-30, Time = 200. These parameters were optimized on each specific pipette puller used, with the resulting needles tested in pilot injections.

In the 30 minutes before collection, 1 µL of a crRNA targeting the 3' end of the coding sequence of *ELAVL3* (at 100 µM in Nuclease-Free Duplex Buffer (IDT, 11-01-03-01); sequence in Supplementary Table 2) and 1 µL of tracrRNA (at 100 µM in Nuclease-Free Duplex Buffer; IDT, 1072532/3/4) were added to 31.3 µL Nuclease-Free Duplex Buffer and annealed at 95°C for 5 minutes to generate the guide RNA (gRNA) solution. After this annealing, 10 µL of the resultant gRNA solution was added to 0.5 µL rCas9 protein (10 µg/µL; IDT, 1081059), and 5.5 µL PBS (Corning, 21-040-CV) and this mixture was heated at 37°C for 10 minutes to generate the ribonucleoprotein complex. After this heating, 8 µL of the ribonucleoprotein complex was added to 1 µL dsDNA homology-directed repair (HDR) template (150 ng/µL; IDT custom-synthesized, sequence in Supplementary Table 2, annotated SnapGene map file in Supplement 1), 1 µL HDR enhancer solution (IDT 10007921; 10 µM), and 0.33 µL phenol red (e.g., Sigma-Aldrich P0290-100ML) to generate the injection solution.

For injection, embryos at the 1 cell stage were aligned in rows on an injection pad (1% agarose in embryo solution, solidified over a custom-3D-printed mold with rows) with the single cell facing upwards placed under a dissecting microscope (Leica, MZ6). Embryos were individually injected with injection solution dispensed through the aforementioned needles (loaded using Microloader

(Calibre Scientific, EPE-5242956003) tips; per-injection volume estimated to be in the nanoliter range). Needles were unsealed by brushing against sides of embryos. Injections were performed with a MPPI-2 Pressure Injector (ASI) with Air Out = Continuous, Pressure ~ 10 psi. This procedure allowed for a constant, slow stream of injection solution flowing out of the needle (visible due to the use of phenol red); the needle was inserted into the single cell of an embryo and injection solution allowed to flow out until the single cell was visibly red (~2-3 seconds).

After injection, embryos were placed in embryo solution in 35 or 60 mm diameter Petri dishes for 2 weeks at 28°C and dead embryos were removed daily. At 9-11 dpf, we identified F0 fish expressing the red fluorescent protein oScarlet in the nervous system (by visual inspection of embryos under a fluorescent dissecting microscope). At 14-16 dpf, embryos were placed on coconut fiber in 35 or 60 mm diameter Petri dishes and maintained at 27-30°C for an additional 2 weeks before hatching by placing in cold humic acid solution left at room temperature overnight (see above), followed by transfer to the aquatic system.

To generate a stable SP-oScarlet line, adult F0 fish (as determined by the visual screening of embryos described above) were crossed with GRZ wildtype fish. F1 fish and some subsequent generations were genotyped to identify SP-oScarlet progeny (see “Genotyping,” below). We outcrossed F1 SP-oScarlet fish with wildtype GRZ fish for >5 generations. Both

GRZ male x SP-oScarlet female and SP-oScarlet male x GRZ female crosses were used. In one cohort, we generated homozygous SP-oScarlet fish by crossing heterozygous parents and noted the homozygotes had relatively poor survival at the fry stage (<10% surviving to one month of age). Therefore, we maintained the line at the heterozygous state and we used heterozygotes for all experiments.

Genotyping

In most generations, SP-oScarlet progeny of SP-oScarlet x GRZ wildtype crosses were identified by visual inspection of embryos. Nonetheless, in the F1 generation and some subsequent generations, we used PCR genotyping to confirm the presence of an insertion at the *ELAVL3* locus, using a three-primer PCR strategy with e.g., primers pFL1, pRL1, and pmCF (sequences in Supplementary Table 2). All primers used were synthesized by IDT.

Genomic DNA was extracted from a small (<1 mg) amount of tail tissue cut from a live fish, either from a 1 day old fry or an adult fish, anesthetized either on a dish placed over ice (for fry) or in 300 mg/L Tricaine (dissolved in system water; e.g., Pentair, TRS1) buffered with sodium bicarbonate to pH ~7 (for adults).

The tail tissue was lysed in 30 µL (for fry) or 100 µL (for adults) 2% (volume/volume) Proteinase K (e.g., Invitrogen, 25-530-049) in DirectPCR lysis solution (Viagen Biotech, 102-T) in a PCR tube (e.g., USA Scientific, 1402-4708) using a thermocycler program of 55°C for 2 hours (lysis) and 80°C for 10 minutes (Proteinase K inactivation).

Next, 2 µL (for fry) or 3 µL (for adults) of the resulting lysate (unpurified) was added to 10 µL 2x GoTaq Green Master Mix (Promega, M7123), 6 µL Milli-Q water, and 0.5 µL each of primers pFL1, pRL1, and pmCF (each at 10 µM in Milli-Q water) following the manufacturer’s instructions for PCR with a total reaction volume of 19-20 µL and a thermocyler program of 98°C (pre-heating); 98°C for 30 seconds; 30 cycles of 98°C for 30 seconds, 55°C for 1 minute, and 72°C for 90 seconds; and finally 72°C for 5 minutes.

Then, 8 µL PCR product was resolved on a 1% agarose gel to verify the size of amplified bands. Samples with only one band of size 971 bp (pFL1, pRL1 band) were identified as wildtype, while samples with two bands (824 bp; pmCF, pRL1 band from knockin allele and 971 bp; pFL1, pRL1 band from wildtype allele) were identified as heterozygous SP-oScarlet (the >1.5 kb pFL1, pRL1 band from the knockin allele would not be expected to be amplified efficiently under these PCR conditions).

Separately, to validate the sequence of the genomic insertion in a SP-oScarlet heterozygous fish, we performed PCR with primers pFL1 and pRL1 outside the homology arms of the knockin construct. For this, genomic DNA was extracted from the sidebody muscle of heterozygous SP-oScarlet

killifish (78 days old male). The fish was sacrificed in ice water and <25 mg of sidebody muscle was cut out with a scalpel (Integra, 4-122), chopped, and placed in 200 µL of DNEasy Blood & Tissue kit (Qiagen, 69504/6) Buffer AL in a 1.5-mL tube (e.g., Eppendorf, 0030108418). The DNEasy Blood & Tissue kit manufacturer's protocol was then followed to extract DNA, which was eluted in 200 µL of Buffer AE.

DNA amount and quality was assessed by NanoDrop and 1 µL (<200 ng) of DNA was used as input in a PCR with 1 µL LongAmp polymerase (New England Biolabs, M0323S), 5 µL 5x LongAmp Taq Reaction Buffer (New England Biolabs, M0323S), 3.75 µL 2 mM DNTPs (e.g., Sigma-Aldrich, D7295-.2ML), 12.25 µL Milli-Q water, and 1 µL each of primers pFL1 and pRL1 (each at 10 µM in Milli-Q water) following the manufacturer's instructions for PCR with a total reaction volume of 25 µL and a thermocyler program of 94°C (pre-heating); 94°C for 30 seconds, 30 cycles of 94°C for 30 seconds, 58°C for 1 minute, 65°C for 3 minutes; and finally 65°C for 10 minutes. Less than 8 µL PCR product was resolved on a 1% agarose gel to verify the size of amplified bands. The remaining PCR product was purified with an NEB Monarch® DNA cleanup kit (New England Biolabs, T1030L) following the manufacturer's protocol exactly and the eluted DNA sent to Primordium Labs for long-read (Oxford Nanopore) sequencing ("Linear/PCR" submission option).

Analysis of the long-read sequencing of the entire locus in SnapGene (by aligning to the expected insertion sequence as listed in Supplementary Table 2) revealed that there were two copies of the SP-oScarlet construct inserted. *In silico* translation with Expasy (*https://web.expasy.org/translate/*; 3'5' Frame 3, oScarlet protein in frame) showed that there was a stop codon after the first copy, compatible with the presence of only one copy of oScarlet protein (Fig. 1 – Fig. Supplement 1a; full sequence of actual insertion in Supplementary Table 2).

Preparation of killifish brain sections

To prepare killifish brain sections, we first sacrificed fish in ice water (in most experiments, unperfused fish; in experiments in Fig. 3b, fish perfused with sulfo-NHS-biotin, see "Intracardial perfusion," below). Whole fish heads were cut off and incubated overnight at 4°C in the dark with rocking in 1-5 mL 4% paraformaldehyde (PFA; e.g., Electron Microscopy Sciences, 15710 diluted 1:4 in phosphate-buffered saline (PBS) (e.g., Corning, 21-040-CV)) in PBS (volume used dependent on fish head size) in a 15-mL conical tube (e.g., Falcon, 352196). The following day, 3 washes with PBS (same volume as 4% PFA used in the preceding step) were performed for at least 1 hour each at 4°C in the dark with rocking. After the final wash, fish brains were dissected out of the heads in cold PBS using forceps (e.g., Fine Science Tools, 11252-20), starting with removal of the lower jaw, then the upper part of the head and eyes, and finally freeing the brain from the skull. The brains were then sunk in 0.5-1 mL 30% (weight/volume) sucrose (Sigma-Aldrich, S0389-1KG) in PBS overnight at 4°C in the dark. Once the brains had sunken, they were embedded in Optimal Cutting Temperature (OCT) compound (Fisher HealthCare, 4585). OCT blocks containing the brains were frozen over dry ice and stored at −80°C until sectioning.

Sagittal sections with a thickness of 50 µm were generated using a cryostat (Leica, CM3050 S) and MX35 Ultra blade (Epredia, 3053835) and added to Superfrost Plus slides (Fisherbrand, 1255015) that were stored at −20°C until further processing. Sections with visible and undamaged forebrain, midbrain and hindbrain tissue were included, with approximately position-matched sections (based on visual inspection of brain tissue gross morphology) used where appropriate for comparisons. RNase-free reagents and technique (namely, spraying tools and surfaces with 70% ethanol and RNaseZap (Invitrogen, AM9780, AM9782)) were used for all experiments in which hybridization chain reaction (HCR) was later performed on the brain sections.

Hybridization chain reaction

To perform hybridization chain reaction (HCR)[73] on killifish brain sections, we first placed slides with 50 µm-thick killifish brain sections were placed in RNase-free PBS at room temperature for at least 20 minutes to wash off excess OCT (preceded by a heating step at 37°C for ~10 minutes in some experiments to minimize the occurrence of sections detaching from the slides).

After washing off OCT, slides were then permeabilized in 1% Triton (e.g., Sigma-Aldrich T8787-50ML) in 100% methanol (e.g., Sigma-Aldrich 34860-100ML-R) for at least 1 hour at −20°C, then washed twice in RNase-free 2x saline sodium citrate (SSC; diluted from 20x SSC (ThermoFisher, AM9763) in RNase-free water) with 0.1% Triton (250 µL per slide) for 15 minutes per wash at room temperature. HCR hybridization buffer (Molecular Instruments, "HCR Probe Hybridization Buffer," for tissue sections; 250 µL per slide; preheated to 37°C) was applied to the slides, which were incubated at 37°C for 30 minutes with a coverslip on top. After the 30 minutes incubation, this hybridization buffer was removed and replaced with hybridization buffer containing the appropriate probe sets diluted 1:100 from stock. Once the hybridization buffer with probes sets had been applied, the slides were then incubated at 37°C overnight with a coverslip on top.

Sequences for all HCR probe sets used in this study are listed in Supplementary Table 2. These sequences were determined by a Python script that used the most 5' or 3' (as noted in Supplementary Table 2) 1012 bp of the longest killifish mRNA sequence for the gene of interest (or the entire mRNA sequence, in the case of shorter genes) to design up to 22 pairs of probes 22 bp in length each, with a 2 bp spacer between probes. Probes sets were ordered in tubes as lyophilized 50 nM oPools (IDT custom-synthesized) and resuspended in 50 µL of TE8.0 (Invitrogen, AM9849). After a 5 minutes wait, the tubes were vortexed and 20 µL of the resuspension solution was added to 20 µL of TE8.0. This diluted resuspension solution was vortexed, spun down, and spit into 5 µL aliquots which were used as the probe set stocks.

After the overnight incubation with probes sets diluted in hybridization buffer, HCR wash buffer (Molecular Instruments, "HCR Probe Wash Buffer," for tissue sections; 250 µL per slide; preheated to 37°C) was applied to was applied to the slides, which were incubated at 37°C for two washes of 30 minutes each with a coverslip on top. The slides were then washed twice in RNase-free 2xSSC with 0.1% Triton (250 µL per slide) for 15 minutes per wash at room temperature. Next, HCR amplification buffer (Molecular Instruments, "HCR Amplification Buffer," for tissue sections; 100 µL per slide; equilibrated to room temperature) was applied to the slides, which were incubated at room temperature for at least 30 minutes with a coverslip on top.

During this incubation, amplification hairpins (Molecular Instruments; 2 µL per hairpin per slide) were prepared. Hairpins were first snap-heated at 95°C for 5 min, followed by 30 minutes of cooling at 4°C. Hairpins used for each probe in this study are listed in Supplementary Table 2 (see "Notes"). Hairpin solution (100 total µL per slide) was prepared by adding hairpins (2 µL per hairpin per slide) to amplification buffer. After applying hairpin solution, slides were incubated at room temperature overnight in the dark.

After overnight incubation with hairpin solution, slides were washed twice in RNase-free 2xSSC with 0.1% Triton (250 µL per slide) for 5 minutes per wash at room temperature in the dark, then washed once in RNase-free 2xSSC with 0.1% Triton (250 µL per slide) for 5 minutes at room temperature in the dark, and then washed twice in RNase-free 2xSSC with 0.1% Triton (250 µL per slide) for 5 minutes per wash at room temperature in the dark before mounting in ProLong Gold with 4',6-diamidino-2-phenylindole (DAPI; Thermo Fisher Scientific, P36931) under a coverslip. Mounted slides were dried overnight at room temperature in the dark and stored at 4°C in the dark until imaging.

For experiments in which HCR and immunofluorescence staining were performed sequentially on the same slides, after overnight incubation with hairpin solution, slides were washed five times in RNase-free 2xSSC with 0.1% Triton (250 µL per slide) for 5 minutes per wash at room temperature in the dark, before proceeding to blocking for immunofluorescence staining.

Immunofluorescence staining

To perform immunofluorescence staining on killifish brain sections, we first heated slides with 50 µm-thick killifish sagittal brain sections for 10 minutes at 37°C, then placed the slides in PBS at room temperature for at least 20 minutes to wash off excess OCT. Slides were then permeabilized in 0.5% Triton in methanol for at least 1 hour at −20°C, then washed twice in PBS for 5 minutes per wash at room temperature.

Next, for blocking, circles were drawn around sections with a hydrophobic pen (Edding 751) blocking buffer (PBS with 5% normal donkey serum (NDS; Fisher Sci., SP-072-VX10) and 1% bovine serum albumin (BSA; from 10% BSA stock; Miltenyi Biotec, 130-091-376)) was added to the areas within the circles for a 30 minutes incubation at room temperature. After blocking, the blocking buffer was removed and primary antibodies were added for overnight incubation at 4°C in the dark. All primary antibodies used in this study are listed in Supplementary Table 3 along with the dilution (in blocking buffer) at which they were used.

After incubation with primary antibodies, slides were washed 6 times with PBS with 0.1% Triton for 10 minutes each at room temperature in the dark, and then washed 3 times with PBS for 5 minutes each at room temperature in the dark, before the PBS was dried off and secondary antibodies and DAPI (Fisher Scientific, 62248) (all diluted 1:500 in blocking buffer) were added for 2 hours incubation at room temperature in the dark. All secondary antibodies used in this study are listed in Supplementary Table 3.

After incubation with secondary antibodies, slides were washed 6 times with PBS with 0.1% Triton for 10 minutes each at room temperature in the dark, and then washed 3 times with PBS for 5 minutes each at room temperature in the dark before mounting in ProLong Gold (ThermoFisher, P36930) under a coverslip. Mounted slides were dried overnight at room temperature in the dark and stored at 4°C in the dark until imaging.

Tissue clearing

To visualize oScarlet protein in SP-oScarlet brains at a whole-brain level, we performed tissue clearing using a modified Adipo-Clear protocol[170]. A dissected young adult SP-oScarlet brain in PBS (processed as described in "Preparation of killifish brain sections," above, up to dissection, then placed in room temperature PBS) was subjected to the Adipo-Clear protocol with ethyl cinnamate (Sigma-Aldrich, 112372) was used in place of dibenzyl ether. An anti-RFP antibody used to visualize oScarlet (details in Supplementary Table 3).

Imaging

Unless otherwise noted, all images were taken with a Zeiss LSM900 confocal microscope with Zen3.0 Blue Edition software. Zeiss Immersol Oil 518F (Zeiss 4Y00-R0DY-1007-3VF3) was used with the 40x and 63x magnification objectives. Imaging parameters, including the magnification objective used for each image, are listed in Supplementary Table 4.

The images in Fig. 1d, Fig. 1e, and Fig. 2 – Fig. Supplement 1a were taken with a Miltenyi Biotec Ultramicroscope Blaze, an EVOS M5000 tissue culture microscope, and a Zeiss Elyra7 structured illumination microscope (at Stanford's Cell Sciences Imaging Facility (*RRID:SCR_017787*)), respectively.

Image processing and quantification

Image analysis scripts are listed in Supplementary Table 4. Confocal images taken were z-stacks with 10-20 slices 0.5 µm apart. Maximum intensity projections of 10 slices per image were generated in Fiji/ImageJ using the macros listed in Supplementary Table 4 and saved as TIF files. The max projection TIF files were loaded into QuPath (v0.6.0)[171] for automated cell detection and, where needed to detect RNA transcripts, subcellular spot detection using Groovy scripts as listed in Supplementary Table 4.

Unless otherwise noted, all images shown in this manuscript were processed (maximum intensity projection, brightness/contrast adjustment, cropping) with Fiji/ImageJ. The image in Fig. 1d was processed in Imaris (specialized software for 3D image processing) and further processed in Fiji/ImageJ. The image in Fig. 2 – Fig. Supplement 1a was pre-processed with Zen Blue Software (for structured illumination mathematical correction) on the microscope used for image acquisition (at Stanford's Cell Sciences Imaging Facility, *RRID:SCR_017787*) prior to processing in Fiji/ImageJ.

Since *APOEB* HCR signal was strong and individual transcript spots were often difficult to distinguish, mean *APOEB* RNA intensity per cell in 10x magnification images was used as a readout of *APOEB* expression. For all other HCR probes used, individual transcript spots were counted in 40-63x magnfiication images. QuPath measurements were exported as .csv files and analyzed in R (v4.5.1).

In quantifications of oScarlet immunofluorescence staining, oScarlet^{HIGH} cells were defined as those with both a mean fluorescence intensity in the oScarlet channel of >2.5 standard deviations higher than the mean of all cells in the image and maximum fluorescence intensity in the oScarlet channel of >25,000, due to the punctate nature of bright oScarlet protein signal.

In quantifications of dextran-Oregon Green 488 native fluorescence, dextran-positive cells were defined as those with both a mean fluorescence intensity in the dextran channel of >2.5 standard deviations higher than the mean of all cells in the image and maximum fluorescence intensity in the dextran channel of >25,000, due to the punctate nature of dextran signal.

In quantifications of *APOEB* HCR signal, cells with high *APOEB* RNA expression were defined as those with a mean fluorescence intensity in the *APOEB* RNA channel of >2.5 standard deviations higher than the mean of all cells in the image, since *APOEB* RNA signal was largely cell body-filling.

In quantifications of colocalization with vasculature, vasculature was defined as cells with a mean fluorescence intensity in the sulfo-NHS-biotin channel of >1.5 standard deviations higher than the mean of all cells in the image, since sulfo-NHS-biotin signal was largely cell body-filling. Cells colocalizing with vasculature were defined as those with a centroid <5 μm from the centroid of any vasculature cell (inclusive of vasculature cells themselves).

For representative sampling of all brain regions for quantification, we imaged one region of interest from each of the forebrain, midbrain, and hindbrain across 1-3 sagittal sections per animal, avoiding areas of visually obvious tissue damage.

In Fig. 3a and Fig. 3 – Fig. Supplement 1a, four images (one image per animal for each of four animals; listed in Supplementary Table 4) were excluded from quantification because they contained regions with a visually obvious very high density of cells with high *APOEB* RNA expression, which could potentially reflect a response to injury (see also “Injection of dextran into killifish brains,” below).

For quantifications in Fig. 3b, brain external borders were generally avoided when selecting regions of interest, because sulfo-NHS-biotin signal was much brighter at these external borders as compared to other areas in the brain, which we could bias quantification. As such, our analysis mostly examined *APOEB*+ cells in the brain interior.

Injection of dextran into killifish brains

To test the endocytic properties of cells in the killifish brain, we injected dextran-Oregon Green 488 (70 kDa) (Thermo Fisher Scientific, D7173), aiming for the ventricle to maximize distribution of dextran through the cerebrospinal fluid. Only females were used for these experiments since adult males have thick muscle above the skull that makes it difficult to visually locate the brain.

The brain injection procedure bears similarities to cerebroventricular microinjection procedures used for adult zebrafish[96,172], though specific adaptations were made for killifish. Brain injection needles (made identically to embryo microinjection needles) were filled with a mixture of 90% dextran (1 mg/mL dissolved in PBS) and 10% phenol red (for visualization), for a final dextran concentration of 900 μg/mL, using Microloader tips.

After loading, the needles were unsealed by breaking their points with fine forceps. Prior to injection, fish were individually anesthetized in 300 mg/L Tricaine (dissolved in system water) buffered with sodium bicarbonate to pH ~7. Successful anesthesia was confirmed by the fish being non-responsive to tail pinching, at which point the fish was placed in between pins on a Tricaine-filled dish underneath the injection microscope.

Injections were performed with a Pneumatic Picopump (World Precision Instruments, PV380) with settings Vacuum = 0 in Hg (vac setting), Hold = 0 psi, Eject = 5-10 psi (Vent = hold), Range = 10 s, Period = 50, Duration = timed, with the needle stabilized and positioned using a DC-3K right apparatus (World Precision Instruments, DC3001R, 00-45-201-0000). We used a micrometer (Fisherbrand, 12-561-SM1) to estimate an approximate ejection volume of <0.5 µL (based 5 test ejections of 10% phenol red in PBS into a mineral oil (e.g., Sigma-Aldrich, M5904-5ML) droplet with similar needles, unsealing procedure, and approximately equal pressure settings as used for brain injections; although injecting through the skull further unseals the needle). We used the minimum Eject pressure necessary to eject liquid for this procedure, to minimize damage to the brain.

To aim for the ventricle, needles were inserted at approximately a 45° angle through the skin and skull at the most medial point of the forebrain/midbrain border (where the two lobes of the telencephalon and two lobes of the optic tectum meet). This point was approximately aligned along the anterior-posterior axis with the most posterior part of the eyes.

No brain coordinates were used to estimate the depth the needle needed to reach before ejection (by pressing foot pedal); the depth of needle insertion was approximately optimized by practice injections, with immediate spread of phenol red used as a readout of successful injection. We note that engulfment of dextran by brain macrophages was observed in some cases where immediate spread of phenol red upon ejection was not observed, possibly due to clogging in the needle limiting the volume of liquid ejected.

Fish were then placed in recovery tanks with fresh system water (not on aquatic system) and sacrificed 1 day (~20-26 hours) after dextran injection.

We excluded one animal from the quantifications in Fig. 3a and Fig. 3 – Fig. Supplement 1a based on visually obvious lack of dextran signal throughout the brain (Fig. 3 – Fig. Supplement 1b). Of the 38 remaining images from six remaining animals, we additionally excluded four images (one each from four different animals) that contained regions of interest with visually apparent very high densities of *APOEB*+ cells, which could reflect a response to injury. These four excluded images are listed in Supplementary Table 4 (row 14, “Notes”).

Intracardial perfusion

To visualize vasculature, we perfused wildtype killifish with sulfo-NHS-biotin (Thermo Scientific, 21335). The perfusion procedure was similar to that described by Costa et al., 2026[55]. Perfusion was performed with a syringe pump (KD Scientific, Legato 200 Series, 788200 syringe pump) with 30-gauge hubless needles with a point style 4 bevel (Hamilton Syringe, custom needle, 22030-01; 30 gauge, Hubless Needle, No Hub, 30 gauge, 1.5 inches length, point style 4 [12°]) attached using ~0.25 meters of BD Intramedic PE Tubing (BD, 427400) to a 30 gauge metal hub blunt-end Luer needle (Hamilton Syringe, custom needle, 7748-16; 30 gauge, Metal Hub Needle, Point Style: 3; Needle Length: 0.375 inches) on a 20-mL disposable syringe with Luer Lock tip (‘Sterile Syringe Only with Luer Lock Tip’, Amazon, B08FJCSLFC).

Adult killifish were anesthetized in 300 mg/L Tricaine (dissolved in system water; e.g., Pentair, TRS1) buffered with sodium bicarbonate to pH ~7, with the underbelly cut so as to expose the heart (full details of cutting described by Costa et al., 2026[55]), with the perfusion needle inserted into the bulbus arteriosus. The perfusion flow rate was 3.5 mL/minute. First, 6 mL of 50 mM Tris pH 8.0 (filled in the disposable syringe; Thermo Fisher Scientific, 15-568-025) was perfused, followed by 4 mL of 0.5 mg/mL sulfo-NHS-biotin in PBS, and then 2 mL of 50 mM Tris pH 8.0.

After perfusion, fish were sacrificed in ice water and their carcasses incubated overnight at 4°C in the dark with rocking in >5 mL 4% paraformaldehyde in PBS (e.g., diluted from 16% paraformaldehyde in PBS (Electron Microscopy Sciences, 15714-S)) in a 15-mL conical tube (e.g., Falcon, 352196). Cuts were made in the underbelly to expose the internal organs and allow for complete fixation. The following day, 3 washes with PBS (same volume as 4% paraformaldehyde used) were performed for at least 1 hour each at 4°C in the dark with rocking. After this, the PBS was exchanged with 100% methanol (Sigma-Aldrich, 34860-4L-R) and the fish were stored long-term (>1 year) at −20°C. Before sectioning, heads were cut off and rehydrated with a reverse

gradient of 2 mL each of (1) 75% methanol and 25% PBS; (2) 50% methanol and 50% PBS; (3) 25% methanol and 75% PBS; and finally (4) 100% PBS, sequentially for 15-45 minutes each on ice. Then, an additional wash in 100% PBS was performed for 15 minutes, and then brains were dissected for preparation of killifish brain sections.

Dissociation of killifish brains for single-cell RNA sequencing

We conducted two single-cell RNA sequencing experiments: one in October 2024 (Fig. 4e) and one in August 2025 (Fig. 1d). In the October 2024 experiment, we sequenced FACS-sorted oScarlet^{HIGH} cells from old male SP-oScarlet brains (n = 3 fish, pooled) as well as FACS-sorted Live cells from old male wildtype brains (n = 3 fish, pooled). In the August 2025 experiment, we sequenced FACS-sorted oScarlet^{HIGH} and oScarlet^{LOW} cells from young male SP-oScarlet brains (n = 4 fish, pooled) as well as FACS-sorted oScarlet^{HIGH} from old male wildtype brains (n = 4 fish, pooled).

For single-cell RNA sequencing experiments, fish were always sacrificed in the morning on a weekday, having not received feeding since the previous afternoon. Males were used for these experiments due to their larger size, maximizing cell yield for single-cell RNA sequencing.

For dissociation, we used protocols similar to those described by Mariën et al., 2024[173]. Fish (not perfused) were sacrificed in ice water and brains were dissected in ice-cold PBS using forceps, starting with removal of the lower jaw, then the upper part of the head and eyes, and finally freeing the brain from the skull. After dissection, brains were cut into pieces approximately the size of a half telencephalon. Per sample (each sample consisted of a pool of 3-4 brains matched in age, genotype, and sex), all tissue pieces were transferred into a 1.5-mL microcentrifuge tube containing 800 µL of ice-cold dissection medium (DMEM/F12 with HEPES (Thermo Fisher Scientific, 11330032) with actinomycin D (transcription inhibitor; Sigma-Aldrich, A1410-2MG) added at 1:200, triptolide (transcription inhibitor; Sigma-Aldrich, T3652-1MG) added at 1:1000, anisomycin (translation inhibitor; Sigma-Aldrich, A9789-5MG) added at 1:368.5 and put on ice until all brains were dissected (up to 2 hours).

Once all the dissected tissues were ready in dissection medium on ice, fresh papain solution was prepared. Papain solution consisted of 50 µL of papain (suspension, from papaya latex; Worthington, LS003126), 20 µL DNase I solution (10 mg/mL; e.g., STEMCELL Technologies, 07900; dissolved in Milli-Q water), and 40 µL of L-cysteine solution (12 mg/mL) per 1 mL of DMEM/F12, with actinomycin D added at 1:200, triptolide at 1:1000, anisomycin at 1:368.5. This solution was sterilized through a 0.2-0.22-µm-pore-size filter (Sigma-Aldrich, WHA9914-2502 or Fisher Scientific, SLGP033RS) and vortexed to mix. L-cysteine solution was prepared by adding 120 mg of L-cysteine hydrochloride (e.g., Sigma-Aldrich, C6852-25G) to 10 mL of filtered, autoclaved Milli-Q water, and stored for up to 2 weeks at 4°C or 1 year at −20°C.

The dissection medium was removed by pipetting and 1 mL fresh papain solution was added to each sample. To start digesting the brain tissue, tubes with the samples were placed in an incubator for ~6 minutes at 37°C. After the 6 minutes, the tubes were removed from the incubator and the brain tissue was dissociated mechanically by pipetting up and down ~13 times with a 1-mL pipette tip (e.g., Fisher Scientific 12-111-164) cut at 0.5 cm. Four additional rounds of incubation and mechanical dissociation were performed. In the second round, mechanical dissociation was performed with a 1-mL pipette tip cut at 0.2 cm, and in subsequent rounds, mechanical dissociation was performed with an uncut 1-mL pipette tip. Papain digest was limited to 5 rounds (30 minutes) total to avoid pre-apoptotic cells. After this digest, cells were transferred into 5-mL FACS tubes with strainer caps (Corning, 352235), using sufficient pressure to make sure that the cells passed through the strainer. Then 3 mL of washing solution for single-cell suspension was passed through the strainer to clean the strainer and stop the enzymatic reaction. Washing solution for single-cell suspension was prepared by adding 975 µL of glucose (e.g., Sigma, G7021-1KG) 15% (weight/volume) in Milli-Q water, 250 µL of HEPES 1 M (e.g., Sigma-Aldrich, H3375-100G; dissolved in Milli-Q water), and 2.5 mL of FBS (fetal bovine serum, e.g., Millipore Sigma, F2442-500ML) to 46.9 mL DPBS (Dulbecco's phosphate-buffered saline; Thermo Scientific, 14190094),

stored for up to 2 months at 4°C, and sterilized with a 0.2-0.22-µm-pore-size filter. After addition of washing solution, contents of the FACS tubes were poured into 50 mL conical tubes (e.g., Thermo Fisher Scientific, 14-432-22) for subsequent centrifugation.

The conical tubes containing the cell suspensions were centrifuged at 500g for 10 minutes at 4°C, and the supernatants were carefully decanted and discarded. Debris was removed using the debris-removal solution, according to the manufacturer's protocol. Cells were resuspended carefully in each tube with 15.5 mL DPBS. Then 4.5 mL of cold debris-removal solution (Miltenyi Biotec, 130-109-398), was added and gently mixed by inverting. This solution was gently overlaid (drop by drop) with 20 mL of cold DPBS (creating two phases), before centrifugation at 3000g for 10 minutes at 4°C, with full acceleration and full brake. After centrifugation, three phases formed; the top two phases were aspirated and discarded. If the phases were hard to distinguish, a conservative approach was taken and the top 20 mL was aspirated and discarded. Then each tube was filled up with cold DPBS (20 mL), closed, mixed by inverting three times with no vortexing and centrifuged at 1000g for 10 minutes at 4°C. The supernatant was aspirated and discarded, and the pellet was resuspended in 500 µL PBS to generate the single-cell suspension.

FACS for single-cell RNA sequencing

Single-cell suspensions were moved to 1.2-mL FACS library tubes (e.g., VWR, 83009-678), to which 5 µL Zombie NIR™ live/dead stain (BioLegend, 423105) diluted 1:10 in PBS was added. These tubes were incubated 15 minutes at room temperature in the dark, and then centrifuged at 300g for 5 minutes at 4°C. For each tube, the supernatant was removed to 100 µL, and the pellet was resuspended in 400 µL of PBS with 0.5% BSA (diluted from 35% BSA; Sigma-Aldrich A7979-50ML).

The contents of each tube were strained through a 5-mL FACS tube with strainer cap, vortexed to minimize cell clumping, and then run on a Sony MA900 cell sorter at about 1500-2000 events per second, with FSC threshold = 6%, FSC gain = 12, BSC gain = 35%, and all fluorophores gain = 40%. Compensation was not used due to the presence of only two fluorophores (oScarlet, same spectra as mScarlet; and Zombie NIR™) whose spectra were determined to be sufficiently non-overlapping per Thermo SpectraViewer. For each sample, 100,000 events were recorded and .fcs files were exported for analysis in FlowJo (v10.0.0). The flow cytometry plot in Fig. 1e was on Live cells as identified from the gating strategy shown in Fig. 1 – Fig. Supplement 1e. oScarlet^{HIGH} cells were defined as those having a FL3-A::mCherry-A (uncompensated) intensity of approximately >800 (October 2024 experiment) or >1000 (August 2025 experiment). oScarlet^{LOW} cells were defined as those having a FL3-A::mCherry-A (uncompensated) intensity of approximately <500.

Each sample from which oScarlet^{HIGH} cells were collected was run in its entirety on Normal mode (maximizes yield) to collect as many oScarlet^{HIGH} cells as possible (with yields ranging from approximately 35,000-65,000 oScarlet^{HIGH} cells according to Sony MA900 event count). For the Live cells collected from wildtype brains in the October 2024 experiment and the oScarlet^{LOW} cells collected from young adult SP-oScarlet fish in the August 2025 experiment, these were also run in Normal mode, but approximately 240,000 and 167,000 cells were collected respectively (according to Sony MA900 event count), which did not represent the entire sample, to avoid overloading the 10x chip in single-cell RNA sequencing. Cells were collected in 500 µL of RNase-free PBS with 1% BSA and 0.1% glucose in 1.5 mL DNA LoBind tubes (Eppendorf, 0030108418).

Single-cell RNA sequencing

After cell collection, tubes containing the cells were centrifuged at 300g for 5 minutes at 4°C. Supernatants were removed to 43.2 µL, and Master Mix was prepared and added to each sample exactly following the instructions in the 10x Genomics Chromium Next GEM Single Cell 3' Reagent Kits v3.1 User Guide. Cells were not counted, in order to load all cells collected in each tube. Once Master Mix was added, the contents of each tube were pipetted up and down (to resuspend the cells fully) and loaded in their entirety onto the 10x chip.

After this, the instructions in the 10x Genomics Chromium Next GEM Single Cell 3' Reagent Kits v3.1 User Guide were followed exactly with 11-12 cycles used in the cDNA amplification PCR and 13-14 cycles used in the Sample Index PCR (October 2024 experiment, 12 and 13 cycles,

respectively; August 2025 experiment; 11 and 14 cycles, respectively).

Libraries were sequenced by Novogene on a NovaSeqX Plus sequencer (150 bp paired-end reads) to an approximate depth of 215-333 million reads per sample.

Identifying homologous genes across species

Killifish gene names were converted to their equivalents in human, mouse, or other species using the table presented in Supplementary Table 5, which was generated as described in the next paragraph. Killifish can have multiple paralogs corresponding to a single mammalian gene, due to whole-genome duplication in teleost fish[174,175]. In such cases, for visualization purposes, one killifish paralog was selected (specified in figure legend). In cases where one killifish paralog had a much higher expression level than the other paralogs, the highest-expressed killifish paralog was selected.

Over half of the killifish NCBI gene names (11,715 out of 22,194) consist of locus numbers. Therefore, we generated new gene symbols for all the killifish protein coding genes, based on NCBI gene descriptions for killifish and human, and orthologs between killifish and other animals. For ortholog identifications, we ran sequence comparison using BLAST (ncbi-blast-2.5.0+) between killifish and 36 other animals, including multiple tetrapod, and fish species. We then generated a prioritized scheme for gene symbol assignment based on the following rules. We kept the gene symbols assigned by NCBI annotation. If there were no gene symbol assigned by NCBI, we matched the NCBI gene description between killifish and human and assigned the human gene symbols where the gene descriptions matched between the two species. For rest of the genes, we generated a consensus gene symbol based on 'majority rules' using ortholog symbols from 36 other animals. In case of ties, priority was given to the tetrapod symbols. We were able to assign proper gene identities to 93% of the locus numbers and improve gene symbols for 96.4% of all protein coding genes.

In the text, figures, and legends of this manuscript, all killifish gene names are capitalized and presented in italics (e.g., *ELAVL3*).

Analysis of single-cell RNA sequencing data

Demultiplexed reads provided by Novogene were aligned to the African turquoise killifish genome (Nfu_20140520) using Cell Ranger. A custom genome including the SP-oScarlet knockin insertion (as determined from sequencing as in Fig. 1 – Fig. Supplement 1a) as a separate chromosome was built according to the instructions provided by 10x Genomics (*https://www.10xgenomics.com/support/software/cell-ranger/latest/tutorials/cr-tutorial-mr*, "Add a custom gene to the FASTA and GTF") for alignment of reads from SP-oScarlet fish, although we note that the *SP-oScarlet* transcript was difficult to detect even in *ELAVL3*+ cells. This is potentially explained by the *SP-oScarlet* transcript's position several kilobases upstream of the 3' end of *ELAVL3*, as *ELAVL3* has a long untranslated region. The *oScarlet* transcript could be detected by HCR in *ELAVL3*+ cells *in situ* (Fig. 1 – Fig. Supplement 1c).

After alignment, raw_feature_bc_matrix outputs were downloaded and a Seurat[176] (v5.3.0) object was created (separately for each sample) using the Read10x and CreateSeuratObject functions (min.cells = 3, min.features = 200). For quality control, each of these Seurat objects was individually filtered to include cells with nCount_RNA > 1000, nFeature_RNA > 500, and <10% mitochondrial reads. No doublet removal was performed. After testing various doublet removal methods in preliminary analyses and ensuring that our key conclusions were robust to doublet removal method, we reasoned that due to the lack of reliable killifish cell type markers (particularly for myeloid cells), it would be challenging to assess the accuracy of singlet vs. doublet classifications. Quality control metrics per individual Seurat object are listed in Supplementary Table 6. Seurat objects were merged as appropriate. After each merge, JoinLayers was run on the merged object to allow Seurat to identify cluster markers and differentially expressed genes.

For all objects, merged or unmerged, clusters were defined by running NormalizeData (normalization.method = "LogNormalize", scale.factor = 10000), FindVariableFeatures (selection.method = "vst", nfeatures = 2000), ScaleData, RunPCA, RunUMAP (dims = 1:30), FindNeighbors (dims = 1:30) and finally FindClusters (resolution = 0.1-0.2). Cell types were defined by running FindMarkers for low-resolution clusters and manually matching markers to cell types based on literature, most notably Ayana et al., 2024[68] (killifish-specific) and Tabula Muris[78]. Full lists of low-resolution cluster marker genes among all young adult cells from the August 2025 experiment can be found in Supplementary Table 7.

For subsetting to macrophages, *APOEB*+ *IBA1*+ *LCP1*+ clusters were selected based on expression from VlnPlot. These markers were used by Ayana et al. to define "Microglia" in their wildtype killifish forebrain single-cell RNA sequencing datasets[68], although our analysis shows that *APOEB*+ *IBA1*+ *LCP1*+ killifish brain cells have an expression profile more similar to that of mouse monocyte-derived macrophages rather than mouse microglia.

Young adult wildtype killifish forebrain macrophages were identified by downloading the dataset SRR24058857 (from Ayana et al., 2024[68]) from NCBI Gene Expression Omnibus/Sequence Read Archive, aligning it to the Nfu_20140520 genome using Cell Ranger, and creating a Seurat object and performing quality control exactly as described above for this study's original datasets, and then subsetting to the (one) *APOEB*+ *IBA1*+ *LCP1*+ cluster.

To compare killifish and mouse brain macrophages, we used a Seurat object corresponding to all young adult mouse brain immune cells analyzed by Barr et al., 2025 (see Barr et al., 2025[75] for details of single-cell RNA sequencing, genome alignment, quality control, annotation of cell types, etc.). This object, which includes cells collected at multiple circadian timepoints, was first subset to the circadian timepoint ZT12 (Time = ZT12), which corresponds to the beginning of the active phase (roughly equivalent to the circadian timepoint at which our killifish single-cell data was collected). The object was then subset to microglia, BAMs, and MDMs (Broad_Cell_Annotation %in% c("Microglia", "PBM", "MDM").

Then, we determined markers of mouse microglia, BAMs, and MDMs using FindAllMarkers (test.use = "wilcox", min.pct = 0.1, logfc.threshold = 0.5). All markers of microglia, BAMs, or MDMs, including genes that were markers of multiple cell types (or all killifish homologs of these genes) were used for principal component analysis (PCA). This PCA was performed starting with a Seurat object for each of the following cell populations:

1. Young adult mouse brain macrophages (subset from all young adult mouse brain immune cells; Barr et al., 2025[75]; Broad_Cell_Annotation %in% c("Microglia", "PBM", "MDM", "IFN-M"))
2. Young adult oScarlet^{HIGH} cells (this study)
3. Young adult wildtype killifish forebrain macrophages (Seurat object generated as described above; Ayana et al., 2024[68])

and subsetting to only the marker genes as described above, then re-running NormalizeData (normalization.method = "LogNormalize", scale.factor = 10000), FindVariableFeatures (selection.method = "vst", nfeatures = 2000), ScaleData, and finally RunPCA.

The strongest markers of mouse microglia, BAMs, and MDMs as depicted in the heatmaps in Fig. 2 – Fig. Supplement 3a and Fig. 2 – Fig. Supplement 4a were defined using using FindAllMarkers (test.use = "wilcox", min.pct = 0.5, logfc.threshold = 3).

DimPlot was used to highlight cells by orig.ident (i.e., sample of origin) or cell type (reduction = "umap") and produce PCA plots (reduction = "pca"). FeaturePlot and VlnPlot were used to highlight expression of specific genes. VlnPlot was also used to highlight sum log-normalized expression of genes in specific Gene Ontology terms. DoHeatmap was used to highlight expression of top killifish cell type marker genes as ranked by area under curve according to Presto[177] (no thresholds applied; cell types defined manually as described above) or to highlight expression of killifish homologs of the strongest mouse microglia, BAM, and MDM markers. Full lists of cell type marker genes among all young adult cells from the August 2025 experiment as determined by Presto can be found in Supplementary Table 8.

Differentially expressed genes between samples were determined using FindMarkers (test.use = "wilcox", min.pct = 0.1, logfc.threshold = 0.5), and Gene Ontology terms upregulated among these genes were determined using enrichR ("GO_Biological_Process_2025") with a background of all human genes with killifish homologs represented among the rownames of the combined Seurat object (containing both samples) and plotted using ggplot2. Differentially expressed genes were always calculated at the level of killifish genes, then converted to human gene names for Gene Ontology analysis (enrichR disregards duplicates). The sizes of the circles in Fig. 4d and Fig. 4 – Fig. Supplement 1d correspond to the numbers of unique human genes with any killifish homologs among the differentially expressed genes for the comparison made. As brains from n = 3-4 individual male fish were pooled to achieve sufficient numbers of oScarlet^{HIGH} cells, statistics were calculated at the per-cell level.

Full lists of differentially expressed genes per comparison made can be found in Supplementary Tables 9 and 12. Full lists of Gene Ontology terms upregulated per condition can be found in Supplementary Tables 10-11 and 13-14.

Dissociation of killifish brains for *ex vivo* engulfment experiments

To assess acute endocytic capacity of killifish brain macrophages, we performed *ex vivo* engulfment of ovalbumin-Alexa Fluor® 647 (a 45 kDa protein) (Fisher Scientific, O34784) as well as dextran-Oregon Green 488 (a 70 kDa polysaccharide) (Thermo Fisher Scientific, D7173). For *ex vivo* experiments, fish were always sacrificed in the morning on a weekday, having not received feeding since the previous day.

Dissociation protocols largely followed those described by Mariën et al., 2024[173]. Fish were sacrificed in ice water and brains were dissected in ice-cold PBS using forceps, starting with removal of the lower jaw, then the upper part of the head and eyes, and finally freeing the brain from the skull. After dissection, brains were cut into pieces approximately the size of a half telencephalon. Per sample (each sample consisted of 1 brain), all tissue pieces were transferred into a 1.5-mL microcentrifuge tube containing 500 µL of ice-cold dissection medium (DMEM/F12 + HEPES) and put on ice.

Once all the dissected tissues were ready in dissection medium on ice, fresh papain solution was prepared. Papain solution consisted of 50 µL of papain (suspension, from papaya latex), 20 µL DNase I solution (10 mg/mL; dissolved in Milli-Q water), and 40 µL of L-cysteine solution (12 mg/mL) per 1 mL of DMEM/F12, with the appropriate substrates added at 25 µg/mL each; see details of individual experiments below, "*Ex vivo* engulfment of ovalbumin" and "*Ex vivo* engulfment of dextran"). This solution was sterilized through a 0.2-0.22-µm-pore-size filter and vortexed to mix. L-cysteine solution was prepared by adding 120 mg of L-cysteine hydrochloride to 10 mL of filtered, autoclaved Milli-Q water, and stored for up to 2 weeks at 4°C or 1 year at −20°C.

The dissection medium was removed by pipetting and 0.5 mL fresh papain solution was added to each sample. To start digesting the brain tissue, tubes with the samples were placed in an incubator for 6 minutes at 37°C. Tubes were covered with foil for all incubations, due to the use of light-sensitive fluorescent substrates. After the 6 minutes, the tubes were removed from the incubator and the brain tissue was dissociated mechanically by pipetting up and down 13 times with a 1-mL pipette tip cut at 0.5 cm. Four additional rounds of incubation and mechanical dissociation were performed. In the second round, mechanical dissociation was performed with a 1-mL pipette tip cut at 0.2 cm, and in subsequent rounds, mechanical dissociation was performed with an uncut 1-mL pipette tip. Papain digest was limited to 5 rounds (30 min) total to avoid pre-apoptotic cells. After this digest, cells were transferred into FACS tubes with strainer caps, using sufficient pressure to make sure that the cells passed through the strainer. Then 2 mL of washing solution for single-cell suspension was passed through the strainer to clean the strainer and stop the enzymatic reaction. Washing solution for single-cell suspension was prepared by adding 975 µL of glucose 15% in water, 250 µL of HEPES 1 M (dissolved in Milli-Q water), and 2.5 mL of FBS to 46.9 mL DPBS, stored for up to 2 months at 4°C, and sterilized with a 0.2-0.22-µm-pore-size filter. After addition of washing solution, contents of the FACS tubes were transferred to 15 mL conical

tubes for subsequent centrifugation. It is easier to see the pellet in conical tubes than in FACS tubes; while a wide variety of tubes are likely suitable for these centrifugation steps, we note that choice of tube can affect yield.

The conical tubes containing the cell suspensions were centrifuged at 500g for 10 minutes at 4°C, and the supernatants were carefully decanted and discarded. Debris was removed using the debris-removal solution, according to the manufacturer's protocol. Cells were resuspended carefully in each tube with 1550 µL DPBS. Then 450 µL of cold debris-removal solution was added and gently mixed by inverting. This solution was gently overlaid (drop by drop) with 2 mL of cold DPBS (creating two phases), before centrifugation at 3000g for 10 minutes at 4°C, with full acceleration and full brake. After centrifugation, three phases formed; the top two phases were aspirated and discarded. If the phases were hard to distinguish, a conservative approach was taken and the top 2 mL was aspirated and discarded. Then each tube was filled up with cold DPBS (2 mL), closed, mixed by inverting three times with no vortexing and centrifuged at 1000g for 10 minutes at 4°C. The supernatant was aspirated and discarded, and the pellet was resuspended in 500 µL PBS with Zombie Aqua™ (BioLegend, 423101) diluted 1:1000 to generate the single-cell suspension.

Flow cytometry and data analysis for *ex vivo* engulfment experiments

To evaluate *ex vivo* engulfment by flow cytometry, 500 µL of single-cell suspension per dissociated brain were moved from 15 mL conical tubes to 1.2-mL FACS library tubes for incubation with Zombie Aqua™ live/dead dye. The suspensions were incubated 15 minutes at room temperature in the dark, and then centrifuged at 300g for 5 minutes at 4°C. For each tube, the supernatant was removed down to 100 µL, and the pellet was resuspended in 400 µL of added PBS with 0.5% BSA.

The contents of each tube were then strained through a 5-mL FACS tube with strainer cap, vortexed to minimize cell clumping, and then run on a Sony MA900 cell sorter at about 1500-2000 events per second (for some more dilute samples, 1000 events per second), with FSC threshold = 6%, FSC gain = 12, BSC gain = 35%, and all fluorophores gain = 40%. Single-color compensation controls were used (see details for individual experiments below). For each sample, 250,000 events were recorded and .fcs files were exported for analysis in FlowJo (v10.0.0). The gating strategy used to identify Live cells was similar to that shown in Fig. 1 – Fig. Supplement 1e, except with Zombie Aqua™ as the live/dead dye rather than Zombie NIR™. Scale data from Live cells were exported as .csv files that were analyzed in R (v4.5.1) for quantification.

Development of an *ex vivo* engulfment assay for ovalbumin

Data for ovalbumin engulfment were acquired over three experiments. In all experiments, ovalbumin-AlexaFluor 647 [ovalbumin] was used at 25 µg/mL (diluted from a 1 mg/mL ovalbumin stock dissolved in PBS) and the fluorophores used on the Sony MA900 sorter were FL3::mCherry (for oScarlet), FL7::BrilliantViolet510 (for Zombie Aqua™ live/dead dye), and FL10::Alexa Fluor® 647 (for ovalbumin).

Importantly, in optimizing the *ex vivo* ovalbumin engulfment assay, we sorted ovalbumin+ cells and verified by confocal microscopy that ovalbumin was localized inside cells rather than binding to the surface of cells.

In the first experiment, four male 41 days old (young adult) and four male 160 days old (old) heterozygous SP-oScarlet killifish were used, as well as single-color compensation controls. The compensation matrix used is included in Supplement 2. Ovalbumin was added to a portion the papain solution after syringe filtration. In this experiment, ovalbumin+ cells were defined as having ovalbumin (FL10-A::Alexa Fluor® 647-A, compensated) intensity of >1000.

In the second experiment, four female 57 days old (young adult) and four female 161 days old (old) heterozygous SP-oScarlet killifish were used, as well as single-color compensation controls (independent compensation controls were used for this experiment). The compensation matrix

used is included in Supplement 3. Ovalbumin was added to a portion the papain solution after syringe filtration. In this experiment, ovalbumin+ cells were defined as having ovalbumin (FL10-A::Alexa Fluor® 647-A, compensated) intensity of >1000.

In the third experiment, two male 63 days old (young adult), and two male 148 days old (old), two female 63 days old (young adult), and two female 167 days old (old) heterozygous

SP-oScarlet killifish were used. No new compensation samples were used in this experiment, as the sex-respective compensation matrices from the previous experiments were re-used. Unlike in the previous experiments, ovalbumin was added to the papain solution before syringe filtration. In this experiment, ovalbumin intensity values were generally lower than observed in the previous two experiments and ovalbumin+ cells were defined as having ovalbumin (FL10-A::Alexa Fluor® 647-A, compensated) intensity of >500.

Our conclusions were not affected by whether ovalbumin was added to the papain solution before or after filtration. However, there was likely some ovalbumin loss when ovalbumin was added before filtration in the third experiment, and the effective ovalbumin concentration in the *ex vivo* engulfment assay was likely lower than the 25 µg/mL reported.

Data on brightness of oScarlet^{HIGH} cells in young adult and old fish were from these ovalbumin engulfment experiments. oScarlet^{HIGH} and oScarlet^{LOW} cells were defined as having oScarlet (FL3-A::mCherry-A, compensated) intensities of >1000 (>500 in Fig. 5 – Fig. Supplement 2b) and <500, respectively. Values presented in Fig. 5c-d, Fig. 5 – Fig. Supplement 1c-d, and Fig. 5 – Fig. Supplement 2b-c were normalized to the average value among for all control samples (always presented as the leftmost category on the x-axis) of the same respective sex and experiment day.

Ex vivo engulfment assay for dextran

Data for dextran engulfment were acquired in one experiment. Dextran-Oregon Green 488 (70 kDa) [dextran] was used at 25 µg/mL (diluted from a 1 mg/mL dextran stock dissolved in PBS) and the fluorophores used on the Sony MA900 sorter were FL1::Alexa Fluor® 488 (for dextran), FL3::mCherry (for oScarlet), and FL7::BrilliantViolet510 (for Zombie Aqua™ live/dead dye).

Four male 56 days old (young adult) and four male 156 days old (old) heterozygous SP-oScarlet killifish were used, as well as single-color compensation controls run the previous day. The compensation matrix used is included in Supplement 4. On the day the eight experimental fish were run, dextran was added to the papain solution before syringe filtration.

In this experiment, dextran+ cells were defined as having dextran (FL1-A::Alexa Fluor® 488-A, compensated) intensity of >800. oScarlet^{HIGH} and oScarlet^{LOW} cells were defined as having oScarlet (FL3-A::mCherry-A, compensated) intensities of >1000 (>500 in Fig. 5 – Fig. Supplement 2d) and <500, respectively. Values presented in Fig. 5e-f, Fig. 5 – Fig. Supplement 1e-f, and Fig. 5 – Fig. Supplement 2d-e were normalized to the average value among for all control samples (always presented as the leftmost category on the x-axis) of the same respective sex and experiment day.

Statistics

No statistical methods were used to determine sample sizes. Sample sizes were determined based on previous experiments with similar types of assays in mice and killifish. No randomization or blinding methods were used, but for dissociation-based experiments, each processing step was carried out in an alternating-by-condition order (e.g., young adult, then old, then young adult, etc.) to minimize the effects of order on the results. All image quantification was automated with scripts in QuPath (v6.0.0). All statistical tests were performed in R (v4.5.1) and plots made with ggplot2 or Seurat. Unless otherwise noted in the figure legends, Wilcoxon rank-sum tests were used to determine statistical significance (paired for matched comparisons; unpaired for all other comparisons). Numbers of experimental replicates, numbers of animals per condition, and whether statistical tests were performed at the per-animal or per-cell level are indicated in individual figure legends.

Figure supplements

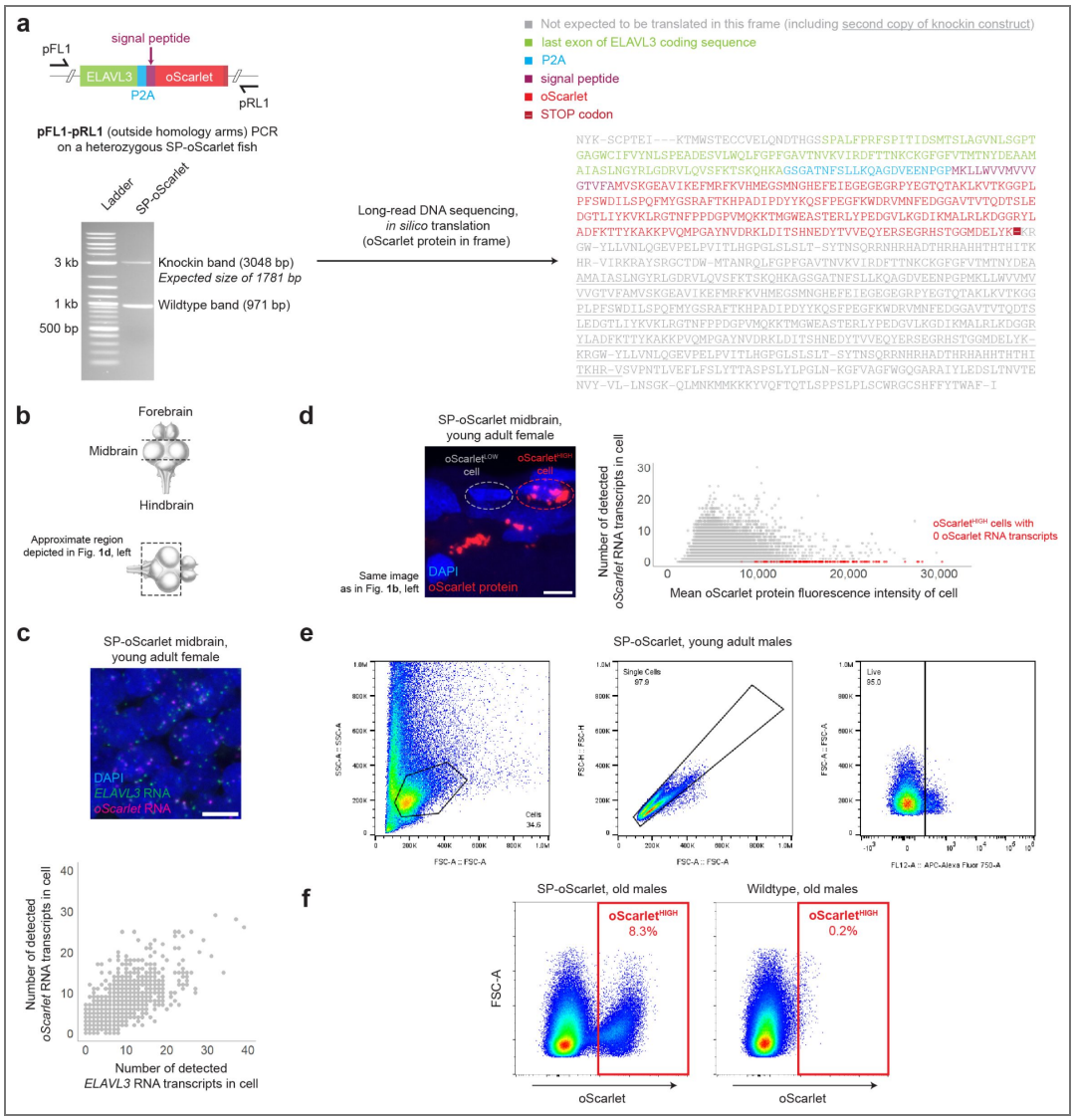

Figure 1 – Figure Supplement 1. **a,** (Left) Schematic for PCR genotyping of a middle-aged (78 days) male heterozygous SP-oScarlet killifish, and DNA gel result (representative of n = 2 fish, 78 days males, in one experiment). (Right) *In silico* translated sequence of sequenced SP-oScarlet insertion (n = 1 fish, 78 days male). **b**, Representation of killifish brain highlighting approximate brain regions as referred to in this study. Art by Massimo Demma (adapted with permission from D'Angelo et al., 2013[169]). **c,** (Above) Representative image of a young adult (59 days) female heterozygous SP-oScarlet killifish brain section, highlighting *ELAVL3* transcripts and *oScarlet* transcripts in the periventricular gray zone, a neuron-dense region of the killifish midbrain. Scale bar = 5 µm. (Below) Per-cell quantification of number of detected *ELAVL3* transcripts and number of detected *oScarlet* transcripts (1,498 cells from n = 4 fish, 59 days females, with 1 region of interest in 1 sagittal brain section per fish, in one experiment). **d**, Same image as in **1b** (left), highlighting examples of oScarlet^{LOW} and oScarlet^{HIGH} cells as detected *in situ*. (Below) Per-cell quantification of mean oScarlet fluorescence intensity and number of detected *oScarlet* transcripts from experiment in **1c** (25,622 cells from n = 10 fish, 59-63 days females, with 3-6 regions of interest over 1-2 sagittal brain sections per fish, over two experiments). Each dot represents one cell. oScarlet^{HIGH} cells that have 0 detected *oScarlet* RNA transcripts are highlighted in red. **e,** FACS plots highlighting gating scheme used to isolate Live cells (as depicted in **1e**) from dissociated young adult male SP-oScarlet brains from experiment in **1d**. **f,** FACS plots highlighting oScarlet^{HIGH} cells notably detected in old (130 days old) male heterozygous SP-oScarlet but not in old (122 days old) male wildtype brains (n = 3 fish per genotype, pooled in one experiment). Each dot represents one cell.

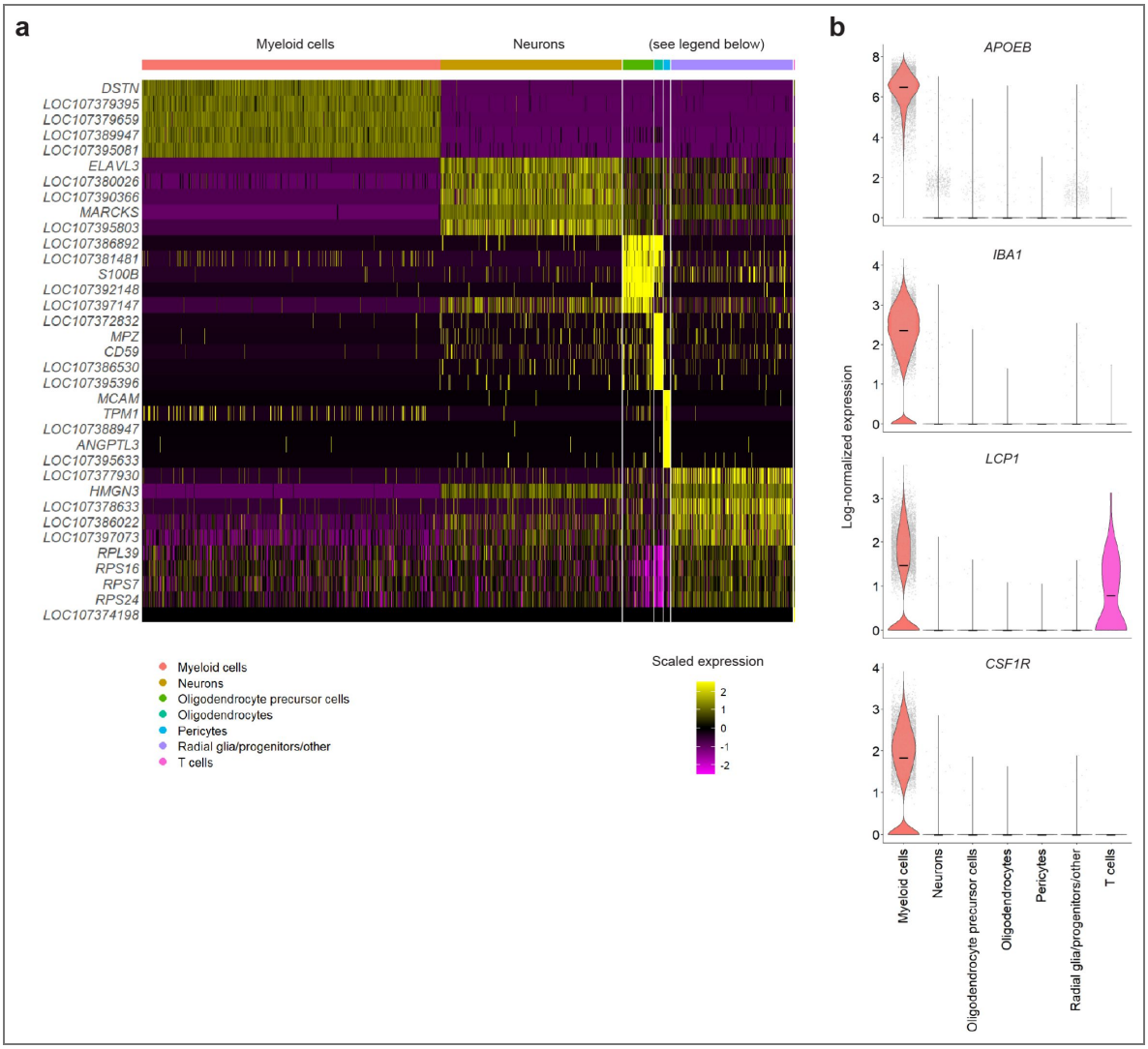

Figure 1 – Figure Supplement 2.

a, Heatmap of expression of top 5 marker genes per cell type, as ranked by area under curve (Presto), in every young adult cell from experiment in **1d**. Full list of cell type marker genes in Supplementary Table 8. **b,** Violin plots from experiment in **1d** highlighting expression of *APOEB* (*LOC10737395*), *IBA1* (*LOC107378674*), *LCP1* (*LOC107389591*), and *CSF1R* (*LOC107387189*) in each cell type. Each dot represents one cell. Lines: medians.

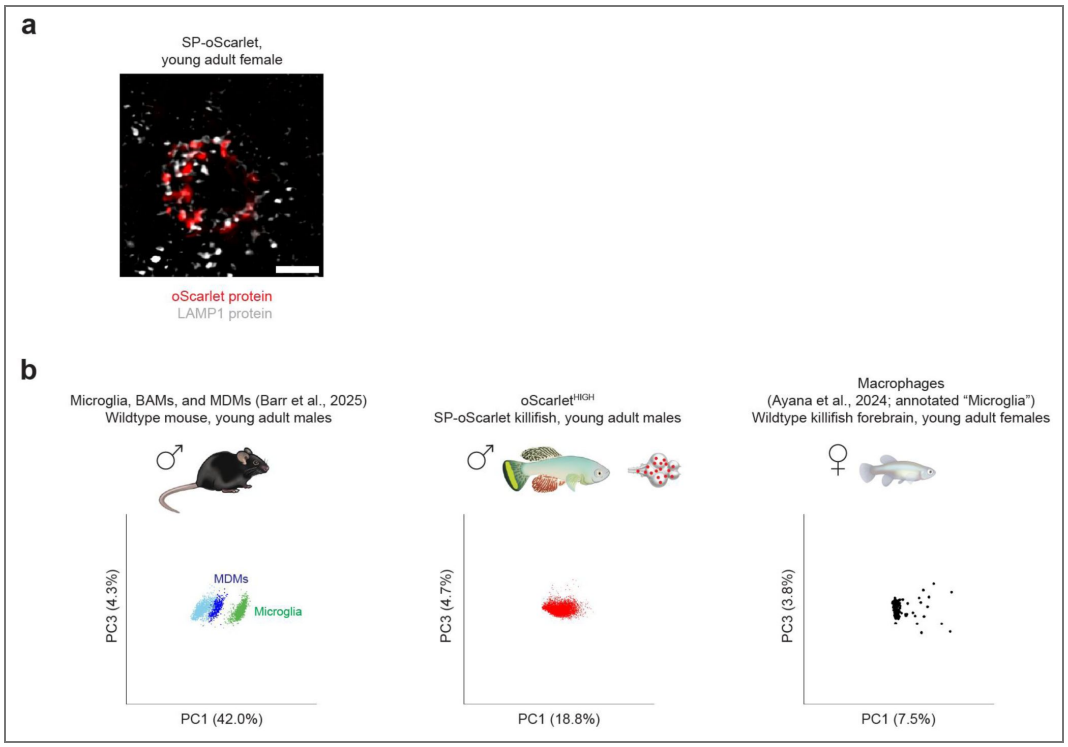

Figure 2 – Figure Supplement 1.

a, Representative image of a young adult (59 days) female heterozygous SP-oScarlet killifish brain section, highlighting oScarlet protein signal colocalized with the late endosome and lysosome marker LAMP1 in an SP-oScarlet brain (representative of n = 8 fish, 59-63 days females, over two experiments). Scale bar = 2 µm. **b,** Principal component analysis (PCA) plots (principal components 1 vs. 3) of wildtype young adult mouse brain macrophages (Barr et al., 2025[75]), young adult oScarlet^{HIGH} cells from experiment in **1d**, and wildtype young adult killifish forebrain macrophages (Ayana et al., 2024[68]) using marker genes of microglia, BAMs, and MDMs from the Barr et al. dataset, or all killifish homologs of these genes. Each dot represents one cell. Percentages on axes represent the percentage of variance explained by each respective principal component.

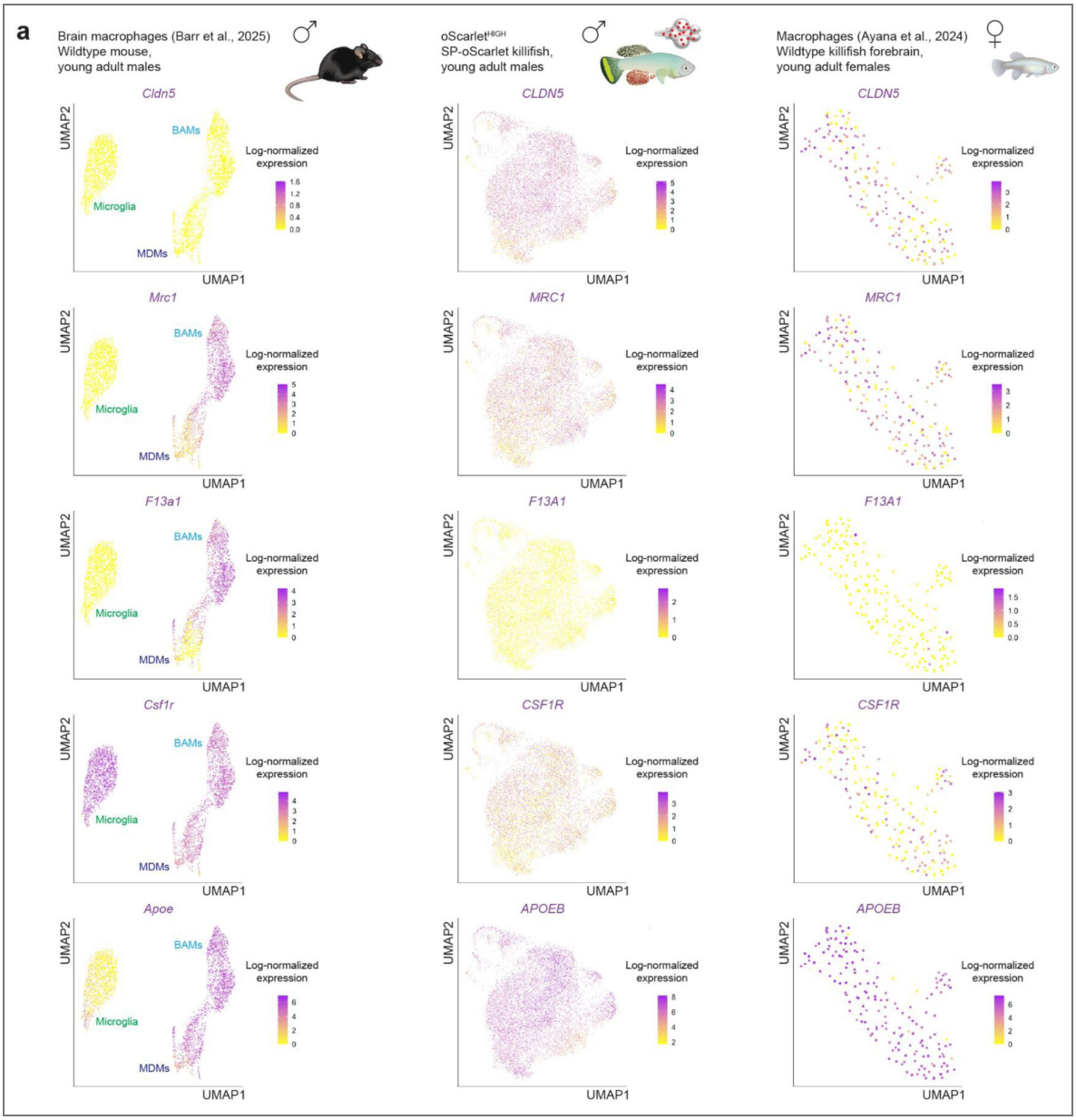

Figure 2 – Figure Supplement 2.

a, UMAPs of wildtype young adult mouse brain macrophages (Barr et al., 2025[75]), young adult oScarlet^{HIGH} cells from experiment in **1d**, and wildtype young adult killifish forebrain macrophages (Ayana et al., 2024[68]) colored according to log-normalized *Cldn5* (or killifish homolog *CLDN5* (*LOC107394244*)), *Mrc1* (or killifish homolog *MRC1* (*LOC107383768*)), *F13a1* (or killifish homolog *F13A1* (*LOC107377057*)), *Csf1r* (or killifish homolog *CSF1R* (*LOC107381415*)), or *Apoe* (or killifish homolog *APOEB* (*LOC107379395*)) expression. Each dot represents one cell.

Figure 2 – Figure Supplement 3.

a, Heatmaps of expression of killifish homologs of strongest microglia, BAM, and MDM marker genes (Barr et al., 2025[75]) in young adult oScarlet^{HIGH} cells from experiment in **1d**.

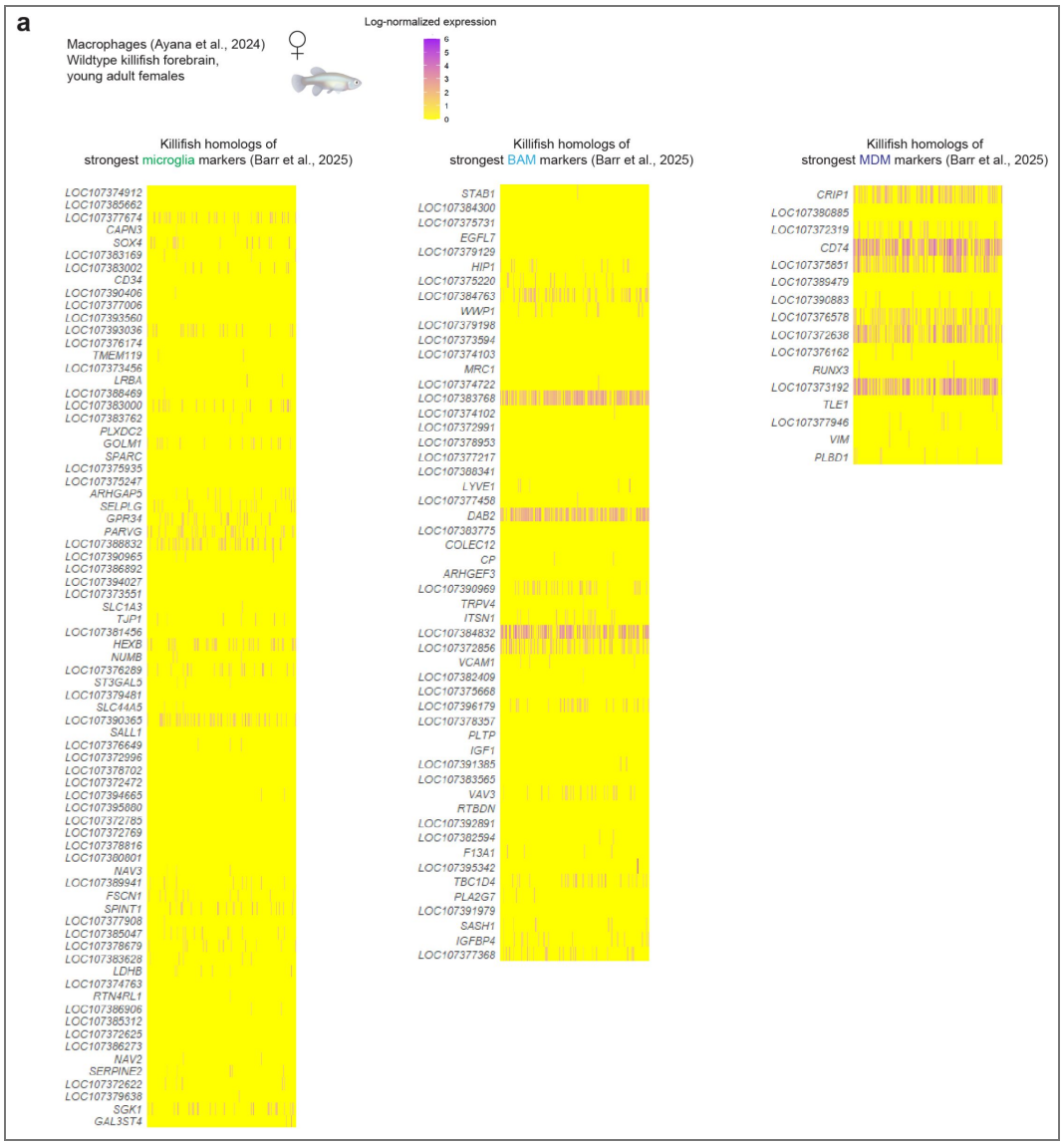

Figure 2 – Figure Supplement 4.

a, Heatmaps of expression of killifish homologs of strongest microglia, BAM, and MDM marker genes (Barr et al., 2025[75]) in wildtype young adult killifish forebrain macrophages (Ayana et al., 2024[68]).

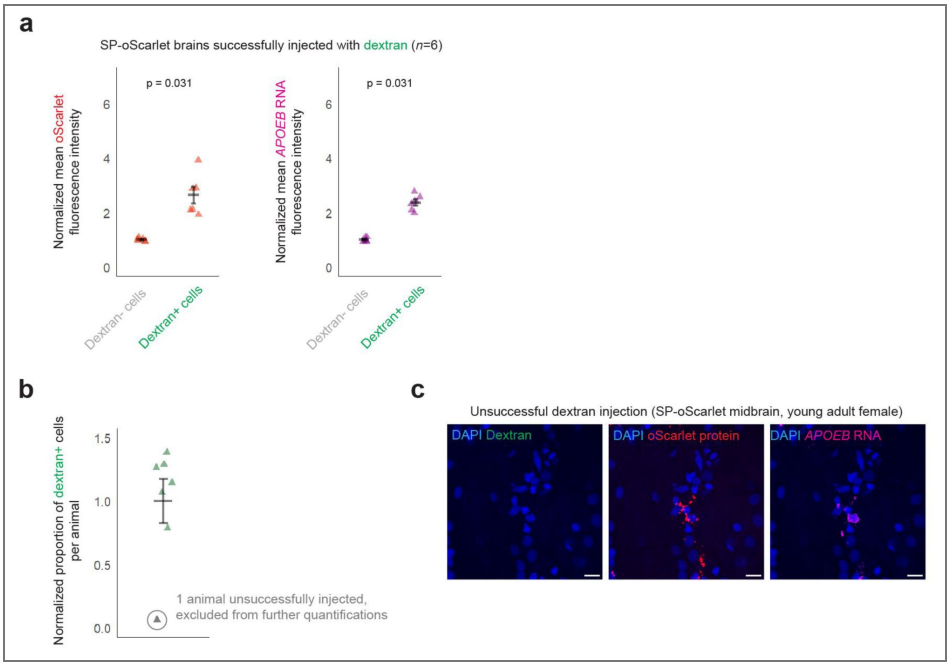

Figure 3 – Figure Supplement 1.

a, Quantification of mean oScarlet fluorescence intensity and mean *APOEB* RNA fluorescence intensity in dextran-negative and dextran-positive cells (n = 6 successfully injected fish, 63-91 days females, with 5-6 regions of interest over 1-2 sagittal brain sections per fish, over two experiments). Four images (one image per fish for each of four fish) of regions of interest with a visually apparent very high density of cells with high *APOEB* RNA expression, which could plausibly reflect an injection-related injury, were excluded from quantifications. The excluded images are listed in Supplementary Table 4. Each triangle represents one fish. Mean +/-standard error of mean; p-values, paired Wilcoxon rank-sum test at per-animal level. **b,** Quantification from experiment in **3a** of proportion of dextran-positive cells per fish (n = 7 fish, 63-91 days females, with 5-6 regions of interest over 1-2 sagittal brain sections per fish, over two experiments), highlighting in grey one fish in which dextran was not observed to circulate throughout the brain (also confirmed by visual inspection of sections). This unsuccessfully injected fish (63 days, female) was excluded from subsequent quantifications. Each triangle represents one fish. **c,** Representative image of brain sections from the young adult (63 days) female heterozygous SP-oScarlet killifish unsuccessfully injected with dextran (n = 1 fish). Scale bars = 10 µm.

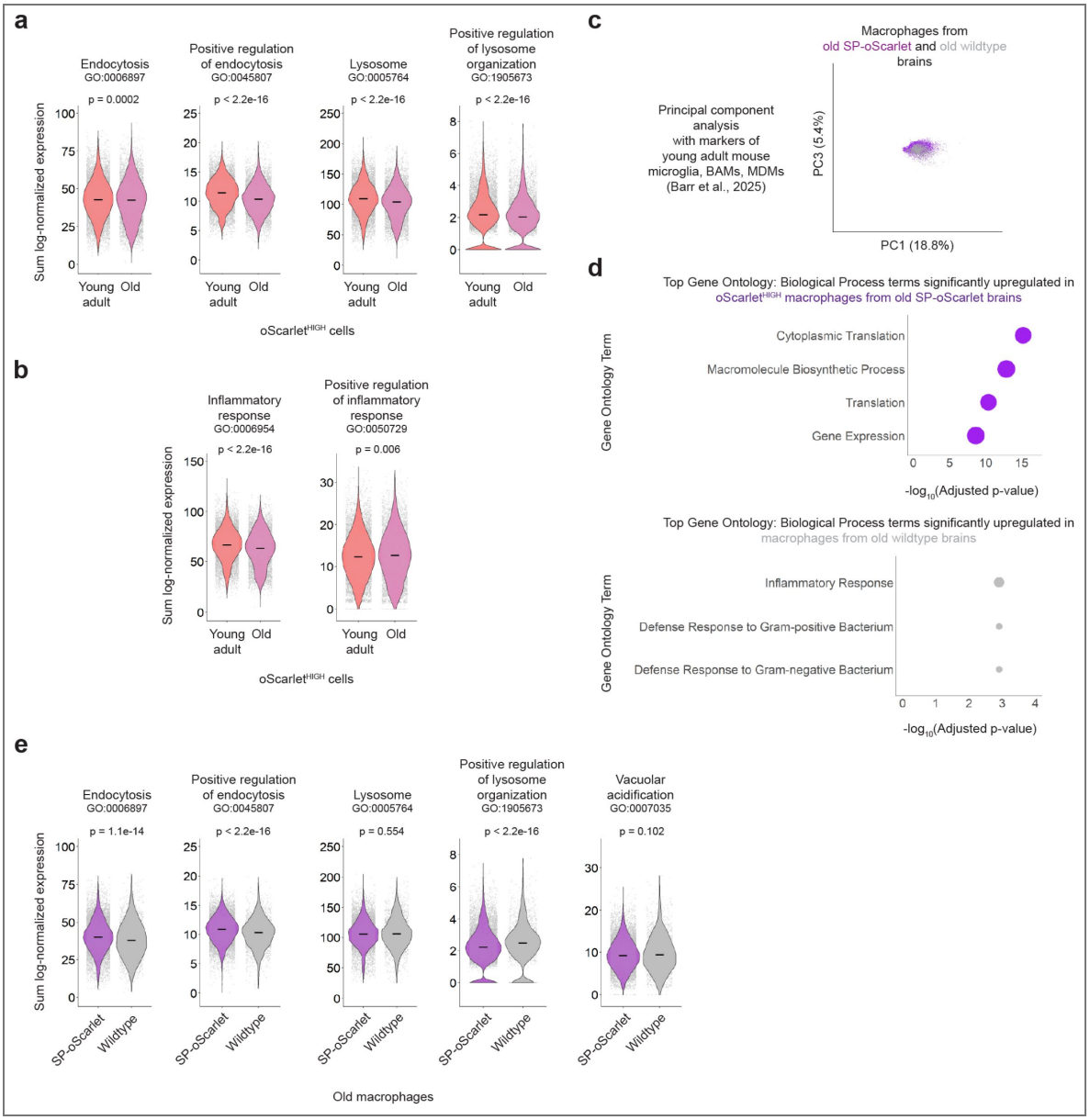

Figure 4 – Figure Supplement 1.

a, Violin plots for sum log-normalized expression of genes in Gene Ontology: Biological Process terms “endocytosis” (GO:0006897), “positive regulation of endocytosis” (GO:0045807), “lysosome” (GO:0005764), and “positive regulation of lysosome organization” (GO:1905673) in young adult and old oScarlet^{HIGH} cells from experiment in **1d**. Each dot represents one cell. Lines: medians; p-values, unpaired Wilcoxon rank-sum test at per-cell level (fish were pooled for single cell RNA-sequencing experiments to obtain sufficient numbers of oScarlet^{HIGH} cells). **b**, Violin plots for sum log-normalized expression of genes in Gene Ontology: Biological Process terms “inflammatory response” (GO:0006954) and “positive regulation of inflammatory response” (GO:0050729) in young adult and old oScarlet^{HIGH} cells from experiment in **1d**. Each dot represents one cell. Lines: medians; p-values, unpaired Wilcoxon rank-sum test at per-cell level. **c,** PCA plot (principal components 1 vs. 3) of oScarlet^{HIGH} and wildtype old killifish brain macrophages from experiment in **4e** using all killifish homologs of marker genes of microglia, BAMs, and MDMs (Barr et al., 2025[75]). Each dot represents one cell. Percentages on axes represent the percentage of variance explained by each respective principal component. **d,** Top Gene Ontology: Biological Process terms upregulated in old oScarlet^{HIGH} macrophages (above) and in old wildtype macrophages (below) from experiment in **4e**, as ranked by adjusted p-value (Fisher’s exact test, Benjamini-Hochberg FDR-corrected). Size of each circle corresponds to number of distinct human homologs among differentially expressed genes from each term. Full lists of differentially expressed genes and upregulated terms in Supplementary Tables 12-14. **e,** Violin plots for sum log-normalized expression of genes in Gene Ontology: Biological Process terms “endocytosis” (GO:0006897), “positive regulation of endocytosis” (GO:0045807), “lysosome” (GO:0005764), “positive regulation of lysosome organization” (GO:1905673), and “vacuolar acidification” (GO: 0007035) in old oScarlet^{HIGH} and old wildtype macrophages from experiment in **4e**. Each dot represents one cell. Lines: medians; p-values, unpaired Wilcoxon rank-sum test at per-cell level.

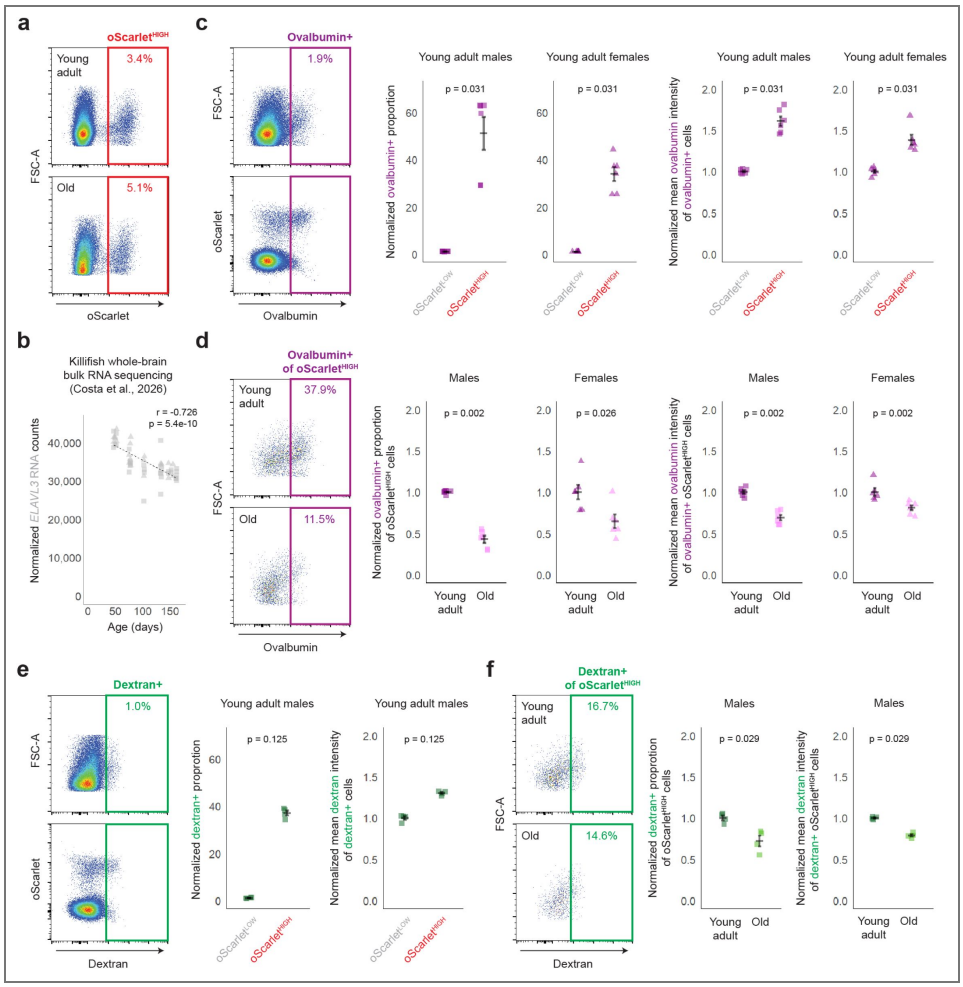

Figure 5 – Figure Supplement 1.

a, Representative flow cytometry plots from young adult (41 days, above) and old (160 days, below) male heterozygous SP-oScarlet killifish brains, highlighting oScarlet^{HIGH} cells. Each dot represents one cell. **b,** Plot of normalized *ELAVL3* (*LOC107378364*) RNA counts across age from bulk RNA sequencing of whole killifish brains (Costa et al., 2026[55]). Each square (male) or triangle (female) represents one fish. Dashed line: linear regression. r: Pearson correlation coefficient; p-value, two-sided t-test. **c,** (Left) Representative flow cytometry plots from young adult (41 days) male heterozygous SP-oScarlet killifish brains, highlighting ovalbumin+ cells as identified from all Live cells, with mean ovalbumin fluorescence intensity plotted against either FSC-A (above) or mean oScarlet fluorescence intensity (below). Each dot represents one cell. (Right) Quantifications of proportion of ovalbumin+ cells and mean ovalbumin fluorescence intensity of ovalbumin+ cells among young adult oScarlet^{LOW} and oScarlet^{HIGH} cells (same experiments as in **5a**). Each square (male) or triangle (female) represents one fish. Mean +/-standard error of mean; p-values, paired Wilcoxon rank-sum test at per-animal level. **d,** (Left) Representative flow cytometry plots from young adult (41 days) (above) and old (160 days) (below) male heterozygous SP-oScarlet killifish brains, highlighting ovalbumin+ oScarlet^{HIGH} cells. Each dot represents one cell. (Right) Quantifications of proportion of ovalbumin+ cells and mean ovalbumin fluorescence intensity of ovalbumin+ cells among young adult and old oScarlet^{HIGH} cells (same experiments as in **5a**). Each square (male) or triangle (female) represents one fish. Mean +/-standard error of mean; p-values, unpaired Wilcoxon rank-sum test at per-animal level. **e,** (Left) Representative flow cytometry plots from young adult (56 days) male heterozygous SP-oScarlet killifish brains, highlighting dextran+ cells as identified from all Live cells, with mean dextran fluorescence intensity plotted against either FSC-A (above) or mean oScarlet fluorescence intensity (below). Each dot represents one cell. (Right) Quantifications of proportion of dextran+ cells and mean dextran fluorescence intensity of dextran+ cells among young adult oScarlet^{LOW} and oScarlet^{HIGH} cells (same experiment as in **5e**). Each square represents one fish. Mean +/- standard error of mean; p-values, paired Wilcoxon rank-sum test at per-animal level. **f,** (Left) Representative flow cytometry plots from young adult (56 days) (above) and old (156 days) (below) male heterozygous SP-oScarlet killifish brains, highlighting dextran+ oScarlet^{HIGH} cells. Each dot represents one cell. (Right) Quantifications of proportion of dextran+ cells and mean dextran fluorescence intensity of dextran+ cells among young adult and old oScarlet^{HIGH} cells (same experiment as in **5e**). Each square represents one fish. Mean +/- standard error of mean; p-values, unpaired Wilcoxon ranksum test at per-animal level.

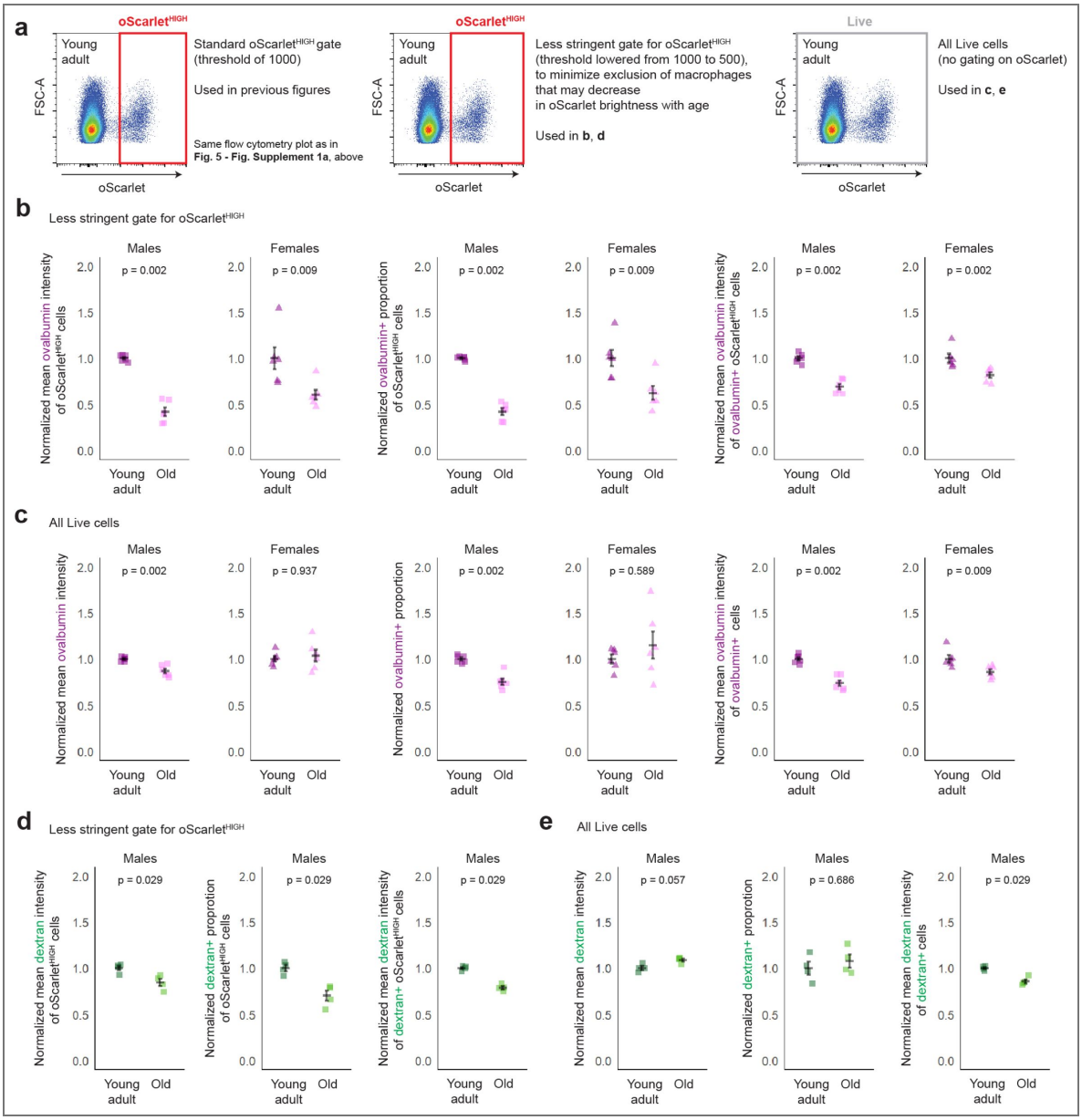

Figure 5 – Figure Supplement 2.

a, Same flow cytometry plot as in **5S1a** (above), illustrating alternative gating schemes used in subsequent panels. **b,** Quantifications of mean ovalbumin fluorescence intensity, proportion of ovalbumin+ cells, and mean ovalbumin fluorescence intensity of ovalbumin+ cells among young adult and old oScarlet^{HIGH} cells (same experiments as in **5a**) with a less stringent oScarlet^{HIGH} gate (lowered from 1000 to 500). Each square (male) or triangle (female) represents one fish. Mean +/-standard error of mean; p-values, unpaired Wilcoxon rank-sum test at per-animal level. **c,** Quantifications of mean ovalbumin fluorescence intensity, proportion of ovalbumin+ cells, and mean ovalbumin fluorescence intensity of ovalbumin+ cells among all young adult and old cells (same experiments as in **5a**, no gating for oScarlet). Each square (male) or triangle (female) represents one fish. Mean +/- standard error of mean; p-values, unpaired Wilcoxon rank-sum test at per-animal level. **d,** Quantifications of mean dextran fluorescence intensity, proportion of dextran+ cells, and mean dextran fluorescence intensity of dextran+ cells among young adult and old oScarlet^{HIGH} cells (same experiment as in **5e**) with a less stringent oScarlet^{HIGH} gate (lowered from 1000 to 500). Each square represents one fish. Mean +/- standard error of mean; p-values, unpaired Wilcoxon rank-sum test at per-animal level. **e,** Quantifications of mean dextran fluorescence intensity, proportion of dextran+ cells, and mean dextran fluorescence intensity of dextran+ cells among all young adult and old Live cells (same experiment as in **5e**, no gating for oScarlet). Each square represents one fish. Mean +/-standard error of mean; p-values, unpaired Wilcoxon rank-sum test at per-animal level.

Data availability

Sequencing reads are publicly available at NCBI GEO (GEO accession: GSE329891). Seurat objects generated in this study are available at Zenodo (record: 19672958). Other raw data (images, etc.) will be made available upon request. Code is available at Github (*https://github.com/RNagvekar/killifish_brain_macrophages*).

Acknowledgements

We thank Jason W. Miklas, Nimrod Rappoport, and Daniel J. Richard for critical reading of the manuscript; Natalie Schmahl and Sarah R. Boyle for help with killifish colony management; Jacob Chung, Rishad Khondker, Maddie Housh, Jason Yang, and Ian H. Guldner for help with killifish husbandry; Justin You, Aleksandra S. Tsenter, Merve Heinzer-Avar, Daniel Heinzer-Avar, and Julliana Ramirez-Matias for advice on brain sectioning and imaging analysis; Giulia Notarangelo, Andy P. Tsai, and Jaeyoon Lee for advice on flow cytometry; Olivia Y. Zhou for advice on design of single-cell RNA sequencing experiments, Nimrod Rappoport and Daniel J. Richard for advice on single-cell RNA sequencing data analysis; Alec J. Walker and Constanze Depp for advice on interpretation of single-cell RNA sequencing data; Ryann M. Fame and Blake J. Laham for advice on brain injections; Katrin I. Andreasson, Kyle G. Daniels, Andrew Z. Fire, Daniel F. Jarosz, and Judith Frydman, Charu Ramakrishnan, Lu Zhou, Gil Vantomme, Katharina Papsdorf, Eric D. Sun and all of the Brunet lab for helpful discussions and advice; and Nimrod Rappoport and Daniel J. Richard for code-checking. This project was supported, in part, by Award Number 1S10OD034400-01A1 from the National Center for Research Resources (NCRR). Its contents are solely the responsibility of the authors and do not necessarily represent the official views of the NCRR or the National Institutes of Health. Funding for this study was provided by the Simons Foundation (to A.B., B.S., T.W.C., and P.M.), the Knight Initiative for Brain Resilience (to A.B., T.W.C., and R.D.N.), the Glenn Foundation for Medical Research (to A.B.), the NOMIS Foundation (to A.B. and T.W.C.), the National Institute on Aging K99 Pathway to Independence Award (to R.D.N. and C.N.B.), the Simons Foundation Fellows-to-Faculty Award (to J.B.J.), and the Stanford Knight-Hennessy Scholars (to R.N.).

Additional information

Author contributions

This study was conceived by R.N., R.D.N., C.N.B., and A.B. R.N. designed the SP-oScarlet killifish line, and R.D.N. generated this line with help from R.N.. C.N.B. designed probes for some hybridization chain reaction experiments and checked code. R.N. designed and performed all experiments and analyses unless noted. A.N.P. performed structured illumination microscopy for LAMP1 imaging and helped with brain dissociations and FACS for *ex vivo* engulfment assays and single-cell RNA sequencing. P.R.K. (under the guidance of B.W.) performed cell type evolution analysis that aided interpretation of single-cell RNA sequencing data. H.J.B. (under the guidance of B.S.) helped design *ex vivo* engulfment assays and interpret single-cell RNA sequencing data, including by sharing unpublished mouse single-cell RNA sequencing datasets. A.M.M.J. (under the guidance of K.R.H.) performed brain clearing and 3D imaging. S.V.P. helped with brain injections. E.K.C. (under the guidance of T.W.C.) and J.C. performed sulfo-NHS-biotin perfusion for vasculature colocalization analysis. J.C. also helped with sample processing for single-cell RNA sequencing. F.B. helped with brain dissociations and flow cytometry for *ex vivo* engulfment assays and checked code. L.A.S. (under the guidance of S.R.Q.) and P.N.N. helped with 10x Genomics single-cell RNA sequencing. J.B.J. (under the guidance of P.M.) helped develop the brain injection protocol. E.K.C. (under the guidance of T.W.C.) and R.B. helped develop the FACS sorting strategy. R.B. also helped with brain sectioning and immunofluorescence staining optimization. P.P.S. produced the gene names conversion table used to identify homologs across species. The manuscript was written by R.N. and A.B., and all authors provided comments.

Funding

Funder	Grant reference number	Author
HHS | NIH | National Institute on Aging (NIA)	K99AG078499	Ravi D Nath Claire Nicole Bedbrook
HHS | NIH | National Institute on Aging (NIA)	K99AG076879	Ravi D Nath Claire Nicole Bedbrook
Simons Foundation (SF)	AN-NC-AB-Research-00811219	Anne Brunet
Glenn Foundation for Medical Research (GFMR)	SPO123100	Anne Brunet
NOMIS Stiftung (NOMIS Foundation)	Agreement-AB-26.2023	Anne Brunet
Knight Initiative for Brain Resilience		Ravi D Nath Anne Brunet Tony Wyss-Coray
Knight-Hennessy Scholars		Rahul Nagvekar
National Center for Research Resources	1S10OD034400-01A1	Angela N Pogson

Author ORCID iDs

Rahul Nagvekar: https://orcid.org/0000-0001-8800-7503
SV Perry: https://orcid.org/0009-0005-9371-5869
Felix Boos: https://orcid.org/0000-0002-1571-9806
Stephen R Quake: https://orcid.org/0000-0002-1613-0809
Tony Wyss-Coray: https://orcid.org/0000-0001-5893-0831
Kristy Red-Horse: https://orcid.org/0000-0003-1541-601X
Beth Stevens: https://orcid.org/0000-0003-4226-1201
Ravi D Nath: https://orcid.org/0000-0003-0905-2707
Anne Brunet: https://orcid.org/0000-0002-4608-6845

Additional files

Supplementary Tables. Supplementary Table 1. Animals used in this study. Supplementary Table 2. Nucleic acid sequences used in this study. Supplementary Table 3. Antibodies used in this study. Supplementary Table 4. Images taken in this study. Supplementary Table 5. Gene names conversion table used to identify homologs across species in this study. Supplementary Table 6. Quality control metrics for Seurat objects generated from raw reads of killifish single-cell RNA sequencing data in this study. Supplementary Table 7. Cluster marker genes based on all young adult cells from August 2025 single-cell RNA sequencing experiment. Supplementary Table 8. Cell type marker genes based on all young adult cells from August 2025 single-cell RNA sequencing experiment. Supplementary Table 9. Differentially expressed genes between young adult and old oScarlet^{HIGH} cells from August 2025 single-cell RNA sequencing experiment. avg_log2FC > 0 indicates enrichment in old oScarlet^{HIGH} cells. avg_log2FC < 0 indicates enrichment in young adult oScarlet^{HIGH} cells. pct. 1 corresponds to the percentage of old oScarlet^{HIGH} cells with detectable expression of the gene. pct. 2 corresponds to the percentage of young adult oScarlet^{HIGH} cells with detectable expression of the gene. Supplementary Table 10. Gene Ontology: Biological Process (2025) terms upregulated in young adult oScarlet^{HIGH} cells from August 2025 single-cell RNA sequencing experiment. Supplementary Table 11. Gene Ontology: Biological Process (2025) terms upregulated in old oScarlet^{HIGH} cells from August 2025 single-cell RNA sequencing experiment. Supplementary Table 12. Differentially expressed genes between old oScarlet^{HIGH} and old wildtype macrophages from October 2024 single-cell RNA sequencing experiment. avg_log2FC > 0 indicates enrichment in old oScarlet^{HIGH} macrophages. avg_log2FC < 0 indicates enrichment in old wildtype macrophages. pct. 1 corresponds to the percentage of old

oScarlet^{HIGH} macrophages with detectable expression of the gene. pct. 2 corresponds to the percentage of old wildtype macrophages with detectable expression of the gene. Supplementary Table 13. Gene Ontology: Biological Process (2025) terms upregulated in old oScarlet^{HIGH} macrophages from October 2024 single-cell RNA sequencing experiment. Supplementary Table 14. Gene Ontology: Biological Process (2025) terms upregulated in old wildtype macrophages from October 2024 single-cell RNA sequencing experiment.

Source Data Tables. Source Data Table 1. Corresponding to Fig. 3a. Source Data Table 2. Corresponding to Fig. 3 – Supplementary Fig. 1a. Source Data Table 3. Corresponding to Fig. 3 – Supplementary Fig. 1b. Source Data Table 4. Supporting information for analysis in Fig. 3b. Source Data Table 5. Supporting information for analysis in Fig. 3b. Source Data Table 6. Corresponding to Fig. 3b. Source Data Table 7. Corresponding to Fig. 5a, Fig. 5c-d, and Fig. 5 – Fig. Supplement 1c-d. Source Data Table 8. Corresponding to Fig. 5 – Fig. Supplement 2b. Source Data Table 9. Corresponding to Fig. 5 – Fig. Supplement 2c. For this analysis, the threshold for oScarlet^{HIGH} was set to 0. Source Data Table 10. Corresponding to Fig. 5e-f and Fig. 5 – Fig. Supplement 1e-f. Source Data Table 11. Corresponding to Fig. 5 – Fig. Supplement 2d. Source Data Table 12. Corresponding to Fig. 5 – Fig. Supplement 2e. For this analysis, the threshold for oScarlet^{HIGH} was set to 0.

Additional Supplements. Supplement 1. SnapGene map file of expected SP-oScarlet insertion. Supplement 2. Compensation matrix from first *ex vivo* ovalbumin engulfment experiment. Supplement 3. Compensation matrix from second *ex vivo* ovalbumin engulfment experiment. Supplement 4. Compensation matrix from *ex vivo* dextran engulfment experiment.

References

1. **Kaur J,** et al. (2021) Waste Clearance in the Brain. *Front Neuroanat* **15**:665803 https://doi.org/10.3389/fnana.2021.665803 | PubMed
2. **Smyth LCD,** Beschorner N, Nedergaard M, Kipnis J (2025) Cellular Contributions to Glymphatic and Lymphatic Waste Clearance in the Brain. *Cold Spring Harb Perspect Biol* **17** https://doi.org/10.1101/cshperspect.a041370 | PubMed
3. **Kipnis J,** et al. (2025) Resolving the mysteries of brain clearance and immune surveillance. *Neuron* **113**:3908-3923 https://doi.org/10.1016/j.neuron.2025.10.036 | PubMed
4. **Kida S,** Steart PV, Zhang ET, Weller RO (1993) Perivascular cells act as scavengers in the cerebral perivascular spaces and remain distinct from pericytes, microglia and macrophages. *Acta Neuropathol* **85**:646-52 https://doi.org/10.1007/bf00334675 | PubMed
5. **Gaudi AU,** et al. (2026) Convergent evolution of scavenger cell development at brain borders. *Nature* https://doi.org/10.1038/s41586-025-10003-3 | PubMed
6. **Venero Galanternik M,** et al. (2017) A novel perivascular cell population in the zebrafish brain. *eLife* **6** https://doi.org/10.7554/elife.24369 | PubMed
7. **Uphoff K,** Suárez I, van Impel A, Schulte-Merker S (2024) dab2 is required for the scavenging function of lymphatic endothelial cells in the zebrafish meninges. *Sci Rep* **14**:27942 https://doi.org/10.1038/s41598-024-76590-9 | PubMed
8. **Mato M,** et al. (1996) Involvement of specific macrophage-lineage cells surrounding arterioles in barrier and scavenger function in brain cortex. *Proc Natl Acad Sci U S A* **93**:3269-74 https://doi.org/10.1073/pnas.93.8.3269 | PubMed
9. **Kim WK,** et al. (2006) CD163 identifies perivascular macrophages in normal and viral encephalitic brains and potential precursors to perivascular macrophages in blood. *Am J Pathol* **168**:822-34 https://doi.org/10.2353/ajpath.2006.050215 | PubMed
10. **Drieu A,** et al. (2022) Parenchymal border macrophages regulate the flow dynamics of the cerebrospinal fluid. *Nature* **611**:585-593 https://doi.org/10.1038/s41586-022-05397-3 | PubMed

11. **Da Mesquita S,** Rua R (2024) Brain border-associated macrophages: common denominators in infection, aging, and Alzheimer's disease?. *Trends Immunol* **45**:346-357 https://doi.org/10.1016/j.it.2024.03.007 | PubMed
12. **Vara-Pérez M,** Movahedi K (2025) Border-associated macrophages as gatekeepers of brain homeostasis and immunity. *Immunity* **58**:1085-1100 https://doi.org/10.1016/j.immuni.2025.04.005 | PubMed
13. **Beiter RM,** Sheehan PW, Schafer DP (2024) Microglia phagocytic mechanisms: Development informing disease. *Curr Opin Neurobiol* **86**:102877 https://doi.org/10.1016/j.conb.2024.102877 | PubMed
14. **Dong Y,** et al. (2021) Oxidized phosphatidylcholines found in multiple sclerosis lesions mediate neurodegeneration and are neutralized by microglia. *Nat Neurosci* **24**:489-503 https://doi.org/10.1038/s41593-021-00801-z | PubMed
15. **Lawrence AR,** et al. (2024) Microglia maintain structural integrity during fetal brain morphogenesis. *Cell* **187**:962-980.e19 https://doi.org/10.1016/j.cell.2024.01.012 | PubMed
16. **Guldner IH,** et al. (2026) Ageing promotes microglial accumulation of slow-degrading synaptic proteins. *Nature* **650**:930-941 https://doi.org/10.1038/s41586-025-09987-9 | PubMed
17. **Sokolowski JD,** Mandell JW (2011) Phagocytic clearance in neurodegeneration. *Am J Pathol* **178**:1416-28 https://doi.org/10.1016/j.ajpath.2010.12.051 | PubMed
18. **Da Mesquita S,** et al. (2018) Functional aspects of meningeal lymphatics in ageing and Alzheimer's disease. *Nature* **560**:185-191 https://doi.org/10.1038/s41586-018-0368-8 | PubMed
19. **Jeong YM,** et al. (2021) Differential Clearance of Aβ Species from the Brain by Brain Lymphatic Endothelial Cells in Zebrafish. *Int J Mol Sci* 22 https://doi.org/10.3390/ijms222111883 | PubMed
20. **Da Mesquita S,** et al. (2021) Aging-associated deficit in CCR7 is linked to worsened glymphatic function, cognition, neuroinflammation, and β-amyloid pathology. *Sci Adv* **7** https://doi.org/10.1126/sciadv.abe4601 | PubMed
21. **Caron NS,** et al. (2022) Cerebrospinal fluid biomarkers for assessing Huntington disease onset and severity. *Brain Commun* **4**:fcac309 https://doi.org/10.1093/braincomms/fcac309 | PubMed
22. **Kaiser S,** et al. (2023) A proteogenomic view of Parkinson's disease causality and heterogeneity. *NPJ Parkinsons Dis* **9**:24 https://doi.org/10.1038/s41531-023-00461-9 | PubMed
23. **Johnson ECB,** et al. (2023) Cerebrospinal fluid proteomics define the natural history of autosomal dominant Alzheimer's disease. *Nat Med* **29**:1979-1988 https://doi.org/10.1038/s41591-023-02476-4 | PubMed
24. **Dammer EB,** et al. (2024) Proteomic analysis of Alzheimer's disease cerebrospinal fluid reveals alterations associated with APOE ε4 and atomoxetine treatment. *Sci Transl Med* **16**:eadn3504 https://doi.org/10.1126/scitranslmed.adn3504 | PubMed
25. **Shen Y,** et al. (2024) CSF proteomics identifies early changes in autosomal dominant Alzheimer's disease. *Cell* **187**:6309-6326.e15 https://doi.org/10.1016/j.cell.2024.08.049 | PubMed
26. **Peña-Bautista C,** et al. (2024) Defining Alzheimer's Disease through Proteomic CSF Profiling. *J Proteome Res* **23**:5096-5106 https://doi.org/10.1021/acs.jproteome.4c00590 | PubMed
27. **Ali M,** et al. (2025) Multi-cohort cerebrospinal fluid proteomics identifies robust molecular signatures across the Alzheimer disease continuum. *Neuron* **113**:1363-1379.e9 https://doi.org/10.1016/j.neuron.2025.02.014 | PubMed
28. **Oh HS,** et al. (2025) A cerebrospinal fluid synaptic protein biomarker for prediction of cognitive resilience versus decline in Alzheimer's disease. *Nat Med* **31**:1592-1603 https://doi.org/10.1038/s41591-025-03565-2 | PubMed
29. **Farinas A,** et al. (2025) Disruption of the cerebrospinal fluid-plasma protein balance in cognitive impairment and aging. *Nat Med* **31**:2578-2589 https://doi.org/10.1038/s41591-025-03831-3 | PubMed

30. **Seo D,** et al. (2025) Cerebrospinal fluid proteomic signatures in cognitively normal individuals identify distinct clusters linked to neurodegeneration. *Nat Aging* **5**:2125-2141 https://doi.org/10.1038/s43587-025-00971-6 | PubMed

31. **Tarasoff-Conway JM,** et al. (2015) Clearance systems in the brain-implications for Alzheimer disease. *Nat Rev Neurol* **11**:457-70 https://doi.org/10.1038/nrneurol.2015.119 | PubMed

32. **van Dyck CH,** et al. (2023) Lecanemab in Early Alzheimer's Disease. *N Engl J Med* **388**:9-21 https://doi.org/10.1056/nejmoa2212948 | PubMed

33. **Sims JR,** et al. (2023) Donanemab in Early Symptomatic Alzheimer Disease: The TRAILBLAZER-ALZ 2 Randomized Clinical Trial. *Jama* **330**:512-527 https://doi.org/10.1001/jama.2023.13239 | PubMed

34. **Li X,** et al. (2024) Promising outcomes 5 weeks after a surgical cervical shunting procedure to unclog cerebral lymphatic systems in a patient with Alzheimer's disease. *Gen Psychiatr* **37**:e101641 https://doi.org/10.1136/gpsych-2024-101641 | PubMed

35. **Bonnar O,** Eyre B, van Veluw SJ (2025) Perivascular brain clearance as a therapeutic target in cerebral amyloid angiopathy and Alzheimer's disease. *Neurotherapeutics* **22**:e00535 https://doi.org/10.1016/j.neurot.2025.e00535 | PubMed

36. **Keil SA,** Jansson D, Braun M, Iliff JJ (2025) Glymphatic dysfunction in Alzheimer's disease: A critical appraisal. *Science* **389**:eadv8269 https://doi.org/10.1126/science.adv8269 | PubMed

37. **Erhardt EB,** et al. (2025) The influence of intermittent hypercapnia on cerebrospinal fluid flow and clearance in Parkinson's disease and healthy older adults. *NPJ Parkinsons Dis* **11**:334 https://doi.org/10.1038/s41531-025-01179-6 | PubMed

38. **Hu CK,** Brunet A (2018) The African turquoise killifish: A research organism to study vertebrate aging and diapause. *Aging Cell* **17**:e12757 https://doi.org/10.1111/acel.12757 | PubMed

39. **Terzibasi E,** et al. (2008) Large differences in aging phenotype between strains of the short-lived annual fish Nothobranchius furzeri. *PLoS One* **3**:e3866 https://doi.org/10.1371/journal.pone.0003866 | PubMed

40. **Terzibasi E,** et al. (2009) Effects of dietary restriction on mortality and age-related phenotypes in the short-lived fish Nothobranchius furzeri. *Aging Cell* **8**:88-99 https://doi.org/10.1111/j.1474-9726.2009.00455.x | PubMed

41. **Tozzini ET,** Baumgart M, Battistoni G, Cellerino A (2012) Adult neurogenesis in the short-lived teleost Nothobranchius furzeri: localization of neurogenic niches, molecular characterization and effects of aging. *Aging Cell* **11**:241-51 https://doi.org/10.1111/j.1474-9726.2011.00781.x | PubMed

42. **Harel I,** et al. (2015) A platform for rapid exploration of aging and diseases in a naturally short-lived vertebrate. *Cell* **160**:1013-1026 https://doi.org/10.1016/j.cell.2015.01.038 | PubMed

43. **Smith P,** et al. (2017) Regulation of life span by the gut microbiota in the short-lived African turquoise killifish. *eLife* **6** https://doi.org/10.7554/elife.27014 | PubMed

44. **Kelmer Sacramento E,** et al. (2020) Reduced proteasome activity in the aging brain results in ribosome stoichiometry loss and aggregation. *Mol Syst Biol* **16**:e9596 https://doi.org/10.15252/msb.20209596 | PubMed

45. **Vanhunsel S,** et al. (2021) The killifish visual system as an in vivo model to study brain aging and rejuvenation. *NPJ Aging Mech Dis* **7**:22 https://doi.org/10.1038/s41514-021-00077-4 | PubMed

46. **Van Houcke J,** et al. (2021) Aging impairs the essential contributions of non-glial progenitors to neurorepair in the dorsal telencephalon of the Killifish Nothobranchius furzeri. *Aging Cell* **20**:e13464 https://doi.org/10.1111/acel.13464 | PubMed

47. **Vanhunsel S,** et al. (2022) The age factor in optic nerve regeneration: Intrinsic and extrinsic barriers hinder successful recovery in the short-living killifish. *Aging Cell* **21**:e13537 https://doi.org/10.1111/acel.13537 | PubMed

48. **Louka A,** et al. (2022) New lessons on TDP-43 from old N. furzeri killifish. *Aging Cell* **21**:e13517 https://doi.org/10.1111/acel.13517 | PubMed

49. **Teefy BB,** et al. (2023) Dynamic regulation of gonadal transposon control across the lifespan of the naturally short-lived African turquoise killifish. *Genome Res* **33**:141-153 https://doi.org/10.1101/gr.277301.122 | PubMed

50. **Van Houcke J,** et al. (2023) A short dasatinib and quercetin treatment is sufficient to reinstate potent adult neuroregenesis in the aged killifish. *NPJ Regen Med* **8**:31 https://doi.org/10.1038/s41536-023-00304-4 | PubMed

51. **Astre G,** et al. (2023) Genetic perturbation of AMP biosynthesis extends lifespan and restores metabolic health in a naturally short-lived vertebrate. *Dev Cell* **58**:1350-1364.e10 https://doi.org/10.1016/j.devcel.2023.05.015 | PubMed

52. **Teefy BB,** et al. (2023) Widespread sex dimorphism across single-cell transcriptomes of adult African turquoise killifish tissues. *Cell Rep* **42**:113237 https://doi.org/10.1016/j.celrep.2023.113237 | PubMed

53. **Moses E,** et al. (2024) The killifish germline regulates longevity and somatic repair in a sex-specific manner. *Nat Aging* **4**:791-813 https://doi.org/10.1038/s43587-024-00632-0 | PubMed

54. **Di Fraia D,** et al. (2025) Altered translation elongation contributes to key hallmarks of aging in the killifish brain. *Science* **389**:eadk3079 https://doi.org/10.1126/science.adk3079 | PubMed

55. **Costa EK,** et al. (2026) Multi-tissue transcriptomic aging atlas reveals predictive aging biomarkers in the killifish. *Nat Aging* https://doi.org/10.1038/s43587-026-01074-6 | PubMed

56. **Morabito G,** et al. (2026) Spontaneous aging-associated inflammation and genome instability in the immune system of turquoise killifish. *Nature Aging* **6**:665-681 https://doi.org/10.1038/s43587-026-01086-2 | PubMed

57. **Rozenberg I,** et al. (2024) A genetic toolbox for the turquoise killifish identifies sporadic age-related cancer. *bioRxiv* https://doi.org/10.1101/2023.05.01.538839

58. **Burgos-Ruiz AM,** et al. (2025) Neotenic transcriptomic features in the adult turquoise killifish brain. *bioRxiv* https://doi.org/10.1101/2025.03.24.645095

59. **Williams RG,** et al. (2026) A multi-omic atlas in the African turquoise killifish reveals increased glucocorticoid signaling as a hallmark of brain aging. *bioRxiv* https://doi.org/10.64898/2026.04.09.717549 | PubMed

60. **Matsui H,** Kenmochi N, Namikawa K (2019) Age- and α-Synuclein-Dependent Degeneration of Dopamine and Noradrenaline Neurons in the Annual Killifish Nothobranchius furzeri. *Cell Rep* **26**:1727-1733.e6 https://doi.org/10.1016/j.celrep.2019.01.015 | PubMed

61. **Bagnoli S,** Fronte B, Bibbiani C, Terzibasi Tozzini E, Cellerino A (2022) Quantification of noradrenergic-, dopaminergic-, and tectal-neurons during aging in the short-lived killifish Nothobranchius furzeri. *Aging Cell* **21**:e13689 https://doi.org/10.1111/acel.13689 | PubMed

62. **de Bakker DEM,** Valenzano DR (2023) Turquoise killifish: A natural model of age-dependent brain degeneration. *Ageing Res Rev* **90**:102019 https://doi.org/10.1016/j.arr.2023.102019 | PubMed

63. **Valenzano DR,** et al. (2006) Resveratrol prolongs lifespan and retards the onset of age-related markers in a short-lived vertebrate. *Curr Biol* **16**:296-300 https://doi.org/10.1016/j.cub.2005.12.038 | PubMed

64. **McKay A,** et al. (2022) An automated feeding system for the African killifish reveals the impact of diet on lifespan and allows scalable assessment of associative learning. *eLife* **11** https://doi.org/10.7554/elife.69008 | PubMed

65. **de Bakker DEM,** et al. (2025) Amyloid beta precursor protein contributes to brain aging and learning decline in short-lived turquoise killifish (*Nothobranchius furzeri*). *bioRxiv* https://doi.org/10.1101/2024.10.11.617841

66. **Bedbrook CN,** et al. (2026) Lifelong behavioral screen reveals an architecture of vertebrate aging. *Science* **391**:eaea9795 https://doi.org/10.1126/science.aea9795 | PubMed

67. **Bedbrook CN,** Nath RD, Nagvekar R, Deisseroth K, Brunet A (2023) Rapid and precise genome engineering in a naturally short-lived vertebrate. *eLife* **12** https://doi.org/10.7554/elife.80639 | PubMed

68. **Ayana R,** et al. (2024) Single-cell sequencing unveils the impact of aging on the progenitor cell diversity in the telencephalon of the female killifish N. furzeri. *Aging Cell* e14251 https://doi.org/10.1111/acel.14251 | PubMed

69. **Bindels DS,** et al. (2017) mScarlet: a bright monomeric red fluorescent protein for cellular imaging. *Nat Methods* **14**:53-56 https://doi.org/10.1038/nmeth.4074 | PubMed

70. **Fenno LE,** et al. (2020) Comprehensive Dual- and Triple-Feature Intersectional Single-Vector Delivery of Diverse Functional Payloads to Cells of Behaving Mammals. *Neuron* **107**:836-853.e11 https://doi.org/10.1016/j.neuron.2020.06.003 | PubMed

71. **Almagro Armenteros JJ,** et al. (2019) SignalP 5.0 improves signal peptide predictions using deep neural networks. *Nat Biotechnol* **37**:420-423 https://doi.org/10.1038/s41587-019-0036-z | PubMed

72. **Szymczak AL,** et al. (2004) Correction of multi-gene deficiency in vivo using a single 'self-cleaving' 2A peptide-based retroviral vector. *Nat Biotechnol* **22**:589-94 https://doi.org/10.1038/nbt957 | PubMed

73. **Choi HMT,** et al. (2018) Third-generation in situ hybridization chain reaction: multiplexed, quantitative, sensitive, versatile, robust. *Development* **145** https://doi.org/10.1242/dev.165753 | PubMed

74. **Marsh SE,** et al. (2022) Dissection of artifactual and confounding glial signatures by single-cell sequencing of mouse and human brain. *Nat Neurosci* **25**:306-316 https://doi.org/10.1038/s41593-022-01022-8 | PubMed

75. **Barr HJ,** et al. (2025) The circadian clock regulates scavenging of fluid-borne substrates by brain border-associated macrophages. *bioRxiv* https://doi.org/10.64898/2025.12.08.693074 | PubMed

76. **Barr HJ,** et al. (2025) Conserved phenotype and function of human brain border-associated macrophages in iPSC-derived models. *bioRxiv* https://doi.org/10.64898/2025.12.11.693582 | PubMed

77. **Becht E,** et al. (2019) Dimensionality reduction for visualizing single-cell data using UMAP. *Nature Biotechnology* **37**:38-44 https://doi.org/10.1038/nbt.4314 | PubMed

78. **Tabula Muris Consortium** (2018) Single-cell transcriptomics of 20 mouse organs creates a Tabula Muris. *Nature* **562**:367-372 https://doi.org/10.1038/s41586-018-0590-4 | PubMed

79. **Hammond TR,** et al. (2019) Single-Cell RNA Sequencing of Microglia throughout the Mouse Lifespan and in the Injured Brain Reveals Complex Cell-State Changes. *Immunity* **50**:253-271.e6 https://doi.org/10.1016/j.immuni.2018.11.004 | PubMed

80. **Rovira M,** et al. (2025) A single-cell transcriptomic atlas reveals resident dendritic-like cells in the zebrafish brain parenchyma. *eLife* **13** https://doi.org/10.7554/elife.91427 | PubMed

81. **Sherr CJ,** et al. (1985) The c-fms proto-oncogene product is related to the receptor for the mononuclear phagocyte growth factor, CSF-1. *Cell* **41**:665-76 https://doi.org/10.1016/s0092-8674(85)80047-7 | PubMed

82. **Stanley ER,** Chitu V (2014) CSF-1 receptor signaling in myeloid cells. *Cold Spring Harb Perspect Biol* **6** https://doi.org/10.1101/cshperspect.a021857 | PubMed

83. **Mildenberger W,** Stifter SA, Greter M (2022) Diversity and function of brain-associated macrophages. *Curr Opin Immunol* **76**:102181 https://doi.org/10.1016/j.coi.2022.102181 | PubMed

84. **Thion MS,** Garel S (2020) Microglial ontogeny, diversity and neurodevelopmental functions. *Curr Opin Genet Dev* **65**:186-194 https://doi.org/10.1016/j.gde.2020.06.013 | PubMed

85. **Utz SG,** et al. (2020) Early Fate Defines Microglia and Non-parenchymal Brain Macrophage Development. *Cell* **181**:557-573.e18 https://doi.org/10.1016/j.cell.2020.03.021 | PubMed

86. **Munro DAD,** et al. (2020) CNS macrophages differentially rely on an intronic Csf1r enhancer for their development. *Development* **147** https://doi.org/10.1242/dev.194449 | PubMed

87. **Wu X,** Saito T, Saido TC, Barron AM, Ruedl C (2021) Microglia and CD206(+) border-associated mouse macrophages maintain their embryonic origin during Alzheimer's disease. *eLife* **10** https://doi.org/10.7554/elife.71879 | PubMed

88. **Masuda T,** et al. (2022) Specification of CNS macrophage subsets occurs postnatally in defined niches. *Nature* **604**:740-748 https://doi.org/10.1038/s41586-022-04596-2 | PubMed

89. **Brioschi S,** et al. (2023) A Cre-deleter specific for embryo-derived brain macrophages reveals distinct features of microglia and border macrophages. *Immunity* **56**:1027-1045.e8 https://doi.org/10.1016/j.immuni.2023.01.028 | PubMed

90. **Ren XS,** et al. (2024) Hematopoietic Growth Factors Regulate the Entry of Monocytes into the Adult Brain via Chemokine Receptor CCR5. *Int J Mol Sci* **25** https://doi.org/10.3390/ijms25168898 | PubMed

91. **Bastos J,** et al. (2025) Monocytes can efficiently replace all brain macrophages and fetal liver monocytes can generate bona fide SALL1(+) microglia. *Immunity* **58**:1269-1288.e12 https://doi.org/10.1016/j.immuni.2025.04.006 | PubMed

92. **Du S,** et al. (2026) Diversity and immune dynamics of choroid plexus macrophages are shaped by distinct developmental origins. *Nat Neurosci* **29**:717-731 https://doi.org/10.1038/s41593-025-02158-z | PubMed

93. **Du S,** et al. (2026) Brain-engrafted monocyte-derived macrophages from blood and skull-bone marrow exhibit distinct properties. *Neuron* https://doi.org/10.1016/j.neuron.2026.01.032 | PubMed

94. **Ferrero G,** et al. (2018) Embryonic Microglia Derive from Primitive Macrophages and Are Replaced by cmyb-Dependent Definitive Microglia in Zebrafish. *Cell Rep* **24**:130-141 https://doi.org/10.1016/j.celrep.2018.05.066 | PubMed

95. **Ferrero G,** Miserocchi M, Di Ruggiero E, Wittamer V (2021) A csf1rb mutation uncouples two waves of microglia development in zebrafish. *Development* **148** https://doi.org/10.1242/dev.194241 | PubMed

96. **Kizil C,** Iltzsche A, Kaslin J, Brand M (2013) Micromanipulation of gene expression in the adult zebrafish brain using cerebroventricular microinjection of morpholino oligonucleotides. *J Vis Exp* e50415 https://doi.org/10.3791/50415 | PubMed

97. **Schonhoff AM,** et al. (2023) Border-associated macrophages mediate the neuroinflammatory response in an alpha-synuclein model of Parkinson disease. *Nat Commun* **14**:3754 https://doi.org/10.1038/s41467-023-39060-w | PubMed

98. **Adler D,** et al. (2026) Functional border-associated macrophages limit Alzheimer's Disease progression. *bioRxiv* https://doi.org/10.64898/2026.01.31.703045 | PubMed

99. **Shi SM,** et al. (2025) Glycocalyx dysregulation impairs blood-brain barrier in ageing and disease. *Nature* **639**:985-994 https://doi.org/10.1038/s41586-025-08589-9 | PubMed

100. **Levard D,** et al. (2024) Central nervous system-associated macrophages modulate the immune response following stroke in aged mice. *Nat Neurosci* **27**:1721-1733 https://doi.org/10.1038/s41593-024-01695-3 | PubMed

101. **Navarro Negredo P,** et al. (2026) Targeting immune cells in the aged brain reveals that engineered cytokine IL-10 enhances neurogenesis and improves cognition. *Immunity* **59**:458-476.e13 https://doi.org/10.1016/j.immuni.2026.01.016 | PubMed

102. **Mrdjen D,** et al. (2018) High-Dimensional Single-Cell Mapping of Central Nervous System Immune Cells Reveals Distinct Myeloid Subsets in Health, Aging, and Disease. *Immunity* **48**:380-395.e6 https://doi.org/10.1016/j.immuni.2018.01.011 | PubMed

103. **Van Hove H,** et al. (2019) A single-cell atlas of mouse brain macrophages reveals unique transcriptional identities shaped by ontogeny and tissue environment. *Nat Neurosci* **22**:1021-1035 https://doi.org/10.1038/s41593-019-0393-4 | PubMed

104. **Zelco A,** et al. (2021) Single-cell atlas reveals meningeal leukocyte heterogeneity in the developing mouse brain. *Genes Dev* **35**:1190-1207 https://doi.org/10.1101/gad.348190.120 | PubMed

105. **Kim JS,** et al. (2021) A Binary Cre Transgenic Approach Dissects Microglia and CNS Border-Associated Macrophages. *Immunity* **54**:176-190.e7 https://doi.org/10.1016/j.immuni.2020.11.007 | PubMed

106. **Karam M,** Janbon H, Malkinson G, Brunet I (2022) Heterogeneity and developmental dynamics of LYVE-1 perivascular macrophages distribution in the mouse brain. *J Cereb Blood Flow Metab* **42**:1797-1812 https://doi.org/10.1177/0271678x221101643 | PubMed

107. **Ostkamp P,** et al. (2022) A single-cell analysis framework allows for characterization of CSF leukocytes and their tissue of origin in multiple sclerosis. *Sci Transl Med* **14**:eadc9778 https://doi.org/10.1126/scitranslmed.adc9778 | PubMed

108. **Silvin A,** et al. (2022) Dual ontogeny of disease-associated microglia and disease inflammatory macrophages in aging and neurodegeneration. *Immunity* **55**:1448-1465.e6 https://doi.org/10.1016/j.immuni.2022.07.004 | PubMed

109. **Benhar I,** et al. (2023) Temporal single-cell atlas of non-neuronal retinal cells reveals dynamic, coordinated multicellular responses to central nervous system injury. *Nat Immunol* **24**:700-713 https://doi.org/10.1038/s41590-023-01437-w | PubMed

110. **Robert SM,** et al. (2023) The choroid plexus links innate immunity to CSF dysregulation in hydrocephalus. *Cell* **186**:764-785.e21 https://doi.org/10.1016/j.cell.2023.01.017 | PubMed

111. **Dissing-Olesen L,** et al. (2023) FEAST: A flow cytometry-based toolkit for interrogating microglial engulfment of synaptic and myelin proteins. *Nat Commun* **14**:6015 https://doi.org/10.1038/s41467-023-41448-7 | PubMed

112. **Jeon J,** et al. (2024) Deciphering perivascular macrophages and microglia in the retinal ganglion cell layers. *Front Cell Dev Biol* **12**:1368021 https://doi.org/10.3389/fcell.2024.1368021 | PubMed

113. **Wang L,** et al. (2024) CCR2(+) monocytes replenish border-associated macrophages in the diseased mouse brain. *Cell Rep* **43**:114120 https://doi.org/10.1016/j.celrep.2024.114120 | PubMed

114. **Jiang X,** et al. (2025) A single-cell atlas of mouse central nervous system immune cells reveals unique infection-stage immune signatures during the progression of meningitis caused by Streptococcus suis. *Commun Biol* **8**:1312 https://doi.org/10.1038/s42003-025-08748-8 | PubMed

115. **Sun L,** et al. (2025) Deciphering the temporal transcriptional landscape of human fetal leptomeninges. *Brain* **148**:2218-2232 https://doi.org/10.1093/brain/awae397 | PubMed

116. **Schweigreiter R,** Roots BI, Bandtlow CE, Gould RM (2006) Understanding myelination through studying its evolution. *Int Rev Neurobiol* **73**:219-73 https://doi.org/10.1016/s0074-7742(06)73007-0 | PubMed

117. **Baraban M,** Mensch S, Lyons DA (2016) Adaptive myelination from fish to man. *Brain Res* **1641**:149-161 https://doi.org/10.1016/j.brainres.2015.10.026 | PubMed

118. **McNamara NB,** et al. (2023) Microglia regulate central nervous system myelin growth and integrity. *Nature* **613**:120-129 https://doi.org/10.1038/s41586-022-05534-y | PubMed

119. **Zupanc GK** (2008) Adult neurogenesis and neuronal regeneration in the brain of teleost fish. *J Physiol Paris* **102**:357-73 https://doi.org/10.1016/j.jphysparis.2008.10.007 | PubMed

120. **Ribeiro Xavier AL,** Kress BT, Goldman SA, Lacerda de Menezes JR, Nedergaard M (2015) A Distinct Population of Microglia Supports Adult Neurogenesis in the Subventricular Zone. *J Neurosci* **35**:11848-61 https://doi.org/10.1523/jneurosci.1217-15.2015 | PubMed

121. **Ganz J,** Brand M (2016) Adult Neurogenesis in Fish. *Cold Spring Harb Perspect Biol* **8** https://doi.org/10.1101/cshperspect.a019018 | PubMed

122. **De Vlaminck K,** et al. (2022) Differential plasticity and fate of brain-resident and recruited macrophages during the onset and resolution of neuroinflammation. *Immunity* **55**:2085-2102.e9 https://doi.org/10.1016/j.immuni.2022.09.005 | PubMed

123. **Rebejac J,** et al. (2022) Meningeal macrophages protect against viral neuroinfection. *Immunity* **55**:2103-2117.e10 https://doi.org/10.1016/j.immuni.2022.10.005 | PubMed

124. **Kim MW,** et al. (2025) Endogenous self-peptides guard immune privilege of the central nervous system. *Nature* **637**:176-183 https://doi.org/10.1038/s41586-024-08279-y | PubMed

125. **Faraco G,** et al. (2016) Perivascular macrophages mediate the neurovascular and cognitive dysfunction associated with hypertension. *J Clin Invest* **126**:4674-4689 https://doi.org/10.1172/jci86950 | PubMed

126. **Park L,** et al. (2017) Brain Perivascular Macrophages Initiate the Neurovascular Dysfunction of Alzheimer Aβ Peptides. *Circ Res* **121**:258-269 https://doi.org/10.1161/circresaha.117.311054 | PubMed

127. **Pedragosa J,** et al. (2018) CNS-border associated macrophages respond to acute ischemic stroke attracting granulocytes and promoting vascular leakage. *Acta Neuropathol Commun* **6**:76 https://doi.org/10.1186/s40478-018-0581-6 | PubMed

128. **Gericke C,** Mallone A, Engelhardt B, Nitsch RM, Ferretti MT (2020) Oligomeric Forms of Human Amyloid-Beta(1-42) Inhibit Antigen Presentation. *Front Immunol* **11**:1029 https://doi.org/10.3389/fimmu.2020.01029 | PubMed

129. **Rajan WD,** et al. (2020) Defining molecular identity and fates of CNS-border associated macrophages after ischemic stroke in rodents and humans. *Neurobiol Dis* **137**:104722 https://doi.org/10.1016/j.nbd.2019.104722 | PubMed

130. **Wan H,** Brathwaite S, Ai J, Hynynen K, Macdonald RL (2021) Role of perivascular and meningeal macrophages in outcome following experimental subarachnoid hemorrhage. *J Cereb Blood Flow Metab* **41**:1842-1857 https://doi.org/10.1177/0271678x20980296 | PubMed

131. **Ochocka N,** et al. (2021) Single-cell RNA sequencing reveals functional heterogeneity of glioma-associated brain macrophages. *Nat Commun* **12**:1151 https://doi.org/10.1038/s41467-021-21407-w | PubMed

132. **Spiteri AG,** et al. (2022) PLX5622 Reduces Disease Severity in Lethal CNS Infection by Off-Target Inhibition of Peripheral Inflammatory Monocyte Production. *Front Immunol* **13**:851556 https://doi.org/10.3389/fimmu.2022.851556 | PubMed

133. **Warrington JP,** et al. (2022) Pial Vessel-Associated Microglia/Macrophages Increase in Female Dahl-SS/Jr Rats Independent of Pregnancy History. *Int J Mol Sci* **23** https://doi.org/10.3390/ijms23063384 | PubMed

134. **Calero M,** et al. (2022) Lipid nanoparticles for antisense oligonucleotide gene interference into brain border-associated macrophages. *Front Mol Biosci* **9**:887678 https://doi.org/10.3389/fmolb.2022.887678 | PubMed

135. **Ivan DC,** et al. (2023) Insulin-like growth factor-1 receptor controls the function of CNS-resident macrophages and their contribution to neuroinflammation. *Acta Neuropathol Commun* **11**:35 https://doi.org/10.1186/s40478-023-01535-8 | PubMed

136. **Mutoh T,** Kikuchi H, Jitsuishi T, Kitajo K, Yamaguchi A (2023) Spatiotemporal expression patterns of ZBP1 in the brain of mouse experimental stroke model. *J Chem Neuroanat* **134**:102362 https://doi.org/10.1016/j.jchemneu.2023.102362 | PubMed

137. **Kearns NA,** et al. (2023) Dissecting the human leptomeninges at single-cell resolution. *Nat Commun* **14**:7036 https://doi.org/10.1038/s41467-023-42825-y | PubMed

138. **Uekawa K,** et al. (2023) Border-associated macrophages promote cerebral amyloid angiopathy and cognitive impairment through vascular oxidative stress. *Mol Neurodegener* **18**:73 https://doi.org/10.1186/s13024-023-00660-1 | PubMed

139. **Colella P,** et al. (2024) CNS-wide repopulation by hematopoietic-derived microglia-like cells corrects progranulin deficiency in mice. *Nat Commun* **15**:5654 https://doi.org/10.1038/s41467-024-49908-4 | PubMed

140. **Ganz T,** et al. (2024) Targeting CNS myeloid infiltrates provides neuroprotection in a progressive multiple sclerosis model. *Brain Behav Immun* **122**:497-509 https://doi.org/10.1016/j.bbi.2024.08.032 | PubMed

141. **Glavan M,** et al. (2024) CNS-associated macrophages contribute to intracerebral aneurysm pathophysiology. *Acta Neuropathol Commun* **12**:43 https://doi.org/10.1186/s40478-024-01756-5 | PubMed

142. **Santisteban MM,** et al. (2024) Meningeal interleukin-17-producing T cells mediate cognitive impairment in a mouse model of salt-sensitive hypertension. *Nat Neurosci* **27**:63-77 https://doi.org/10.1038/s41593-023-01497-z | PubMed

143. **Xu H,** et al. (2024) The choroid plexus synergizes with immune cells during neuroinflammation. *Cell* **187**:4946-4963.e17 https://doi.org/10.1016/j.cell.2024.07.002 | PubMed

144. **Anfray A,** et al. (2024) A cell-autonomous role for border-associated macrophages in ApoE4 neurovascular dysfunction and susceptibility to white matter injury. *Nat Neurosci* **27**:2138-2151 https://doi.org/10.1038/s41593-024-01757-6 | PubMed

145. **Yang S,** et al. (2025) Amantadine modulates novel macrophage phenotypes to enhance neural repair following spinal cord injury. *J Transl Med* **23**:60 https://doi.org/10.1186/s12967-024-05916-y | PubMed

146. **Xiong XY,** et al. (2025) Single-nucleus RNA sequencing reveals the specific molecular signatures of myeloid cells responding to brain injury after microglial replacement. *Front Immunol* **16**:1625673 https://doi.org/10.3389/fimmu.2025.1625673 | PubMed

147. **Okuno N,** et al. (2025) Brain macrophages and pial fibroblasts promote inflammation in a hypomyelination model. *Acta Neuropathol Commun* **13**:145 https://doi.org/10.1186/s40478-025-02063-3 | PubMed

148. **Strehle J,** et al. (2025) The border-associated macrophage marker MRC1 contributes to an early neuroprotective inflammatory response to traumatic brain injury in mice. *Acta Neuropathol Commun* **13**:220 https://doi.org/10.1186/s40478-025-02156-z | PubMed

149. **Ohki T,** et al. (2025) Depletion of CD169(+) border-associated macrophages induces Parkinson's disease-like behavior. *Front Neurosci* **19**:1688394 https://doi.org/10.3389/fnins.2025.1688394 | PubMed

150. **Van Hove H,** et al. (2025) Interleukin-34-dependent perivascular macrophages promote vascular function in the brain. *Immunity* **58**:1289-1305.e8 https://doi.org/10.1016/j.immuni.2025.04.003 | PubMed

151. **Wu X,** Miller JA, Lee BTK, Wang Y, Ruedl C (2025) Reducing microglial lipid load enhances β amyloid phagocytosis in an Alzheimer's disease mouse model. *Sci Adv* **11**:eadq6038 https://doi.org/10.1126/sciadv.adq6038 | PubMed

152. **Dyckhoff-Shen S,** et al. (2025) Pharmacologic depletion of border-associated macrophages worsens disease in a mouse model of meningitis. *Acta Neuropathol Commun* **13**:191 https://doi.org/10.1186/s40478-025-02126-5 | PubMed

153. **Hu M,** et al. (2025) Senescent-like border-associated macrophages regulate cognitive aging via migrasome-mediated induction of paracrine senescence in microglia. *Nat Aging* **5**:2039-2054 https://doi.org/10.1038/s43587-025-00956-5 | PubMed

154. **Zhou J,** et al. (2025) Remote ischemic postconditioning improves cognitive dysfunction after subarachnoid hemorrhage by driving metabolic reprogramming of border-associated macrophages through the IL-33/ST2 axis. *J Neuroinflammation* **22**:257 https://doi.org/10.1186/s12974-025-03587-0 | PubMed

155. **Baluszek S,** et al. (2025) Determining the Biological Features of Aggressive Meningioma Growth with Transcriptomic Profiling. *Cancers* **17** https://doi.org/10.3390/cancers17203324 | PubMed

156. **Yu N,** et al. (2026) Changes in border-associated macrophages after stroke: Single-cell sequencing analysis. *Neural Regen Res* **21**:346-356 https://doi.org/10.4103/nrr.nrr-d-24-01092 | PubMed

157. **Gao Y,** et al. (2026) Meningeal blood vessel blockage enhances anti-glioblastoma immunity. *Cell* **189**:1305-1322.e28 https://doi.org/10.1016/j.cell.2025.12.045 | PubMed

158. **Liu N,** et al. (2026) Early glymphatic failure in AppNL-F knock-in mice is linked to parenchymal border macrophages loss. *Brain* awag080 https://doi.org/10.1093/brain/awag080 | PubMed

159. **Guo P,** et al. (2026) Glibenclamide alleviates hydrocephalus after intraventricular hemorrhage by targeting metabolic reprogramming of border-associated macrophages. *Exp Neurol* **401**:115751 https://doi.org/10.1016/j.expneurol.2026.115751 | PubMed

160. **Seferbekova Z,** et al. (2026) Spatial Transcriptomics Characterisation of Radionecrotic Changes in Glioblastoma Patients. *Neuro Oncol* https://doi.org/10.1093/neuonc/noag026 | PubMed

161. **Tang F,** et al. (2026) BMAL1-GPX3 axis in the choroid plexus mitigates Aβ pathology in an amyloid mouse model. *J Neuroinflammation* **23** https://doi.org/10.1186/s12974-026-03691-9 | PubMed

162. **Garcia-Bonilla M,** et al. (2026) Post-hemorrhagic hydrocephalus of prematurity is associated with disruption of tight junctions and increased macrophage activity in the choroid plexus. *Fluids Barriers CNS* https://doi.org/10.1186/s12987-026-00800-x | PubMed

163. **Ratzabi A,** et al. (2026) Brain metastases exhibit distinct spatial patterns of resident and infiltrating macrophages. *Cell Death Discov* https://doi.org/10.1038/s41420-026-03084-0 | PubMed

164. **Philippe TJ,** et al. (2025) A Multi-omic Atlas of Human Choroid Plexus in Alzheimer's Disease. *bioRxiv* https://doi.org/10.1101/2025.11.23.690014 | PubMed

165. **Zawadzki ME,** et al. (2025) Fluid-Niche and Microglial Signatures Prime Robust Intraventricular Macrophage Response to Blood During Brain Development. *bioRxiv* https://doi.org/10.1101/2025.10.02.679906 | PubMed

166. **Bhatta S,** Grzybowski A, Ortiz G, DiStasio M (2026) Mechanobiological Specialization of Choroid Plexus Macrophages Defined by Titin Expression. *bioRxiv* https://doi.org/10.64898/2026.01.20.700716 | PubMed

167. **Kim S,** et al. (2026) Meningeal inflammation and arachnoid barrier breakdown in a mouse model of neonatal bacterial meningitis. *bioRxiv* https://doi.org/10.64898/2026.03.04.709573 | PubMed

168. **Colacurcio DJ,** Nixon RA (2016) Disorders of lysosomal acidification-The emerging role of v-ATPase in aging and neurodegenerative disease. *Ageing Res Rev* **32**:75-88 https://doi.org/10.1016/j.arr.2016.05.004 | PubMed

169. **D'Angelo L** (2013) Brain atlas of an emerging teleostean model: Nothobranchius furzeri. *Anat Rec* **296**:681-91 https://doi.org/10.1002/ar.22668 | PubMed

170. **Chi J,** Crane A, Wu Z, Cohen P (2018) Adipo-Clear: A Tissue Clearing Method for Three-Dimensional Imaging of Adipose Tissue. *J Vis Exp* https://doi.org/10.3791/58271 | PubMed

171. **Bankhead P,** et al. (2017) QuPath: Open source software for digital pathology image analysis. *Sci Rep* **7**:16878 https://doi.org/10.1038/s41598-017-17204-5 | PubMed

172. **Bhattarai P,** et al. (2016) IL4/STAT6 Signaling Activates Neural Stem Cell Proliferation and Neurogenesis upon Amyloid-β42 Aggregation in Adult Zebrafish Brain. *Cell Rep* **17**:941-948 https://doi.org/10.1016/j.celrep.2016.09.075 | PubMed

173. **Mariën V,** Arckens L, Van Houcke J (2024) Preparation of High-Viability Single-Cell Suspensions from African Turquoise Killifish Brain Tissue. *Cold Spring Harb Protoc* **2024**:107829 https://doi.org/10.1101/pdb.prot107829 | PubMed

174. **Glasauer SM,** Neuhauss SC (2014) Whole-genome duplication in teleost fishes and its evolutionary consequences. *Mol Genet Genomics* **289**:1045-60 https://doi.org/10.1007/s00438-014-0889-2 | PubMed

175. **Singh PP,** et al. (2024) Evolution of diapause in the African turquoise killifish by remodeling the ancient gene regulatory landscape. *Cell* **187**:3338-3356.e30 https://doi.org/10.1016/j.cell.2024.04.048 | PubMed

176. **Butler A,** Hoffman P, Smibert P, Papalexi E, Satija R (2018) Integrating single-cell transcriptomic data across different conditions, technologies, and species. *Nat Biotechnol* **36**:411-420 https://doi.org/10.1038/nbt.4096 | PubMed

177. **Korsunsky I,** Nathan A, Millard N, Raychaudhuri S (2019) Presto scales Wilcoxon and auROC analyses to millions of observations. *bioRxiv* https://doi.org/10.1101/653253

Nagvekar R (2026) Engulfment by brain macrophages in a short-lived vertebrate. NCBI Gene Expression Omnibus. ID GSE329891 https://www.ncbi.nlm.nih.gov/geo/query/acc.cgi?acc=GSE329891

Ayana R, Zandecki C, Van Houcke J, Mariën V, Seuntjens E, Arckens L (2024) Single cell sequencing unravels the cellular diversity that shapes neuro- and gliogenesis in the fast aging killifish (N. furzeri) brain. NCBI Gene Expression Omnibus. ID GSE213154 https://www.ncbi.nlm.nih.gov/geo/query/acc.cgi?acc=GSE213154

Peer reviews

Reviewer #1 (Public review):

Summary:

The manuscript by Nagvekar et al. studies engulfing macrophages in the killifish brain upon aging. It first describes the development of a transgenic knock-in killifish line overexpressing a secreted fluorescent protein in neurons. This becomes a tool for isolating myeloid cells that are capable of endocytosis or phagocytosis of the fluorescent protein, which seem to comprise the majority of the myeloid cells within the young adult brain. The paper then demonstrates the similarities of what they call "engulfing macrophages" to brain myeloid cell types of other species and investigates changes to this population upon aging. Overall, the study combines multiple complementary technologies to support their data, that are nicely presented and well described in the legends, while the textual description remains very concise. The findings are of interest to scientists studying brain aging, and microglia/macrophages.

Major comments:

(1) Although the authors describe and analyze their data from the viewpoint of engulfing macrophages, the paper would benefit from a broader perspective and a comparison to other studies on microglia in different species. Along this line, the title does not really seem to cover the data presented here very well, and the introduction lacks a proper explanation of terminology on microglia/brain macrophages and their known roles, cell types versus cell states and the current state of the art in fish versus other model species in the context of aging.

(2) The result that nearly all myeloid cells in the killifish brain are of the engulfing macrophage type is somewhat surprising. This appears to differ from other studies in for instance zebrafish (e.g. ref 80, that describes the heterogeneity of the myeloid cells in detail). There are two questions we like to raise: (Q1) What is the evidence towards this homogeneity? and (Q2) Could there be a technical bias?

Regarding (Q1): What is the evidence towards this homogeneity? The markers used are overlapping with markers for microglia. It would be helpful to clarify how canonical microglia populations are represented in the dataset. What is the heterogeneity of the oScarletHIGH cells? On several plots (Fig1f, Fig2d, Fig4a) this population of cells seems more heterogeneous than described. Are there different cell states or types? What is the percentage of myeloid cells that is oScarletLOW? To what extent do these cells compare transcriptionally to the oScarletHIGH cells?

a. Fig1f-i depict an enriched oScarletHIGH group alongside oScarletLOW cells. This representation is a bit misleading since it seems to indicate that really all myeloid cells are of the engulfing macrophage type whereas it is the majority, but not all.

b. Line 52: The authors describe that the oScarletHIGH cell group is "enriched for signatures characteristic of macrophage functions". This finding is logical, as the isolation procedure of this population of cells was based on the endocytic and phagocytic properties of the cells. This result appears more consistent with a validation of the isolation strategy than with definitive evidence for myeloid cell identity.

Regarding (Q2): Could there be a technical bias? An alternative explanation that may warrant discussion is whether aspects of the experimental pipeline (cell dissociation, FACS, scRNA-seq) could influence myeloid cell states. For instance, it is conceivable that dissociation induces a reactive program that enhances uptake of fluorescent protein, potentially enriching for oScarletHIGH cells. As the authors use a similar experimental setup to prove uptake of dextran and ovalbumin, such a technical artefact may merit consideration. As this would influence the major conclusions of the paper, the authors might want to address this comment with additional experimental controls, such as single-nuclei RNA-seq on control young and aged brains to profile the natural myeloid population when not submitted to a cell dissociation and FACS procedure.

(3) The authors compare the oScarletHIGH cell transcriptomes to mouse and killifish datasets. Both the mouse (Barr et al) and killifish (Nagvekar, this paper) dataset are from enriched immune cells (mouse= CD45+ cells, and the 3 cell types selected from that). Why did the authors not compare to the whole mouse CD45+ dataset? Including zebrafish (Rovira et al, 2025) here would strengthen the evolutionary comparison. I also feel that the additional comparison with young killifish (Ayana et al) might not be that solid since this dataset was initially not enriched and has a significantly lower number of myeloid cells, and thus much less power. The old age time point in that study contained more myeloid cells and might be interesting to include for cell type comparison. There are other, perhaps more unbiased ways of comparing cell types across species, for instance SAMap, developed by co-author Bo Wang. Did the authors consider using this or other methods?

(4) Regarding the comparison with the aged brain:

a. Figure 4: It would be nice to include the same comparisons as for young fish (cfr Fig.1 panels F-I).

The percentage of oScarletHIGH cells in the aged condition is 8% (Fig1-suppl1) compared to 4% at young age. On the other hand, a lower number of cells was isolated at old age compared to young age (Figure4a). Can the authors elaborate on this difference? Later on, it is stated that the engulfing capacity declines with aging, but could this be linked to the lower or potentially biased recovery of cells?

b. Figure4a: Transcriptional differences are stated between young and old (line 226), can a relevant selection be shown in e.g. a dot plot or heatmap?

The UMAP clustering does seem to indicate batch effects on panels a and g. Can the authors provide sub clustering and show that young and old/ FACS sorted high and low cover similar cell types/states? The PCA plot (panel f) and marker analysis is not fully convincing, as PC1 and 2 alone do not suffice to explain all the variance in these cells, and the markers are common ones for many microglia/macrophage cell types (and thus likely to be expressed similarly).

c. Figure 5: It would be informative to include the corresponding aged condition for panels c and e.

Significance:

General assessment

Strengths: This manuscript introduces a valuable new transgenic tool to isolate and characterize myeloid cells in the brain of the fast-aging killifish (Nothobranchius furzeri), an emerging model organism in aging research. The study combines multiple complementary approaches, including transgenesis, FACS, histology, and single-cell transcriptomics, to investigate brain immune populations and their changes upon aging. The cross-species comparison and aging analyses provide useful datasets and candidate markers for the field of neuroimmunology and comparative brain aging. Overall, the data are clearly presented, the experiments are logically structured, and the manuscript provides a useful resource for future studies on brain immune cells in teleosts.

Limitations/points for improvement: The major limitation of the study concerns a potential technical bias introduced by the experimental pipeline (cell dissociation, FACS isolation, and transcriptomic profiling), which may have influenced the observed predominance and transcriptional state of the oScarletHIGH/engulfing macrophage population. At present, it remains difficult to fully exclude whether the protocol itself contributes to the apparent homogeneity of the myeloid compartment or induces a shared reactive state. Because this issue affects some of the central conclusions, the manuscript would benefit either from additional controls (e.g., dissociation-independent approaches such as single-nuclei RNA-seq) or from a more cautious interpretation and discussion of this possibility in the text.

Advance: The fast-aging killifish is becoming an important vertebrate model for studying aging, yet the brain immune compartment in this species remains relatively underexplored. This manuscript provides both a novel experimental tool and a transcriptomic resource for studying myeloid cells in the killifish brain. To my knowledge, the study is among the first to profile engulfing/endocytic myeloid populations in the context of brain aging in this model organism and to compare these cells across species. The advance is primarily technical and descriptive/resource-generating, while also offering conceptual insight into how brain myeloid populations may change during aging and how they compare evolutionarily across vertebrates. Although the mechanistic interpretation would benefit from additional validation, the study clearly extends current knowledge and provides a framework for future work on neuroimmune aging in fish.

Audience: The manuscript will primarily be of interest to a specialized basic research audience, including researchers in neuroimmunology, brain aging, microglia/macrophage biology, and comparative neuroscience. It will also be relevant to scientists using killifish or other emerging vertebrate models for aging research. Beyond the immediate field, the study may be of broader interest to researchers investigating immune-brain interactions and the evolutionary conservation of myeloid cell states across species. The transgenic line and transcriptomic datasets are likely to serve as a useful resource for future comparative and functional studies.

https://doi.org/10.7554/eLife.112503.1.sa3

Reviewer #2 (Public review):

Summary:

The work by Nagvekar et. al., reports the development of a new model in the African Killifish to study the engulfment of extracellular proteins. Specifically, they expressed oScarlet with a signaling peptide under the control of a neuronal promoter/gene to induce secretion into the extracellular space. Using this model, they found that the secreted protein was predominantly taken up by brain macrophages. Leveraging this finding, they were able to conduct RNAseq on brain macrophages from young and aged fish, where they reported differences in translation and vacuolar acidification at the transcriptional level among others. Finally, they show that the engulfment capacity of brain macrophages from old killifish is reduced when compared to their young counterparts.

Major comments:

(1) Red fluorescent proteins are notorious for being prone to aggregation. Are oScarlet proteins being internalized by macrophages aggregates or soluble proteins? This distinction is important as the clearance of extracellular molecules could be mediated by most cells, yet aggregates could be removed specifically by macrophages. Can experiments be conducted to distinguish between these two possibilities? We realize this may be challenging. If not feasible, the discussion should be tempered to reflect this possibility.

(2) Brain dissociation tends to generate a lot of debris, especially from sheared neurons. Therefore, the high level of oScarlet inside macrophages could be an artifact of dissociation rather than a reflection of in vivo clearance. Authors should use internalization inhibitors during dissociation (CytoD, Dynasore, and pitstop) to exclude this possibility. Alternatively, if they have a transgenic killifish that expresses another fluorescent reporter in neurons (and preferably at a similar level to that of oScarlet), authors should dissociate brains together and quantify how many oScarlet+ cells are now also positive for that other fluorescent reporter. This could give an idea of how much engulfment is occurring due to the dissociation processes. It is not ideal, as macrophage eating could be happening during dissociation but before cells are in single cell suspension. However, given that RNAseq is needed to identify macrophages, this reviewer would be satisfied by this alternative approach if the aforementioned pitfall is also presented in the discussion.

(3) Related to the above, it appears based on the scRNAseq that dissociation heavily enriched for brain macrophages. Therefore, the claim that clearance is mostly macrophage mediated could be due to an enrichment of this population during dissociation rather than this cell type being responsible for most of the extracellular waste disposal. Authors should quantify the % of total oScarlet that is specifically in macrophages in the brain sections they already have that are stained against oScarlet and CSF1R/ApoEB transcript.

(4) The flow cytometry strategy used does not distinguish between oScarlet protein that has been internalized versus that which is sticking to the surface of macrophages. Authors should stain non-premeabilized and permeabilized cell suspensions with a flow antibody against mCherry/RFP to get a sense of how much oScarlet is inside versus outside of the macrophage. For most antibodies this can be done on the same sample sequentially if the antibodies have a different fluorophore.

(5) It is concerning that dextran and oScarlet are almost perfectly colocalized in the image presented (Figure 3a). It raises the possibility, among others, that dextran is sticking to potential oScarlet aggregates and then being internalized by macrophages. Therefore, it could be an artifact of the transgenic line. Authors should repeat the experiment in wildtype fish and use HCR against CSF1R/ApoEB to address this issue.

Significance:

We believe that this is an important finding as such a model in African Killifish lays the groundwork to study the pathways that mediate the clearance of extracellular molecules by

brain macrophages, the impact that this process has on brain homeostasis, and how it changes in aging. In particular, this reviewer is excited about the future potential of this model to uncover the molecular processes behind macropinocytosis, a process that occurs frequently in brain macrophages yet the mechanisms regulating it remain elusive, and how it contributes to overall brain health.

https://doi.org/10.7554/eLife.112503.1.sa2

Reviewer #3 (Public review):

Summary:

Rahul Nagvekar et al. generated a novel genetic model (SP-oScarlet) to label brain macrophages via their engulfment activity in the naturally short-lived African turquoise killifish. They found that these brain phagocytes exhibit transcriptional features resembling mammalian BAMs/MDMs and provided evidence that their engulfment capacity declines with age. The model and topic are interesting, but some of the central conclusions require more precise calibration to match the strength of the supporting evidence.

Major comments:

The SP-oScarlet model enriches cells based on phagocytic capacity - by design, any phagocytic cell, including microglia, can be labeled. Only 0.5% of oScarlet^{LOW} cells were myeloid cells, confirming that this method captures virtually the entire myeloid population. The transcriptional resemblance to BAMs/MDMs is therefore a post hoc characterization of brain phagocytes broadly, rather than evidence for a selectively labeled subset. The authors show examples of apoeb^{+} cells near vasculature (Fig. 3b), but do not provide a comprehensive quantification of the full spatial distribution of oScarlet^{HIGH} cells. Importantly, neither the SP-oScarlet macrophages nor previously published wild-type killifish brain macrophages could be transcriptionally separated into three subgroups analogous to mammalian microglia, BAMs, and MDMs by PCA. This suggests that fish brain macrophages may not exist as subpopulations that correspond with their mammalian counterparts. The authors should therefore describe these cells as brain myeloid cells that exhibit BAM/MDM-like transcriptional characteristics, rather than implying they are a population equivalent to mammalian BAMs/MDMs.

The age-related decline in oScarlet fluorescence in oScarlet^{HIGH} cells in vivo could reflect either reduced phagocytic capacity of macrophages, or reduced oScarlet secretion by neurons, as the authors have discussed (Fig. 5a). The ex vivo assay addresses this by standardizing substrate concentration, which is a strength, but an in vivo functional assessment would provide a more physiologically relevant complement. The authors have already established the methodology for in vivo substrate injection (Fig. 3a, dextran). A similar experiment comparing substrate uptake in young and old fish would circumvent potential artifacts of the ex vivo approach, such as enzymatic dissociation altering surface receptor availability, and would directly test whether engulfment declines in the native brain environment.

Significance:

General assessment: This study presents a novel genetic model (SP-oScarlet) for visualizing chronic engulfment by brain macrophages in a short-lived vertebrate. The finding that killifish brain phagocytes exhibit BAM/MDM-like transcriptional features is interesting. Leveraging the killifish's naturally short lifespan, the authors further provide functional evidence that brain macrophage engulfment capacity declines with age. However, the authors should exercise caution when defining these cells as a distinct population specialized

for engulfment of material from the brain extracellular space, since the SP-oScarlet model labels nearly the entire myeloid population in the brain.

Advance: This study establishes a novel genetic model for chronic, in vivo visualization of engulfment in a vertebrate brain. The conceptual insight that killifish brain phagocytes transcriptionally resemble BAMs/MDMs rather than classical microglia is novel and may reflect evolutionary differences in brain clearance strategies.

Audience: This research will interest a broad audience across developmental biology, genetics, neuroimmunology, aging research, and evolutionary biology.

https://doi.org/10.7554/eLife.112503.1.sa1

Author response:

> ***General Statements***

Please find below a revision plan for our manuscript entitled 'Engulfment by brain macrophages in a short-lived vertebrate' that was reviewed by Review Commons and that we wish to be considered for publication in *eLife*.

We were very happy to see that all three Reviewers were interested in our study and we are sincerely grateful to all of them for their constructive suggestions, which we believe can largely be addressed and will improve our manuscript.

We would like to inquire whether you would consider publishing our manuscript at *eLife* in its current form, along with the reviews. We will then provide an updated version of the manuscript, based on our revision plan below when we are able.

Thank you so much for your consideration.

> ***Description of the planned revisions***
>
> ***Reviewer #1:***
>
> *Major comments*
>
> *Comment 1: Although the authors describe and analyze their data from the viewpoint of engulfing macrophages, the paper would benefit from a broader perspective and a comparison to other studies on microglia in different species. Along this line, the title does not really seem to cover the data presented here very well, and the introduction lacks a proper explanation of terminology on microglia/brain macrophages and their known roles, cell types versus cell states and the current state of the art in fish versus other model species in the context of aging.*

We thank the Reviewer for these suggestions. We will expand the introduction to add more information and references on microglia/brain macrophages across fish and other species. We will also edit the title to more closely reflect the data in the manuscript.

> *Comment 2: The result that nearly all myeloid cells in the killifish brain are of the engulfing macrophage type is somewhat surprising. This appears to differ from other studies in for instance zebrafish (e.g. ref 80, that describes the heterogeneity of the myeloid cells in detail). There are two questions we like to raise: (Q1) What is the evidence towards this homogeneity? and (Q2) Could there be a technical bias?*

We agree with the Reviewer, and we were also surprised to find a fairly homogenous myeloid population even in wildtype (non-transgenic) killifish brains, especially given that all these 3 different populations of myeloid cells (microglia, non-microglial macrophages, and dendritic-

like cells), could be found in the adult zebrafish brain by Rovira et al. using single-cell RNA sequencing of *cd45*+ cells (ref. 80).

We will better describe our evidence towards this homogeneity among killifish brain myeloid cells in the manuscript by adding a paragraph in the text at the end of the section referring to Figure 2. We will also provide additional experiments and analyses (see also below, our detailed responses to Q1 and Q2):

i) In our and Ayana et al.'s single-cell RNA sequencing datasets, we could not find distinct populations of myeloid cells corresponding to microglia, non-microglial macrophages, and dendritic-like cells, even in wildtype (non-transgenic) killifish young adult and old brain, and even when subclustering only the myeloid cells. However, *cd45*+ cells were not specifically enriched in these experiments.

ii) When using PCA, we also could not separate killifish brain macrophages into microglia, border-associated macrophages, and monocyte-derived macrophages (whereas we could separate mouse brain macrophages into these three groups as a positive control for this approach).

iii) As noted by the Reviewer below, our analysis of the Ayana et al. wildtype dataset was limited to the young adult timepoint from this dataset. In the revised version of our manuscript, we will also include analysis of the old timepoint from this dataset.

iv) As described in our responses to Q1 and Q2 below, we will provide more detailed subclustering that highlights the heterogeneity we do observe among killifish brain myeloid cells. We find this heterogeneity to be subtle and likely corresponding to different cell states rather than functionally distinct cell types. We will also use hybridization chain reaction (HCR) to test whether *cd74*, a key marker we use to propose a monocyte-derived macrophage-like identity for almost all detected killifish brain macrophages, labels *apoeb*+ cells in young wildtype brains in situ (as would be predicted based on our single-cell RNA sequencing analysis). We will additionally use HCR to test whether *batf3*, a key marker used by Rovira et al. to identify dendritic-like cells, labels any cells in the killifish brain (based on our single-cell RNA sequencing analysis, we do not expect to find *batf3*+ cells in the killifish brain).

We agree that there could be technical confounds that could lead to the observed homogeneity of the myeloid population and lack of canonical microglia and dendritic-like cells even in wildtype killifish in our analysis. These could include our/Ayana et al.'s protocol for brain dissociation, our FACS-sorting step, or the step of loading cells into the 10x Genomics chip for single-cell RNA sequencing – each of these could be a step where canonical microglia and/or dendritic-like cells could be lost. In addition, we did not enrich for *cd45*+ cells, so it is possible that rare populations of immune cells in the killifish brain may not be represented in our dataset. As described below in our responses to Q1 and Q2, we will perform additional analyses that we hope will help address some of these key points, and we will more extensively discuss all possible technical confounds leading to potential cell type bias in the Discussion section.

In addition to discussing potential technical confounds, we will also better highlight biological possibilities that could explain the differences between our and Rovira et al.'s findings. For example, the observed lack of microglia and dendritic-like cells in killifish brains could reflect a species (killifish vs. zebrafish) difference. Alternatively, even though both studies analyzed young adult timepoints, there could also be differences in biological age between the young adult killifish and zebrafish analyzed, which may be additionally influenced by husbandry conditions (e.g., feeding, pathogen exposure).

> *Regarding (Q1): What is the evidence towards this homogeneity? The markers used are overlapping with markers for microglia. It would be helpful to clarify how canonical*

> *microglia populations are represented in the dataset. What is the heterogeneity of the oScarletHIGH cells? On several plots (Fig1f, Fig2d, Fig4a) this population of cells seems more heterogeneous than described. Are there different cell states or types? What is the percentage of myeloid cells that is oScarletLOW? To what extent do these cells compare transcriptionally to the oScarletHIGH cells?*

The Reviewer makes a series of excellent points. To address them:

i) We will more prominently highlight markers not expressed by canonical microglia (e.g., *mrc1*, *cd74*) that are expressed by nearly all detectable killifish brain myeloid cells, even in wildtype datasets. We could not find canonical microglia (e.g., *tmem119+*, *sall1+*) in any of our killifish datasets. We will highlight these results in the text and will move some of the relevant graphs in the main figure.

ii) We agree that oScarlet^{HIGH} cells are somewhat heterogeneous. To better understand the source of this heterogeneity, we will present UMAPs/Seurat FeaturePlots focusing on cell state markers (e.g., cycling [*mki67+*] and activated [*iba1+*] cells) as well as specific cell type markers from mammalian/zebrafish literature (canonical microglia, non-microglia macrophages, dendritic-like cells, etc.). We expect this analysis to show distinct cell states, but fairly uniform expression of cell type markers across all oScarlet^{HIGH} cells in our datasets.

iii) The percentage of detected myeloid cells that are oScarlet^{LOW} is very low (<1%). However, as noted in the next comment from the Reviewer, our sorting protocol de-enriches for oScarlet^{LOW} myeloid cells, so the actual percentage of all myeloid cells that is oScarlet^{LOW} may be higher. We will include additional panels to illustrate this point.

iv) oScarlet^{LOW} myeloid cells are largely transcriptionally similar to oScarlet^{HIGH} cells (which are almost all myeloid). The main differentially expressed genes in oScarlet^{LOW} vs oScarlet^{HIGH} myeloid cells are markers of non-myeloid genes (e.g., *elavl3*, *mpz*). These could reflect phagocytosis of non-myeloid cells by oScarlet^{LOW} myeloid cells but could also reflect ambient RNA contamination, since oScarlet^{LOW} myeloid cells (but not oScarlet^{HIGH} cells) were sequenced alongside non-myeloid cells. We will include the differential expression analysis and add commentary in the text to discuss these possibilities.

> *Fig1f-i depict an enriched oScarletHIGH group alongside oScarletLOW cells. This representation is a bit misleading since it seems to indicate that really all myeloid cells are of the engulfing macrophage type whereas it is the majority, but not all.*

We agree with the Reviewer. We will also include different representations that provide more accurate estimates of the proportion of all myeloid cells that are oScarlet^{LOW}/not engulfing macrophages.

> *Line 52: The authors describe that the oScarletHIGH cell group is "enriched for signatures characteristic of macrophage functions". This finding is logical, as the isolation procedure of this population of cells was based on the endocytic and phagocytic properties of the cells. This result appears more consistent with a validation of the isolation strategy than with definitive evidence for myeloid cell identity.*

We agree and we will reframe this result as a validation of the isolation strategy.

> *Regarding (Q2): Could there be a technical bias? An alternative explanation that may warrant discussion is whether aspects of the experimental pipeline (cell dissociation, FACS, scRNA-seq) could influence myeloid cell states. For instance, it is conceivable that dissociation induces a reactive program that enhances uptake of fluorescent protein, potentially enriching for oScarletHIGH cells. As the authors use a similar experimental setup to prove uptake of dextran and ovalbumin, such a technical artefact may merit consideration. As this would influence the major conclusions of the paper, the authors*

> *might want to address this comment with additional experimental controls, such as single-nuclei RNA-seq on control young and aged brains to profile the natural myeloid population when not submitted to a cell dissociation and FACS procedure.*

We agree with the Reviewer that brain dissociation, FACS, and single-cell RNA sequencing could all represent technical biases that could all influence the representation of different myeloid cell types in our dataset. We will clearly note this potential confound in the Results and the Discussion.

We agree that it would be valuable to test some of these issues experimentally. We will perform non-dissociative HCR (in situ) to test (1) whether in young wildtype brains, *apoeb*+ cells (macrophages) express *cd74* (a key marker for our argument re: MDM-like cell type identity) and (2) whether we can find cells expressing *batf3* (a key marker used by Rovira et al. to identify dendritic-like cells, which we cannot detect in the killifish brain in our single-cell RNA sequencing data). We will also acknowledge that these are only individual markers and would not provide as comprehensive a picture of cell type identity as single-nuclei RNA sequencing.

> *Comment 3: The authors compare the oScarletHIGH cell transcriptomes to mouse and killifish datasets. Both the mouse (Barr et al) and killifish (Nagvekar, this paper) dataset are from enriched immune cells (mouse= CD45+ cells, and the 3 cell types selected from that). Why did the authors not compare to the whole mouse CD45+ dataset? Including zebrafish (Rovira et al, 2025) here would strengthen the evolutionary comparison. I also feel that the additional comparison with young killifish (Ayana et al) might not be that solid since this dataset was initially not enriched and has a significantly lower number of myeloid cells, and thus much less power. The old age time point in that study contained more myeloid cells, and might be interesting to include for cell type comparison. There are other, perhaps more unbiased ways of comparing cell types across species, for instance SAMap, developed by co-author Bo Wang. Did the authors consider using this or other methods?*

We thank the Reviewer for these excellent suggestions. We will do the following in our revised manuscript:

i) We will include comparisons to all immune (CD45+) cells from mice (Barr et al.).

ii) We will include comparisons to all immune (*cd45*+) cells in zebrafish (Rovira et al.).

iii) We will also analyze the old age time point from the Ayana et al. wildtype killifish dataset.

> *The percentage of oScarletHIGH cells in the aged condition is 8% (Fig1-suppl1) compared to 4% at young age. On the other hand, a lower number of cells was isolated at old age compared to young age (Figure4a). Can the authors elaborate on this difference? Later on, it is stated that the engulfing capacity declines with aging, but could this be linked to the lower or potentially biased recovery of cells?*

We appreciate the Reviewer's point. We will elaborate on the percentage differences in oScarlet^{HIGH} cells recovered in the different experiments, and more clearly indicate what they could originate from and whether they could influence the engulfment results:

i) We will indicate more clearly that in each single-cell RNA sequencing experiment, we loaded the entire set of Live oScarlet^{HIGH} cells collected from each condition onto the 10x Genomics chip. In the young vs. old comparison, more Live old oScarlet^{HIGH} cells were loaded than Live young oScarlet^{HIGH} cells (66K vs. 42K, based on the FACS sorter counts, though these numbers are likely overestimates). One possibility is that the lower recovery of successfully sequenced old oScarlet^{HIGH} cells might be explained by differences with age in oScarlet^{HIGH} cells' ability to remain intact during loading onto the 10x Genomics chip.

ii) In the *ex vivo* experiments where we find that engulfment capacity declines with age (current Fig. 5), the proportion of oScarlet^{HIGH} cells among all Live cells slightly increased with age. We will include the data illustrating this, and indicate more clearly in the text that the differences in engulfment capacity observed in these experiments are unlikely to be explained solely by lower recovery of oScarlet^{HIGH} cells from old brains.

iii) We will more clearly acknowledge in the Discussion the possibility of potentially biased cell recovery with age.

> *Figure4a: Transcriptional differences are stated between young and old (line 226), can a relevant selection be shown in e.g. a dotplot or heatmap?*

This is another great point from the Reviewer. We will show these genes in a dotplot/heatmap in a Supplemental Figure. We will also clearly indicate in the main text that many of the genes most strongly enriched in old oScarlet^{HIGH} cells in our young vs. old comparison experiment were not strongly expressed in an independent old oScarlet^{HIGH} cells dataset (which was compared to old wildtype cells, without a young counterpart).

> *The UMAP clustering does seem to indicate batch effects on panels a and g. Can the authors provide subclustering and show that young and old/ FACS sorted high and low cover similar cell types/states? The PCA plot (panel f) and marker analysis is not fully convincing, as PC1 and 2 alone do not suffice to explain all the variance in these cells, and the markers are common ones for many microglia/macrophage cell types (and thus likely to be expressed similarly).*

The Reviewer has another excellent suggestion. We will provide subclustering, which indeed shows that young and old oScarlet^{HIGH} cells generally represent similar cell types and states. This analysis also shows a subcluster specific to old oScarlet^{HIGH} cells, but this subcluster is far less pronounced in a second old oScarlet^{HIGH} dataset (see our previous comment), so we will clearly indicate in the main text that this subcluster may not be robust. We will also remove the PCA plot.

> *Figure 5: It would be informative to include the corresponding aged condition for panels c and e.*

We agree and we will include this.

> *Minor comments*
>
> *The authors use the oScarlet fish in a heterozygous state. Is the homozygous line not viable? Or what is the reason to use the heterozygous state? Too high expression of OScarlett? Is apoptosis of neurons checked for this line? Compared to wild type?*

The homozygous SP-oScarlet line has not been characterized, and we will include this information in the Results. We did not check apoptosis of neurons in the SP-oScarlet line or in wildtype killifish, and we will indicate this in the Methods and Discussion.

> *Is the secretion of OScarlett completely proven? Maybe the signal is engulfed by the clearance of cell debris from apoptotic neurons?*

This is a great point. We have not directly tested the secretion of oScarlet in the SP-oScarlet line, and it remains possible that engulfed oScarlet also comes from apoptotic neurons that are being engulfed by myeloid cells. We will acknowledge this possibility in the Discussion.

We will also more clearly highlight references that adding a signal peptide to proteins (as we did for the SP-oScarlet line) is sufficient to induce their secretion in several contexts in different species (although this does not prove secretion in this particular case).

We also do have another line (built for a separate project) in which oScarlet is expressed cytoplasmically in *elavl3*+ cells. In this line, in pilot data, we did not observe oScarlet^{HIGH} cells by flow cytometry. While these experiments are not of publishable quality, these observations also suggest that the presence of a signal peptide on oScarlet is necessary for the engulfment phenotype.

> *Line 329. What exact difference between teleosts and mice are you pointing at?*

We will edit the text to clarify that we are referring to our inability to find a cell population with a transcriptional profile like that of canonical adult mouse microglia in the adult killifish brain.

> *Suggestions for Figures*
>
> *General remark IHC/HCR figures: Please add overview figures to guide the reader to ROI shown.*
>
> *Fig1.*
>
> *1.b Please add overview figures to show the overall distribution of the signal in the brain. Are there any hotspots or low-abundant regions?*
>
> *1.d/1.e Please add numbers of cells on figure panels.*
>
> *1.d: overview figure is unclear. Telencephalon seems to be missing? Can annotation be added to regions of the structure?*
>
> *Additional in vivo evidence of the homogeny/heterogeneity of oScarlet protein+/RNA- cells would be informative, e.g. double labeling (HCR) with some of the markers of panel Fig. 2a). This also would exclude location bias. One could expect myeloid cells that are not in close proximity to secreting neurons, for instance in dense neurogenic niches*
>
> *Fig. 2*
>
> *2.c Please add number of cells on graph*
>
> *2.d Please add brain regions to graphs of published datasets like was done for the own dataset.*
>
> *Subtext: Why is there a different number of cells for Barr in c and d? Please add number of cells of own killifish dataset in legend.*
>
> *Supplement fig. 2 Please add additional microglia-specific markers such as for instance HEXB, GPR34, SELL1, C1Q.*
>
> *Fig.3*
>
> *Please add overview pictures.*
>
> *Fig.4*
>
> *4.g grey color not very visible*
>
> *It would be informative to have the markers of 4.h plot on top of the UMAP to show the distribution/differences, maybe in supplementary information.*

We will implement all of these changes. We will add *cd74* HCR labeling of oScarlet^{HIGH} cells that do not express *oScarlet* RNA transcripts in situ. The different numbers of cells from the Barr et al. dataset in the current panels 2c and 2d do not reflect differences in brain regions

from which macrophages were isolated (in both cases, the same whole-brain dataset was used). Instead, in this dataset, there is a small population of interferon-responsive macrophages that are not microglia, BAMs, or MDMs; these cells were included in the analysis in 2d but not 2c. We will clarify this and update the analysis in current panel 2d to include all immune cells from the Barr et all. dataset, as suggested by the Reviewer above.

> ***Reviewer #2:***
>
> *Red fluorescent proteins are notorious for being prone to aggregation. Are oScarlet proteins being internalized by macrophages aggregates or soluble proteins? This distinction is important as the clearance of extracellular molecules could be mediated by most cells yet aggregates could be removed specifically by macrophages. Can experiments be conducted to distinguish between these two possibilities? We realize this may be challenging. If not feasible, the discussion should be tempered to reflect this possibility.*

The Reviewer makes a great point, and we were also interested in this question. mScarlet and its derivatives (including oScarlet) would generally be expected to remain in the monomeric state to a greater extent than other red fluorescent proteins like mCherry (Bindels et al., Albakri et al.). We will indicate this with references in the Results section.

But this does not preclude the possibility of oScarlet aggregation in SP-oScarlet brains. We did collect soluble and insoluble fractions from SP-oScarlet brains using a gentle lysis method that would be expected to preserve aggregates in the insoluble fraction (Avar et al.). However, we found that the levels of oScarlet in both fractions were below the limit of detection by western blot and by a plate reader-based fluorescence assay, thereby precluding us from directly testing how much oScarlet was aggregated. We will address the possibility of oScarlet aggregation, and its potential impact on engulfing macrophages, in the Results and Discussion sections.

> *Brain dissociation tends to generate a lot of debris, especially from sheared neurons. Therefore, the high level of oScarlet inside macrophages could be an artifact of dissociation rather than a reflection of in vivo clearance. Authors should use internalization inhibitors during dissociation (CytoD, Dynasore, and pitstop) to exclude this possibility. Alternatively, if they have a transgenic killifish that expresses another fluorescent reporter in neurons (and preferably at a similar level to that of oScarlet), authors should dissociate brains together and quantify how many oScarlet+ cells are now also positive for that other fluorescent reporter. This could give an idea of how much engulfment is occurring due to the dissociation processes. It is not ideal, as macrophage eating could be happening during dissociation but before cells are in single cell suspension. However, given that RNAseq is needed to identify macrophages, this reviewer would be satisfied by this alternative approach if the aforementioned pitfall is also presented in the discussion.*

This is another excellent suggestion, and we have already done the following experiments:

i) We have performed bulk RNA sequencing from FACS-sorted oScarlet^{HIGH} cells from middle-aged SP-oScarlet brains dissociated with five inhibitors (cytochalasin D, dynasore, Pitstop 2, bafilomycin A, and wortmannin) in addition to transcription/translation inhibitors. Deconvolution analysis of these bulk RNA sequencing data showed that oScarlet^{HIGH} cells in the presence of cytochalasin D, dynasore, Pitstop 2, bafilomycin A, and wortmannin are also almost all macrophages. While these data are not at single-cell resolution, they indicate that engulfment by macrophages is unlikely to solely occur during the dissociation process. We will include a revised Supplementary Figure with these experiments.

ii) We have also already performed a pilot co-dissociation experiment (in a different genetic background) as suggested by the Reviewer using a *ubb*

:GFP reporter as the second transgenic and observed very few GFP+ oScarlet^{HIGH} cells (see Author response image 1). We will include co-dissociation data in the revised version of the manuscript.

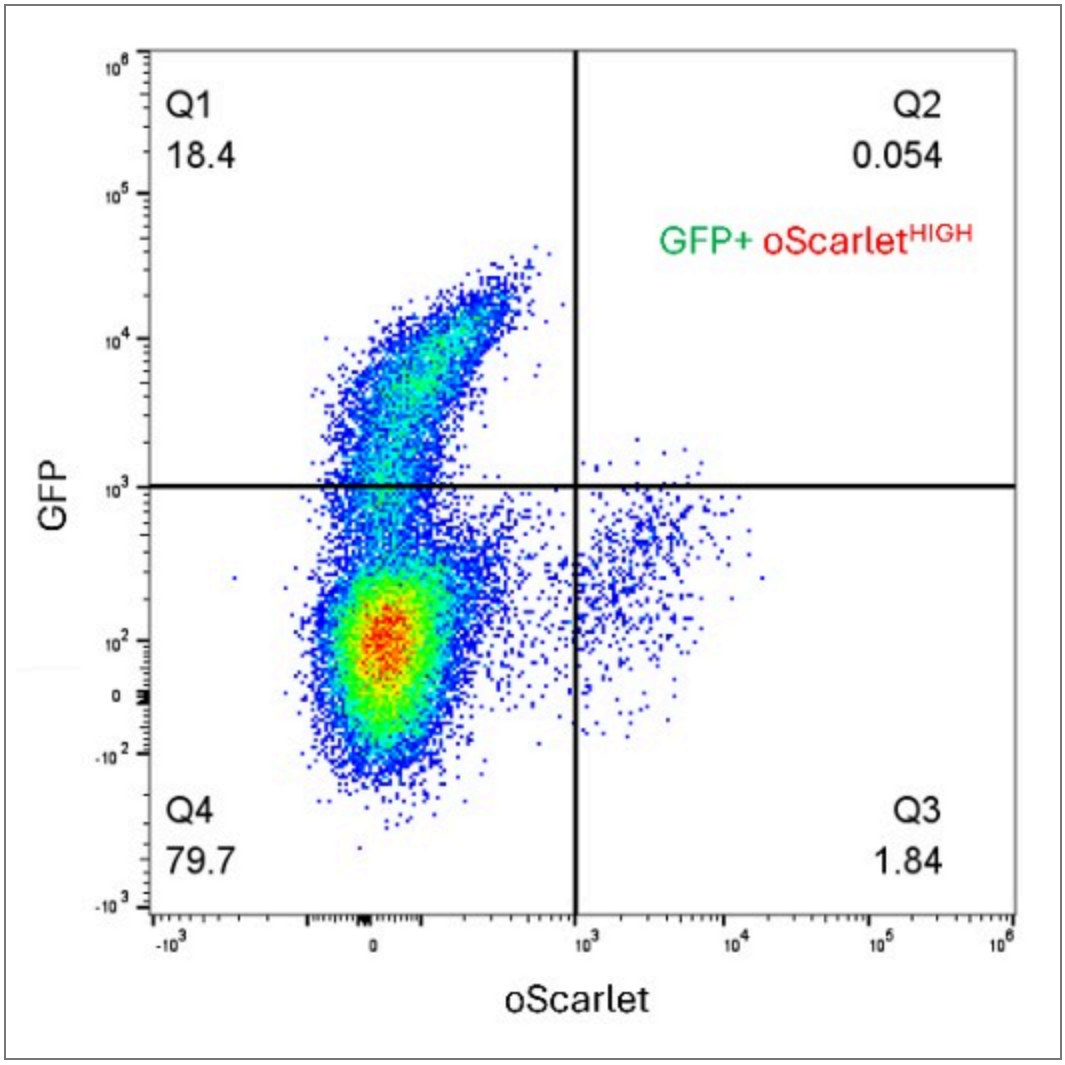

Author response image 1.

We believe that the results of these experiments are consistent with the notion that oScarlet^{HIGH} cells have engulfed oScarlet in vivo, prior to dissociation step. Nevertheless, we will also make note in the Discussion of the pitfall mentioned by the Reviewer.

> *Related to the above, it appears based on the scRNAseq that dissociation heavily enriched for brain macrophages. Therefore, the claim that clearance is mostly macrophage mediated could be due to an enrichment of this population during dissociation rather than this cell type being responsible for most of the extracellular waste disposal. Authors should quantify the % of total oScarlet that is specifically in macrophages in the brain sections they already have that are stained against oScarlet and CSF1R/ApoEB transcript.*

The Reviewer's point is well taken and we agree that experiments in intact brain sections are important to orthogonally test whether macrophages are responsible for engulfment. As suggested by the Reviewer, we will quantify the percentage of total oScarlet that is in *apoeb*+ macrophages in the brain sections we already have (current Fig. 3a). We note that it may not

accurately reflect the actual in vivo percentage, as we have found that it can be challenging to draw cell boundaries around macrophages due to their irregular shapes.

> *It is concerning that dextran and oScarlet are almost perfectly colocalized in the image presented (Figure 3a). It raises the possibility, among others, that dextran is sticking to potential oScarlet aggregates and then being internalized by macrophages. Therefore, it could be an artifact of the transgenic line. Authors should repeat the experiment in wildtype fish and use HCR against CSF1R/ApoEB to address this issue.*

We agree with the Reviewer. We have already injected dextran into non-transgenic killifish brains and observed dextran engulfment by *apoeb*+ cells. We will include this experiment in the revised version of the manuscript.

> ***Reviewer #3:***
>
> *Major comments*
>
> *The SP-oScarlet model enriches cells based on phagocytic capacity - by design, any phagocytic cell, including microglia, can be labeled. Only 0.5% of oScarlet^{LOW} cells were myeloid cells, confirming that this method captures virtually the entire myeloid population. The transcriptional resemblance to BAMs/MDMs is therefore a post hoc characterization of brain phagocytes broadly, rather than evidence for a selectively labeled subset. The authors show examples of apoeb^{+} cells near vasculature (Fig. 3b), but do not provide a comprehensive quantification of the full spatial distribution of oScarlet^{HIGH} cells. Importantly, neither the SP-oScarlet macrophages nor previously published wild-type killifish brain macrophages could be transcriptionally separated into three subgroups analogous to mammalian microglia, BAMs, and MDMs by PCA. This suggests that fish brain macrophages may not exist as subpopulations that correspond with their mammalian counterparts. The authors should therefore describe these cells as brain myeloid cells that exhibit BAM/MDM-like transcriptional characteristics, rather than implying they are a population equivalent to mammalian BAMs/MDMs.*

We agree with the Reviewer and will describe killifish brain macrophages as "brain myeloid cells that exhibit BAM/MDM-like transcriptional characteristics."

As described in our responses to Reviewer 1's comments, we will also provide/more prominently highlight analysis of killifish brain myeloid cell datasets showing:

i) Markers (e.g., *mrc1*, *cd74*) that are shared between mammalian BAM/MDMs and killifish brain myeloid cells.

ii) The heterogeneity we observe among killifish brain myeloid cells, which we believe corresponds to different cell states, but is not likely pronounced enough to correspond to functionally distinct cell types.

iii) The presence of oScarlet^{LOW} killifish brain myeloid cells, which are de-enriched by our sorting strategy.

> *Minor comments*
>
> *The authors acknowledge that oScarlet is relatively resistant to degradation and could affect the state of cells that engulf it. The independent single-cell experiment comparing old SP-oScarlet and old wild-type macrophages addresses this concern at the transcriptional level. However, it remains possible that chronic accumulation of degradation-resistant protein in lysosomes could itself impair phagocytic capacity. If so, the age-related decline in ex vivo engulfment might be partially attributable to oScarlet burden accumulated over a lifetime, rather than to aging per se. While a direct*

> *functional comparison with old wild-type macrophages is experimentally challenging, the authors should at least acknowledge this interpretive caveat in the Discussion.*

The Reviewer makes a great point, and we will acknowledge this caveat in the Discussion.

> *The transcriptional data show only modest changes in engulfment- and lysosome-related pathways with age. The authors should offer one or more specific, testable hypotheses (e.g., which phagocytic receptors or lysosomal components might be affected) to guide future investigation.*

We will provide a list of top engulfment-relevant genes that change the most with age, which also show only modest changes. We will better acknowledge that the age-related transcriptional changes in engulfment-relevant genes observed in our single-cell RNA sequencing experiment are modest and are unlikely to directly serve as a resource for testable hypotheses. We will also move our single-cell RNA sequencing data to the Supplementary Figures.

> *In the text, gene names such as APOEB are capitalized, whereas the convention for fish gene nomenclature is lowercase italics (e.g., apoeb). The authors should ensure gene formatting follows species-appropriate conventions throughout the manuscript.*

We thank the Reviewer for this suggestion, and we will change killifish gene names to be lower-case italicized throughout the manuscript.

> ***Description of analyses that authors prefer not to carry out***
>
> ***Reviewer #1:***
>
> *Regarding (Q2): Could there be a technical bias? An alternative explanation that may warrant discussion is whether aspects of the experimental pipeline (cell dissociation, FACS, scRNA-seq) could influence myeloid cell states. For instance, it is conceivable that dissociation induces a reactive program that enhances uptake of fluorescent protein, potentially enriching for oScarletHIGH cells. As the authors use a similar experimental setup to prove uptake of dextran and ovalbumin, such a technical artefact may merit consideration. As this would influence the major conclusions of the paper, the authors might want to address this comment with additional experimental controls, such as single-nuclei RNA-seq on control young and aged brains to profile the natural myeloid population when not submitted to a cell dissociation and FACS procedure.*

We believe that generating our own single-nuclei RNA sequencing dataset would be beyond the scope of this study. However, a preprint by Williams et al. from the Benayoun Lab (*https://doi.org/10.64898/2026.04.09.717549*) includes single-nuclei RNA sequencing data from wildtype killifish brains and could provide an excellent test of our findings. We will point readers to this preprint in the Discussion.

> *Comment 3: The authors compare the oScarletHIGH cell transcriptomes to mouse and killifish datasets. Both the mouse (Barr et al) and killifish (Nagvekar, this paper) dataset are from enriched immune cells (mouse= CD45+ cells, and the 3 cell types selected from that). Why did the authors not compare to the whole mouse CD45+ dataset? Including zebrafish (Rovira et al, 2025) here would strengthen the evolutionary comparison. I also feel that the additional comparison with young killifish (Ayana et al) might not be that solid since this dataset was initially not enriched and has a significantly lower number of myeloid cells, and thus much less power. The old age time point in that study contained more myeloid cells, and might be interesting to include for cell type comparison. There are other, perhaps more unbiased ways of comparing cell types across species, for instance SAMap, developed by co-author Bo Wang. Did the authors consider using this or other methods?*

We thank the Reviewer for the SAMap suggestion. We did perform SAMap with a mouse reference from the Allen Brain Atlas. Our SAMap analysis identifed distinct microglia-, BAM-, and dendritic-like myeloid populations. However, we were not confident in these SAMap results because the differences between the populations were subtle and we thought they would be unlikely to represent differences between functionally distinct cell types. Of note, the dendritic-like cells we identified by SAMap in the killifish brain did not express canonical markers of dendritic/dendritic-like cells from mammalian and zebrafish literature (e.g., *batf3*). Additionally, other SAMap studies from the Wang Lab analyzing non-neural cell types in other vertebrates do not separate microglia from non-microglial macrophages (Kalakuntla et al., in preparation).

> *Comment 4: Regarding the comparison with the aged brain:*
>
> *Figure 4: It would be nice to include the same comparisons as for young fish (cfr Fig.1 panels F-I).*

We agree with the Reviewer. Unfortunately, we did not sequence oScarlet^{LOW} cells from old brains, for cost reasons, and this precludes the comparison requested by the Reviewer. We will more clearly indicate that we do not have the oScarlet^{LOW} cells from old brain in the Results section.

> ***Reviewer #2:***
>
> *The flow cytometry strategy used does not distinguish between oScarlet protein that has been internalized versus that which is sticking to the surface of macrophages. Authors should stain non-premeabilized and permeabilized cell suspensions with a flow antibody against mCherry/RFP to get a sense of how much oScarlet is inside versus outside of the macrophage. For most antibodies this can be done on the same sample sequentially if the antibodies have a different fluorophore.*

The Reviewer makes an important point, and we will address this caveat in the Methods. We have performed a pilot of the flow cytometry experiment suggested by the Reviewer and, encouragingly, observed a higher proportion of cells labeled by the antibody (the same anti-mCherry antibody we used to label oScarlet in situ) in the permeabilized condition. However, we do not wish to publish these results as even in the permeabilized condition, the antibody labeled <0.2% of cells – meaning it likely did not label most oScarlet^{HIGH} cells, making it difficult to draw strong conclusions about internalized vs. surface oScarlet in these cells.

> ***Reviewer #3:***
>
> *The age-related decline in oScarlet fluorescence in oScarlet^{HIGH} cells in vivo could reflect either reduced phagocytic capacity of macrophages, or reduced oScarlet secretion by neurons, as the authors have discussed (Fig. 5a). The ex vivo assay addresses this by standardizing substrate concentration, which is a strength, but an in vivo functional assessment would provide a more physiologically relevant complement. The authors have already established the methodology for in vivo substrate injection (Fig. 3a, dextran). A similar experiment comparing substrate uptake in young and old fish would circumvent potential artifacts of the ex vivo approach, such as enzymatic dissociation altering surface receptor availability, and would directly test whether engulfment declines in the native brain environment.*

We agree with the Reviewer and performed a pilot of the suggested experiment, which did not show age-related differences in in vivo engulfment of injected dextran. However, in developing the brain injection procedure, we concluded that this procedure works well for comparisons within a sample, but not for comparisons across samples and conditions (e.g., young vs. old). This is because the injection site is determined by sight (aiming for the most

medial point on the telencephalon/optic tectum border, with no standardized way to control injection depth), and not stereotactically with coordinates. With our current procedure, it is challenging to perform reproducible injections across ages due to known age-related differences in fish/brain size and skull thickness.

We are interested in developing stereotactic injection approaches that would be compatible with comparisons across ages and other conditions, but we believe that this is beyond the scope of this manuscript. We will discuss this possibility as a future direction in the manuscript.

https://doi.org/10.7554/eLife.112503.1.sa0